Multitemporal assessment of crop parameters using multisensorial flying platforms

Dissertation
zur
Erlangung des Doktorgrades (Dr. rer. Nat.)
der
Mathematisch-Naturwissenschaftlichen Fakultät
der
Rheinischen Friedrich-Wilhelms-Universität Bonn

vorgelegt von

Dipl.Biol. Andreas Burkart

aus

Düsseldorf

Bonn Mai, 2015

Angefertigt mit Genehmigung der Mathematisch-Naturwissenschaftlichen Fakultät der Rheinischen Friedrich-Wilhelms-Universität Bonn

1. Gutachter: Prof. Gunter Menz

2. Gutachter: Prof. Uwe Rascher

Tag der Promotion: 21.09.2015

Erscheinungsjahr: 2016

Abstract

Agriculture is the source of food for mankind. The increase of yield and the efficient use of resources are key elements for a sustainable food production. This increase is essential to fulfill the demand of the earth´s growing population. In the present study we investigated the opportunities and challenges of unmanned aerial vehicle (UAV) based measurement systems that can provide detailed data on agricultural crops. This novel way of rapid data acquisition with high spatial resolution opens up new possibilities in precision farming and management of huge breeding experiments. In total 4 studies were carried out which investigated key elements for the retrieval of valid remote sensing data from optical UAV sensors.

A spectrometer was developed to be carried by an octocopter UAV and its calibration and quality assessment are presented. Over a spectral range from 350 nm to 800 nm, the UAV spectrometer has shown excellent correlation with ground based reference instruments ($r^2 > 0.99$), while having a 6 time smaller standard deviation.

In a second experiment four different UAV sensors suitable for precision farming (Sony NEX-5n RGB camera; Canon Powershot modified to infrared sensitivity; MCA6 Tetracam; UAV spectrometer) were compared over differently treated grassland. The high resolution infrared and RGB camera allows spatial analysis of vegetation cover while the UAV spectrometer enables detailed analysis of spectral reflectance at single points. The high spatial and six-band spectral resolution of the MCA6 combines the opportunities of spatial and spectral analysis, but requires huge calibration efforts to acquire reliable data. All investigated systems were able to provide useful information in different distinct research areas of interest in the spatial or spectral domain.

The UAV spectrometer was further used to assess multiangular reflectance patterns of wheat. By flying the UAV in a hemispherical path and directing the spectrometer towards the center of this hemisphere, the system acts like a large goniometer. Other than ground based goniometers, this novel method allows huge diameters without any need for infrastructures on the ground. Our experimental results shows good agreement with models and other goniometers, proving the approach valid.

UAVs are capable of providing airborne data with a high spatial and temporal resolution due to their flexible and easy use. This was demonstrated in a two year survey a high resolution RGB camera was flown every week over experimental plots of barley. From the RGB imagery a time series of the barley development was created using the color values. From this analysis we could track differences in the growth of multiple seeding densities and identify events of plant development such as ear pushing.

These results lead towards promising practical applications that could be used in breeding for the phenotyping of crop varieties or in the scope of precision farming. With the advent of high endurance UAVs such as airships and the development of better light weight sensors, an exciting future for remote sensing from UAV in agriculture is expected.

Content

Introduction

The ultimate goal of agricultural research is the sustainable provision of food to mankind for now and in the future. As the population continues its exponential growth, agriculture has to face the huge task of feeding 9 billion until the middle of this century (Godfray et al. 2010). In history, more crop output was achieved by transforming wilderness into farmland. By applying crop rotation, fertilizer and pesticides, the productivity of the available area was further enhanced leading to the "green revolution" (Cassman 1999; Evenson and Gollin 2003). In recent decades the huge potential of breeding and genetic engineering has generated another gain in yield (Tester and Langridge 2010; Fischer and Edmeades 2010). But the capabilities of traditional techniques to increase agricultural production are reaching their limits and must be complemented by new methods to sustain the steady gain in yield (Jain 1986; Reilly and Fuglie 1998). But as improving the yield is converging the limit and environmental issues arise from the extensive use of fertilizers and herbicides, the optimization of the use of resources is coming into the focus of the farm management. So new approaches can be identified to further optimize the overall efficiency of agricultural food production.

In this context two recent approaches are promising to complement the work of crop breeders and farmers.

1) Precision farming makes use of precise and current knowledge about spatial heterogeneity of the farmlands as well as the current state of crop development. By the adaptive use of fertilizers and pesticides, the farmer applies only the necessary amount. This strategy has a huge potential for saving valuable resources (McBratney et al. 2005). However, the farmers are in need for accurate sensing technologies which support the decision making by detailed spatial and temporal information about the plants development (Auernhammer 2001). These methods must be available on short notice and must be able to cover large areas within short times, to deliver the necessary data to the decision makers in almost real time.
2) Phenotyping characterizes the development of a plant under different environmental conditions. While the genotype of a crop is fixed as a variety, the phenotype of a crop can show extreme variations as a result of its surrounding parameters such as soil, fertilizer, pathogens and weather (Araus and Cairns 2014). The phenotype is the main driver for plant productivity. So breeders are finally interested in optimizing phenotypes for specific conditions, rather than genotypes that may react in unpredictable ways under changing environments. The problem is, that the amount of possible phenotypes of a plant is very numerous, as the permutation of environmental conditions are endless. To encounter this challenge high throughput phenotyping methods are necessary, that can screen thousands of plants and identify relevant breeding traits (Fiorani and Schurr 2013). Using phenotyping the impact on the plants of the relevant environmental conditions, which define the present ecosystem or will be occurring throughout the global climate change can be assessed. Phenotyping efforts go from lab, to greenhouse and finally to field level. To survey large agricultural phenotyping fields, devices and sensors are required, that deliver detailed temporal and spatial information on the planted phenotypes on a regular base.

The recent development of Unmanned Aerial Vehicles (UAV) provides platforms, which allow to place light weight sensors over agricultural fields. By changing the perspective to view of a whole field from above, new insights become possible. This opens the door for a whole new information technology that is going to change the way farmland is managed in the future. The development of high powered and light weight batteries, together with miniature attitude sensors, coupled with high efficiency electric motors and data

processing devices enabled the construction of a new class of flying vehicles. So called multicopters have from 3 to 16 rotors delivering vertical thrust to lift the vehicle in the air. At the same time, by accurately controlling each single motor, the UAV can perform directional maneuvers and allows defined positioning in the 3D space. The ability to hover over a fixed position is the main difference to airplanes that on the other hand have longer endurance and can cover larger areas (J. A. J. Berni et al. 2008). Both concepts are widely used in science and first steps are undergoing towards commercial use (Anderson and Gaston 2013).

The UAV only acts as a platform, in other words it is a versatile tripod that enables the positioning of a sensor almost everywhere over agricultural fields. By observing areas of interest from a nadir perspective, comparison of spatially distributed plant traits is straight forward, compared to an oblique view. While common RGB cameras already enable outstanding insights, if positioned above agricultural fields (Sakamoto et al. 2012; Juliane Bendig et al. 2014), other sensor types allow complementing analyses. The technical development towards small high performance electronics recently allowed the production of thermal cameras that can be carried by UAVs to detect water stress (P. J. J. Zarco-Tejada, González-Dugo, and Berni 2011). Furthermore, multispectral cameras allow the detection of distinct spectral bands that bear information on various plant parameters (Kelcey and Lucieer 2012). Exceeding a few multispectral bands, spectroradiometers look at the full spectrum of reflected light. Just recently spectrometers became available, which are both, highly accurate and light weight, which makes them suitable for the use on UAVs. These devices allow the deepening of insights into the plant´s structure and biochemistry (Milton et al. 2009) via collecting hyperspectral reflectance measurements of plants.

In remote sensing, the concept of reflectance is used to describe the measurable interaction of incident light with the land cover. For top of canopy measurements, the formula for reflectance is the quotient of upwelling reflected radiance by incident irradiance (eq.1).

$$eq.1 \quad Reflectance = \frac{Radiance}{Irradiance}$$

When observing vegetation, reflection is strongly associated with the plant´s architecture, biochemistry and growth state (Knipling 1970; Sims and Gamon 2002; Asner 1998). By using cameras or spectrometers, the reflectance can be investigated in the visible or near-infrared (NIR) spectral range. In addition, the thermal range can be observed using thermal cameras. The visible light, however, is the driver for photosynthesis. Thus, a vast amount of relevant information about the plants can be derived from the visible range of light (wavelength range 400 nm – 700 nm) (Peñuelas and Filella 1998). The continuous spectrum of a plant´s reflectance has distinct spectral regions that are known to represent information about the plant´s condition. These regions are commonly exploited using so called “Vegetation Indices” (VI), which rely on two or more single bands of the continuous spectrum. The most prominent VI is the normalized differentiated vegetation index (NDVI), which is based on comparing the red and NIR range of reflection (Blackburn 1998). An increasing number of VIs has been developed which correlate to different plant traits (Bannari et al. 1995) or plant diseases (Mahlein et al. 2013). But reflectance mirrors not only the plant´s properties, it is also dependent on variations of the measurement setup, such as sensor-illumination geometry. The so called Bidirectional Reflection Distribution Function (BRDF) is the theoretical base to describe the effects of the geometry of the measurement setup in relation to the investigated surface (Nicodemus 1965; Schaepman-Strub et al. 2006). The angular reflection properties of a surface covered with plants is largely dependent on the structure of the plants and the illumination conditions.

The Influence of such effects must be understood to eliminate their impact on the actual plant parameter that could be estimated from the reflectance measurement.

The retrieval of small differences in the reflectance of the plants is necessary to detect relevant differences in traits. But to identify these small differences the quality of the measurements must allow such discrimination. However, field measurements under outdoor conditions are prone to a large variety of undesired influences, which increase uncertainty. These can be divided in three categories which have to be addressed separately to achieve a high quality of data acquisition:

1) Environmental factors such as changes in light conditions by clouds, different sun elevations or strong wind, can alter the reflection signal of plants.
2) Instrumental characteristics are the limiting factors in data retrieval. Depending on the type of sensor a full quality assessment has to be performed that delivers spatial and spectral accuracy as well as a quantification of instrumental errors. A well characterized sensor produces data with known quality and uncertainty which is the essential base for the estimation of plant parameters.
3) Measurement protocols that are suited to the given environmental factors and instruments characteristics need to be developed to insure consistent data quality. By intelligent design these protocols can eliminate issues of the sensors that would otherwise appear in the data.

Additional awareness has to be given to metadata. All acquired sensor data is worthless without an adequate context. For phenotyping experiments as well as observational studies of agricultural fields, the measurements must be adapted to the given circumstances. Experimental treatments and meteorological conditions must be known. Only proper knowledge about the actual condition of the plant at ground level leads to meaningful analysis of any airborne sensor data. In this study, the new field of UAV-based remote sensing of agricultural crops and its opportunities are explored. But as outlined in the introduction a couple of challenges stand between the plants, the UAV based method and the desired results. This leads to the main task of this study:

“Identification of key elements for the retrieval of valid remote sensing data from optical UAV sensors.”

Along with this question we carried out different studies: 1) a UAV platform for agricultural research was introduced and heavily tested. It is based on a commercially available octocopter and was used throughout the three years of this study; 2) different optical sensors such as a RGB camera or a spectrometer were calibrated and tested to retrieve meaningful results from the raw data; 3) a novel UAV-based spectrometer was developed and tested. This first small UAV based flying spectrometer was intensively calibrated and its performance was assessed compared to ground based standard instruments; 4) the influence of angular effects on hyperspectral data was investigated to contribute to the efforts of understanding the impact of such effects on vegetation. The novel method presented in this study was based on an UAV spectrometer and allows the coverage of larger areas as compared to common ground based tools for angular measurements; 5) time series of UAV imagery of an agricultural experiment were analyzed over two vegetation periods. With this dataset it was possible to track the development of crops with high spatial and temporal resolution and to extract meaningful parameters referring to growth-stages. In summary, we give an outlook on future scientific opportunities and possible applications in this rapidly developing field of plant science and remote sensing.

Methods and Instruments

The UAV Platform

In this study, it was intended to acquire a mature flying platform that enables the user to focus on sensors and the scientific work itself, rather than design and build an UAV from scratch. So the various flying systems that are currently available on the market (Anderson and Gaston 2013) were compared and evaluated after their suitability for the present work. The following key parameters should be fulfilled by the UAV: 1) a payload of more than 500 g; 2) simple handling, which includes fast setup and a small form factor for the ease of transportation; 3) autonomous control of a stable and reliable flight, which relieves the operator from stressful piloting work; 4) low risk for injuries for the operator and third persons; 5) hover over a point and vertical take-off capability. Following this list of requirements, we decided to acquire the Falcon-8 UAV (Ascending Technologies, Krailing, Germany). Furthermore this UAV has a good reputation in the scientific community and was successfully used in various previous studies (Israel 2012; Eisenbeiss and Sauerbier 2011; Wefelscheid, Hänsch, and Hellwich 2012).

Fig. 1 Falcon-8 UAV used within the present study, during flight, equipped with the UAV spectrometer.

Design and Handling – The Falcon-8 (Fig. 1) is a rotary wing copter with 8 propellers that weighs approximately 1.8 kg including payload. The unique V-shaped motor arrangement allows the sensors to look down, as well as forward or upwards, without components of the UAV inside the field of view. This feature enabled the “multiangular experiment” [A3]. The UAV has an actively stabilized gimbal to correct the orientation of the sensor against the UAVs movements. This gimbal can be exchanged quickly to mount different sensors, facilitating the “comparison of UAV sensors” [A2]. The sophisticated flight stabilization system lets the UAV fly almost autonomously, which makes flying an easy job that can be done by anyone with little training. This allows, the operator to focus on scientific work. In contrast to various earlier studies (P. J. J. Zarco-Tejada, González-Dugo, and Berni 2011; Mitchell et al. 2012), the Falcon-8 and its sensors could be controlled by a single person. The system performed well during three years of operation and several hundred flight hours. The compact design allows to store the UAV in a case, which fits in the back of a car and is suitable for air-mail. By this, we could use the UAV at various sites in Germany as well

as throughout Europe (France, Spain, Portugal, Italy) and New Zealand. A software package for waypoint planning is included with the UAV, that enables semi-autonomous flight of the device, as well as sensor triggering.

Accuracy – For precision farming and phenotyping, an accurate positioning of the UAV and a proper pointing of the optical sensor are critical to investigate the area of interest. The positioning of the UAV during autonomous waypoint flight is based on GPS data and is commonly given within 10 m deviation from the actual desired position. During the study [A3] we tested the positioning and pointing accuracy of the UAV, using a 3D reconstruction approach (Structure from motion, Agisoft Photoscan, St. Petersburg, Russia), based on multiple images of the same scene shot by the UAV´s high resolution RGB camera. Using this, the error in waypoint flights could be assessed and is given in Tab. 1.

Deviation of:	Heading [°]	Camera Tilt [°]	Altitude [m]	Position X [m]	Position Y [m]
Average	0.11	6.07	0.03	-1.15	-2.22
SD	8.67	1.22	0.70	0.68	0.82
Max	26.20	9.74	1.44	0.67	-0.39
Min	-17.99	3.68	-1.09	-2.79	-4.60

Tab. 1 Accuracy of the UAV pointing and positioning calculated by structure from motion using 75 high resolution RGB images.

Robustness – The UAV was extensively used during the three years of this study and often performed multiple flights per day. No hardware related critical failure was observed in this period. One serious crash, due to the operator, who ignored battery warnings happened with structural damage to the UAV itself, but without harm to the payload. An in-field repair using tape and wire could restore flying capability to complete the ongoing experiment. The UAV was sent for maintenance and calibration to the manufacturer once a year.

Legal issues – Within Germany a couple of legal issues had to be solved for scientific/commercial use of small flying platforms that are below 5 kg of take-off weight. The operator has to prove experience in the handling of remotely controlled aircrafts. An insurance that covers eventual damage of third parties has to be filed as well. With this prerequisites, an official license can be requested from the “Dezernat 26 Luftverkehr, Bezirksregierung Düsseldorf”, which allows the use of the specific UAV in flying altitudes of up to 100 m above ground level. The landowner, however, has to agree with the flying activities on his property. Flying above persons is strictly forbidden, as well as flying at night. Each mission has to be logged in a flight book.

Efficiency – The flying time is one of the major limitations of rotary wing UAVs. As compared to planes or airships, their extremely inefficient way of flying, requires huge amounts of energy. This electrical power is stored in batteries, which are heavy and thus again decrease the flight time. With the Falcon-8 flight times of up to 16 minutes were achieved, depending on the payload. But for safety reasons we limited the mission time to 10 minutes, since a depleted battery is the main risk for crashes. Within the work with the UAV up to 9 additional batteries were acquired that could be exchanged in seconds after landing of the UAV. This way multiple sequential flights could be performed. The coverage of large areas (bigger than 1 km²), however, is an extremely big effort with the Falcon-8 and for these purposes fixed wing UAVs (planes) are preferable.

The UAV sensors and their calibration

RGB Camera

The sensor that is most often used in current UAV studies is a common consumer RGB digital camera. These cameras are light-weight, have a high resolution of multiple megapixels, are equipped with a SD card to save images and have a built-in battery. These cameras are designed to capture similar information as the human eye does. This is achieved by employing the three channels red, green and blue for each pixel, by inserting a so called Bayer-Matrix (Bayer 1976) filter in front of a monochrome Charged Coupled Device (CCD). The spectral transmittance of the Bayer-Matrix mimics the sensitivity of the receptor cells for red, green and blue light in the retina of the human eye. This implies that from a RGB picture, in theory, all information can be derived that can be derived by human vision. Installing a camera on a UAV enhances the human vision by flying it towards points and perspectives of interest that are otherwise hard to reach. For agriculture, with a focus on phenotyping and precision farming, this means rather than walking through never ending fields with countless plots, a single picture taken from above describes the whole experiment. A RGB camera can give information about spatial distribution of plants, their color and by employing post-processing methods 3D information can be derived (Juliane Bendig et al. 2014). To use a camera on an UAV for scientific purposes to generate meaningful data, a couple of modifications, calibrations and in-field preparations are necessary. This is essential to finally transform the raw imagery of the camera into useful values of reflectance which represents information about the plant state.

Fig. 2 Sony NEX-5n camera attached to the Falcon-8 UAV. Image provided by Ralf-Uwe Limbach.

UAV Integration – In this study, we use a Sony NEX-5n (Sony Cooperation Inc.) with a 16 mm fixed lens. The camera features 4912 x 3264 pixels. The field view is 73° x 53°, which leads to an observation area of approximately 150 m by 100 m from a flying altitude of 100 m over ground. At the same altitude a spatial

resolution for a single pixel of 30 mm by 29 mm, is achieved in theory. This resolution is often not reached in the image due to the quality of the optical path, and largely depends on the environmental parameters such as illumination conditions and wind. This camera was modified by Ascending Technologies, to be integrated into the Falcon-8. The LCD display on the back of the camera was removed and the image is directly streamed to the ground control station. The operator has a life-view of the camera and can assess shutter speed or ISO from the ground. Triggering of the camera is done either manually by a button on the remote control, or by the UAV itself, whenever it reaches a waypoint. The vertical pitch angle is accurately defined within one degree of precision by the operator during flight, or can be set in a preprogrammed waypoint flight.

Calibration – Depending on the further use of the acquired UAV imagery, the camera must be properly calibrated in the lab and with additional in-field methods [A2]. In this study we use the RGB camera for 1) color analysis and 2) 3D scene reconstruction. To derive valid color analysis from JPG images that are captured with automatic camera settings (eg. automatic shutter speed, ISO or white balance), the camera must be characterized for vignetting effects and color references must be present in each image (Lebourgeois et al. 2008). The vignetting effect appears in an image with darker edges compared to the center. This is dependent on the quality of the lens and can have a large impact on the derived color values. To correct for the vignetting effect, we employed an averaging approach. By averaging more than thousand fully different images of various scenes, the only information that remains is the lens dependent vignetting effect. By applying the inverse of this averaged vignetting image (Fig. 3) to the images of interest, the effect of the vignetting is removed.

Fig. 3 RGB image averaged from >1000 different images. The image represents the vignetting pattern of the Sony NEX-5n 16 mm lens camera setup. The corners and edges appear slightly darker than the center of the image.

To solve the problem of different illumination conditions (cloudy, sunny) and the cameras automatic white balance, colored targets on the ground were used (Sakamoto et al. 2012). These targets, which consist of colored squares of different reflectivity, which remain rather stable over the years. Using their colors as

reference, influence of illumination on the images of interest can be corrected, as long as the references are visible in the images.

To derive 3D models via structure from motion, we used the software Agisoft Photoscan. This is an enhanced processing tool that incorporates the calibration of the optical path of a camera, based on the images that are processed. In other words, all calibration procedures are performed by the software and the user just supplies multiple images of the ROI from different positions. The software then calculates the 3D scene including camera positions and the structure of the surface. This is used in an increasing number of scientific studies for a variety of surfaces from landfills to agricultural fields (Juliane Bendig et al. 2014; Siebert and Teizer 2014).

UAV spectrometer

At the time of this study, no spectrometer has been deployed on a small rotary wing UAV. As field spectroscopy using hand carried spectrometers (Milton 1987), as well as plane based airborne systems (Birk and McCord 1994) are frequently used with good results, the approach of mounting a spectrometer on a UAV system was highly promising. A UAV based spectrometer would not only facilitate speed of measurements compared to hand spectrometers, but it would also enable the spectrometer to be flown over hardly accessable areas and without disturbing eventual ground cover. To measure reflectance, several prerequisites have to be fulfilled: 1) the spectrometer needs a controller, that triggers via remote connection or at waypoints; 2) a reference must be available that allows to calculate the irradiance, while the flying spectrometer measures the upwelling reflected irradiance; 3) the whole system must be properly calibrated with a focus on influences that might arise from the implementation on an UAV; 4) accurate georeferencing must be available by the flying platform or an attached inertial measurement units (IMU). Latter is essential to allocate the field of view of the spectrometer to the actual measured spot in the field.

Fig. 4 UAV spectrometer Version 1, attached to the Falcon-8 using an active gimbal that stabilizes the viewing direction against the movement of the flying platform. Image provided by Ralf-Uwe Limbach.

Design – The development of the UAV spectrometer (Fig. 4) as well as practical testing and calibration is described in [A1]. In the following, an overview about the critical parts of the work with the UAV spectrometer is given, which serves as base for the later comparison to the other optical UAV sensors [A2] and the multiangular experiment [A3]. The limiting parameter for an UAV based sensor is weight. The Falcon-8, used for this instrument cannot lift anything that exceeds 500 g. At the time of the study, the Ocean Optics STS micro spectrometer (STS) became available. This device weighs only 68 g. It has up to 1024 spectral bands in the wavelength range from 300 nm to 800 nm and a field of view of about 12°. It provides a performance in spectral resolution and signal to noise similar to larger units, so we decided to base the UAV spectrometer on this unique device. The STS, however, does not provide the capability of saving spectra, nor has a battery for autonomous operation. To solve this problem, we designed a small control unit based on an open source Arduino microcontroller (Banzi 2008). This control unit provides data storage for spectral data on micro SD card and triggers the spectrometer. Via a wireless remote connection, the user can set the integration time and receive a draft of the last acquired spectrum. Spectrometer and control unit are both powered by a 1.000 mAh 3.7 V lithium polymer battery, which keeps the system running for about 4 hours. Thereby, the UAV spectrometer is fully independent from the UAVs electrical system. We further integrated the option to automatically trigger the spectrometer when the UAV reaches a predefined waypoint. Using the UAVs waypoint planning software, a fully automatic operation of the spectrometer on board of the Falcon-8 could be achieved. To measure reflectance, a second spectrometer is placed on the ground, which measures the incident radiance over a white reference, at the same time, the UAV spectrometer is triggered (Fig.5). Thereby, the impact of changing illumination conditions during flight can be eliminated. By this measurement protocol, the spectrometer system is also almost independent from atmospheric influence, as the UAV´s flying altitude is usually between 10 m and 30 m. Both spectrometers, however, must be thoroughly inter-calibrated to warrant high data quality.

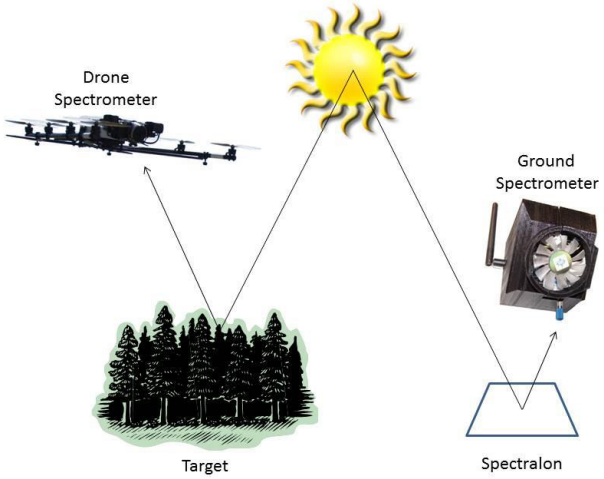

Fig. 5 reflectance measurements conducted with an airborne spectrometer over forest and a ground based device over a white reference, both wirelessly synchronized to adapt to changing light conditions.

Calibration – Additionally to common calibration efforts that must be addressed in every spectrometer (Schaepman and Dangel 2000), a technique after Kuusk (J. Kuusk 2011) was applied, to remove the influence of dark current (DC) from the raw data. The DC is an underlying noise that is introduced by electrical effects in the linear CCD which converts incident light quants into electrical current. Commonly

the DC is measured and subtracted by closing the spectrometer´s optics to characterize its DC excluding light. But the light weight STS has no internal shutter, nor is it possible to cover the optics during flight. The noise is largely dependent on the temperature of the device and integration time (IT). By measuring the DC with different IT and raising temperature, a model was developed that estimates the DC of every single pixel depending on actual IT and temperature. Thereby, we could eliminate the effects of DC for each spectrum, even though environmental conditions might affect the temperature of the device. Because we rely on two spectrometer units, both must be inter-calibrated, because they have slightly different responses in spectral shift and sensitivity. The spectral shift is a mismatch of wavelengths and was corrected by using the software SPECCAL (Busetto et al. 2011), which exploits the defined positions of Fraunhofer lines in the solar spectrum. The different sensitivities of the two spectrometers were assessed by measuring the same lambertian reflectance targets (Spectralon) under equal illumination conditions. A correction factor that accounts for this linear difference is then applied in the post-processing.

Test – To check the practical use of the instrument and its performance compared to ground based field spectrometers, a field experiment was conducted. The same agricultural areas were measured at approximately the same time of the day with an ASD field spectrometer and the UAV-based spectrometer. The measurements were performed in a way that the same areas were covered. After post-processing, the results were compared [A1].

Field sites and experimental setup

Comparison of UAV sensors experiment

A variety of optical sensors that are suitable for UAVs are available on the market. These sensors range from simple consumer RGB cameras towards more complex multispectral systems to expensive hyperspectral line scanners or snapshot cameras. However, most of these sensors, are novel and poorly characterized. To evaluate, which sensor is most applicable for specific research questions, we chose 4 different devices, which were available at the time of the study, for an in-field comparison experiment. In [A2] the Sony NEX-5n, a converted Canon Powershot sensible to infrared, a MCA 6 Tetracam (Tetracam Inc., Chatsworth, USA) multispectral camera and one UAV spectrometer [A1] were inter-compared over different types of grassland. In the following section we will focus on the Sony-NEX-5n RGB camera and the UAV spectrometer, as they were the primary sensors used in the other presented studies of this work.

Setup – The study site was a dairy farm of the Massey University in Palmerston North, New Zealand (lat. - 40.376, long. 175.606). Flights were performed in February 2013 around noon at a clear blue sky day. The RGB camera and the UAV spectrometer were flown on board of the Falcon-8 by exchanging gimbal and sensor straight after landing. We chose 8 waypoints which were resembling different grassland conditions from dry to irrigated. Along with the UAV sensors, a handheld spectrometer (ASD handheld 2, ASD. Inc) was used to characterize the spectral signature of the observed WPs with a standard method. The UAV spectrometer was used with its ground reference as described in [A1]. To refer the RGB images of the camera to reflectance, big colored tarps were put in the field of view. Using the handheld measurements of reflectance over the reference targets, the RGB images could be converted into

estimates of actual reflectance, using the empirical line method (Smith and Milton 1999). Both sensors, RGB camera and UAV spectrometer were calibrated as described before. The reflectance values as derived from the two sensors and postprocessing chains, were compared and their correlation over the eight waypoints was assessed. As a spectral 3 band, but high spatial resolution RGB camera is compared to a single point hyperspectral radiometer, fully different scientific analyses can be performed. These possible applications were identified, according to the sensors capabilities.

Multiangular experiment

Angular effects that are the result of the trigonometry in the illumination-surface-sensor setup are an intensively studied field of remote sensing (Liang et al. 2000). Various earlier studies have performed ground-, plane- and satellite based research that led to an understanding of angular effects on the macro (Comar et al. 2012) or landscape scale (Verrelst et al. 2008). But vegetation canopies are subject to continuous change, thus a high temporal resolution of angular measurements is necessary to understand the underlying effects. At the same time the small spots that can be assessed by ground based angular measurement instruments are often too small to represent the whole canopy. This is why we developed the novel approach of an UAV based goniometer. Goniometers are devices that allow to characterize the angular reflectance properties of a surface by changing the angle of view of the sensor around a fixed center point of interest. For homogeneous surfaces such as snow or sand, small goniometers are suitable (Bourgeois et al. 2006). But for more structured surfaces such as vegetation, larger fields of view are necessary, as the angular effects arise from the complex 3D structure of the canopy. Common ground based goniometers are limited in size and thus in their field of view. With the UAV based approach, the goniometer is replaced by a distinct flight pattern. This flight pattern along with the viewing angle of the spectrometer enables the investigation of a center point from different directions, as shown in Fig. 6.

Fig. 6 exemplary path as flown by the UAV over an agricultural area to act as a goniometer. On each nook of the flight pattern, the UAV stops and points and triggers the spectrometer towards the center of the hemisphere, described by the path. Visualization captured from Google Earth.

The experiment was performed over a wheat field at Merzenhausen, Germany (lat. 50.93039, long, 6.29689), at a clear sky day in June 2013. The center point of the multiangular flight pattern was placed according to high resolution UAV imagery in a homogenous part of the wheat field. A pattern with 25 waypoints covering 8 different heading angles (45° steps) and 4 different vertical tilt angles (20°; 43°; 60°; 90°), was programmed for the UAV. The pattern was flown at 12:43 and 14:47 local time, to compare two different time points around solar noon. At each of the 25 waypoints, the spectrometer was triggered 3 times, to assess the reproducibility of the spectral measurements at a single waypoint. A ground reference measured a white reference each time the airborne spectrometer was triggered. Using this dataset, a variety of angular effects in the spectral range could be investigated. Among a variety of analyses that were described in [A3], we investigated the effects of the sun angle on vegetation indices such as the NDVI or the red edge inflection point (REIP).

UAV image time series of barley

For precision farming and phenotyping, not single snapshots of the plants development are important, but an overview of the whole growth cycle. Only by the use of time series, the reaction of the plant to environmental parameters can be investigated. This is a huge effort in large field experiments, because each of hundreds of plots, has to be observed manually. By the use of satellite imagery agricultural fields can be assessed on low spatial resolution. But in general, satellite imagery is available only once per month. So the dynamic plant growth that can happen in days, cannot be tracked. This lack of survey capability was addressed in this study with a UAV, carrying a high resolution RGB camera. To this end an experimental barley field was observed from 100 m altitude with a weekly frequency, covering the whole growth period.

Year 2013	Year 2014
9-May-2013	27-Mar-2014
14-May-2013	3-Apr-2014
23-May-2013	10-Apr-2014
5-Jun-2013	16-Apr-2014
11-Jun-2013	22-Apr-2014
19-Jun-2013	5-May-2014
26-Jun-2013	15-May-2014
30-Jun-2013	21-May-2014
6-Jul-2013	22-May-2014
1-Aug-2013	26-May-2014
	31-May-2014
	5-Jun-2014
	10-Jun-2014
	18-Jun-2014
	24-Jun-2014
	3-Jul-2014
	18-Jul-2014

Tab. 2 dates of UAV flights over the barley density experiment at the campus Klein-Altendorf. In 2013 a total of 10 surveys were performed and in 2014 we flew 17 times.

Setup – A density experiment with 2 barley varieties (Scarlett, Barke) was planted in 2013 and 2014 at the campus Klein-Altendorf next to Bonn. Ten different seeding densities ranging from 24 to 340 grains per m² were sown in plots of 16 x 1.5 m in 5 randomly spread repeats. The whole experiment was arranged in a rectangular field with paths between the plots. The UAV was flown at the dates given in Tab. 2 over the experiment in an altitude of 100 m to make a single image of the current growth state of the whole experiment. Colored references were placed in the center of the image to correct for different illumination conditions. Ground based plant scoring was performed along with the flights, whenever time allowed.

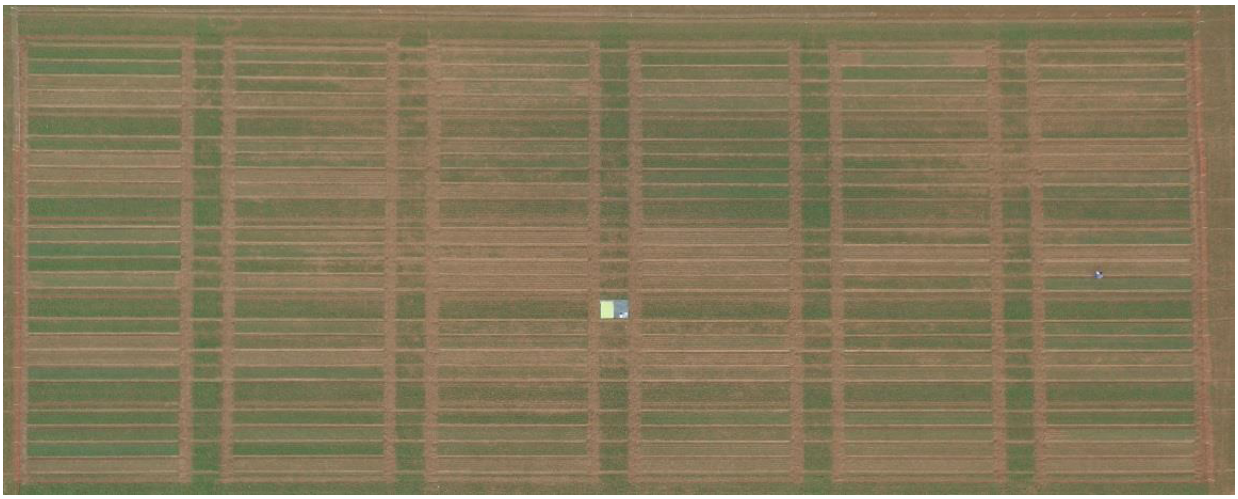

Fig. 7 rectified and vignetting corrected image of the density experiment as photographed with the UAV at the 22th of April 2014. In the center of the image the color references are visible.

Image processing – Images were corrected for vignetting and rectified towards a base image using ENVI (Fig. 7). Regions of interest were defined for each seeding density and variety, covering all 5 repeats. The average RGB values for each point in time and region of interest were extracted and corrected against the color reference. Using the green red vegetation index GRVI (eq. 2), a relative greenness was calculated (Motohka et al. 2010).

$$eq.2 \;\; GRVI \;\; = \frac{(Green - Red)}{(Green + Red)}$$

With this value we assessed the development of each plot over time. The processed image data was compared to ground based coverage of the experiment to check its relevance for the description of the plants development.

Results and discussion

Comparison of UAV sensors

Throughout the experiments of this study, the two main UAV sensors RGB Camera and UAV spectrometer were used intensively for different applications. In the following, the differences between the two sensors is described and afterwards the performance of each single instrument in their specific application is discussed. Both sensors are observing the optical domain of the electromagnetic spectrum. While the RGB camera has a high spatial resolution of 4912 x 3264 pixels (16 megapixels), it separates only 3 spectral

bands with the broadly defined bands red, green and blue. The UAV spectrometer on the other hand has a high spectral resolution of up to 1024 bands with a very narrow bandwidth. It covers the spectral range from 300 to 800 nm, but has only a single spatial pixel. While these are the main differences of the two sensors, there are other parameters that preclude the RGB camera from accurate reflectance measurements, while the spectrometer suits well for the retrieval of reflectance. Nowadays RGB cameras have a huge variety of automation, which is intended to create visually appealing images. This, however, is in conflict with the accurate quantification of light in specific bands. For this kind of measurements, the UAV spectrometer is suitable, because it reacts almost linear to the amount of the incident light and can be calibrated radiometrically. The camera on the other hand captures detailed spatial information in an image which can be used to generate detailed 3D models (J. Bendig et al. 2013). The UAV spectrometer, in contrast, allows the calculation of narrow band spectral Vis, that are highly useful for plant research.

We tested the retrieval of reflectance from both sensors over the same areas, to assess how the retrieved values differ. The correlation over the 8 waypoints for three comparable bands (R,G,B) of the both sensors was $R^2 = 0.681$ (Tab. 3). The reason for this rather low correlation is mainly found in the non-linear radiometric response of the RGB camera. The JPG compression, as well as non-linear adaptions to light, decrease the accurate retrieval of reflectance values from RGB imagery. Scientific grade cameras or RAW imagery could enhance the quality of this data compared to the presented approach (Lebourgeois et al. 2008).

R^2	RGB	IR	MCA6	UAV Spec
RGB	1			
IR	0.9136 (16)	1		
MCA6	0.3773 (16)	0.9452 (16)	1	
OO UAV	0.6807 (24)	0.8906 (24)	0.8259 (48)	1
ASD	0.6736 (24)	0.6474 (24)	0.9242 (48)	0.9777 (3856)

Tab. 3 Correlation of reflectance, retrieved from different UAV sensors measuring over the same eight grassland targets. In brackets the number of measurements n is given. RGB = Sony NEX-5n, IR = Canon Powershot modified to near-infrared sensitivity, MCA6 = 6 band Tetracam, UAV Spec = STS spectrometer, enhanced for mounting on an UAV.

Another limitation of the RGB camera, compared to the UAV spectrometer is the low dynamical range. While the UAV spectrometer has a 14-bit response range, the JPG compression of the RGB camera saves only 8-bit per color channel. The spatial resolution, however, gives a useful insight in the grassland heterogeneity and allows fast assessment of clearly visible features, such as dry vs. healthy vegetation. Within [A2] two additional UAV sensors were tested for the use in vegetation monitoring. The third sensor was a Canon PowerShot consumer camera that was modified towards extended sensitivity in the near infrared. It was easy to use and provided high resolution (4000 by 3000 pixels) imagery, but had the same shortcomings as the RGB camera. The infrared sensitivity is not only affecting the red pixels, but also the blue and green. This leads to rather unseparated bands and thus decreases the value of the retrieved information (Sakamoto et al. 2012). The fourth sensor was a MCA6 Tetracam. The MCA6 has six bands that can be adjusted by selectable filters with a bandwith of about 10 nm. Further it is a scientific grade sensor

that features a 10-bit dynamical range and a resolution of 1280 by 1024 pixels. The camera, however, required extraordinary calibration efforts (Kelcey and Lucieer 2012). But after applying the calibration procedures, the correlation to the UAV spectrometer was satisfying ($R^2 = 0.826$). In contrary to the other three sensors, the MCA6 is a rather heavy sensor that exceeded the payload of the Falcon-8 and was lifted by another copter. Within [A2] we could show that four different optical UAV sensors deliver comparable results, but each should be used for a specific range of measurement topics. The recent technological development in the camera sector has produced a rapid advance in miniaturization and quality. This trend has an impact on scientific devices and several of manufacturers are now providing multi- and hyperspectral cameras suitable for UAVs (Tab. 4).

Name	Manufacturer	Weight [g]	Bands
Rikola Hyper.	Rikola Ltd.	600	adjustable
UHD 185 Firefly	Cubert GmbH	840	125
Nano-Hyperspec	Headwall Photonics Inc.	700	270
OXI-VNIR-40	Gamaya SA	100	40
MCA6	Tetracam Inc.	700	6

Tab. 4 List of manufacturers for multi- and hyperspectral camera systems that are suitable for integration in UAV platforms. The list is a snapshot of devices available in early 2015. All cameras work with fundamentally different principles of the optical path and thus have huge varieties in how to perform measurements and post-processing.

These cameras are closing the gap between single point spectrometers and high spatial but low spectral resolution cameras. Once the calibration and validation issues are mastered, these cameras will provide the sensing capabilities, needed for accurate determination of valid plant parameters. Recent studies with such cameras on board of UAVs point towards the retrieval of highly relevant data allowing the identification of drought stress, nitrogen deficit or upcoming plant diseases (Quemada, Gabriel, and Zarco-Tejada 2014; P J Zarco-Tejada et al. 2009; Baluja et al. 2012; Mitchell et al. 2012). Other studies work towards combining 3D information with hyperspectral data to increase the informative value of the data (Juliane Bendig et al. 2014; Aasen et al. 2014). Even very small, but highly meaningful signals like the chlorophyll fluorescence (Meroni and Colombo 2006; Porcar-Castell et al. 2014), could be measured from UAV based sensors (P. J. J. Zarco-Tejada, González-Dugo, and Berni 2011; P.J. Zarco-Tejada et al. 2009). This opens up new possibilities for insights into plant biochemistry from remote sensing data.

Multiangular effects on optical UAV data

Not only sensors are a limiting aspect of the optical remote sensing of plant parameters. The setting of the investigated vegetation, illumination or sensor angle have an effect as well. We have investigated this effect using a novel setup, based on the UAV spectrometer. In the multiangular study [A3] we first checked the accuracy of the approach. Our data revealed that the positioning and pointing accuracy were acceptable (Tab. 1), although they were worse than ground based devices. The reproducibility of spectra, taken at the same waypoint, however, was satisfying (Fig. 8).

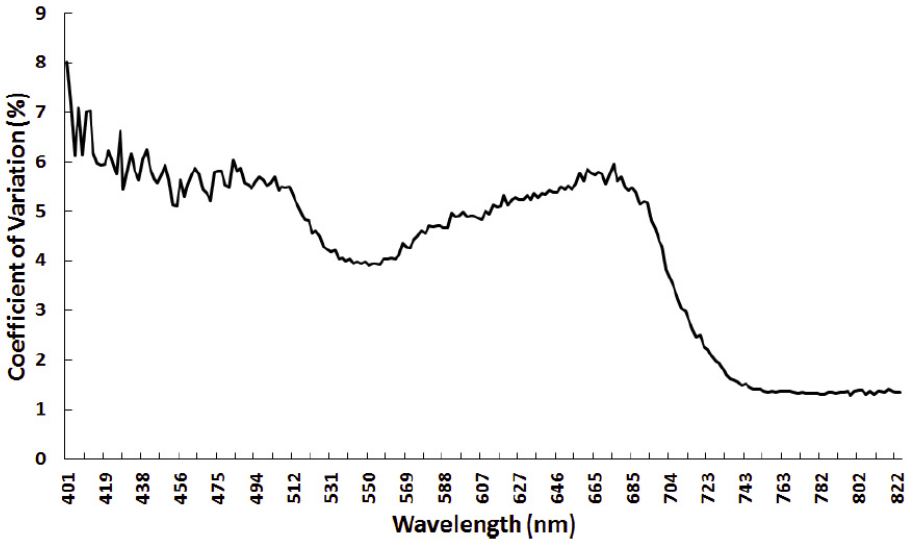

Fig. 8 The spectrometer of the UAV goniometer was triggered three times at each waypoint. The overall variation of these three reflectance spectra for all waypoints is shown over the whole spectrum.

We then investigated the impact of the observation angle to the NDVI and REIP. The difference in the NDVI ranged from 0.83 to 0.95 with a nadir value of 0.89. In the REIP the values ranged from 729 nm to 735 nm with a nadir value at approximately 733 nm (Fig. 9). The multiangular data, derived in this experiment, however, is in line with earlier studies with ground based goniometers or satellite approaches (A. Kuusk 1991; Verrelst et al. 2008; A. Kuusk, Kuusk, and Lang 2014). In this experiment extreme sensor tilt angles down to 20° were investigated, but even at 66° a significant difference is observed.

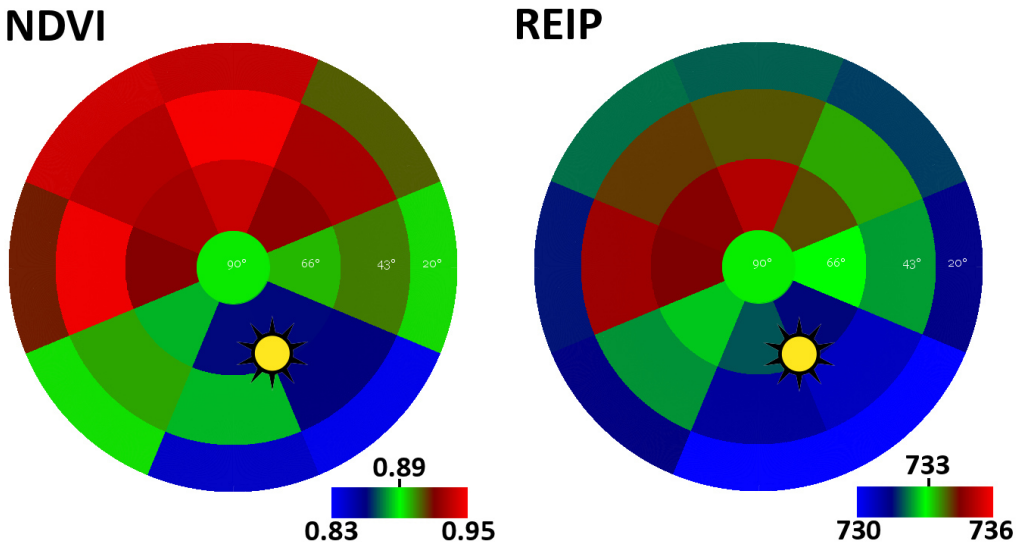

Fig. 9 Values of NDVI and REIP in nm at all 25 waypoints shown as a circular graph, or polar plot. Each "slice" represents a heading while each ring represents a sensor tilt angle. The indices magnitude is color coded from low values of light blue, to high values in bright red. The angular position of the sun is depicted by the sun-symbol. In this figure no interpolation between waypoints is performed.

This difference is driven by the position of the sun. This was confirmed by comparing a measurement before and one after noon. The pattern of the angular reflectance difference changes with the position of the sun, which is seen in the data as hot spot, with higher reflectance values. This impact of surface and sensor illumination geometry, also known as BRDF effects (Nicodemus 1965), is a frequently discussed topic in the remote sensing technology (Schaepman-Strub et al. 2006). Up to now huge efforts have been conducted to address this issue and various steps towards good BRDF corrections have been performed (Bourgeois et al. 2006; Hautecoeur and Leroy 1996; Schlapfer, Richter, and Feingersh 2015; Sandmeier and Itten 1999; Meggio et al. 2014). For heterogeneous surfaces such as vegetation, which is also affected by continuous changes throughout the year, the BRDF effects are not yet fully understood, nor characterized. With the presented UAV spectrometer, used as goniometer, we have introduced a method for fast and easy retrieval of the multiangular parameters of vegetation. The huge advantage of the system is its independence from ground based structures. This also enables the UAV goniometer to be used over surfaces that are difficult to access by foot. An approach towards convenient correction of BRDF effects are mathematical models, which are optimized to estimate the angular influences depending on vegetation structure and sun/observer position. Using the SCOPE model (Soil Canopy Observation Photochemistry and Energy fluxes) (Tol et al. 2009), we have found good correlation of modelled angular reflection to measured data in angles close to nadir (Fig. 10). At lower tilt angles, however, the correlations are worse. This shows that using novel sensor-platform combinations, like the UAV goniometer, models can be trained and evaluated to further enhance the knowledge about angular effects of vegetation. Once these effects are understood in detail, the opposite way of using angular measurements to derive information about vegetation, will become feasible.

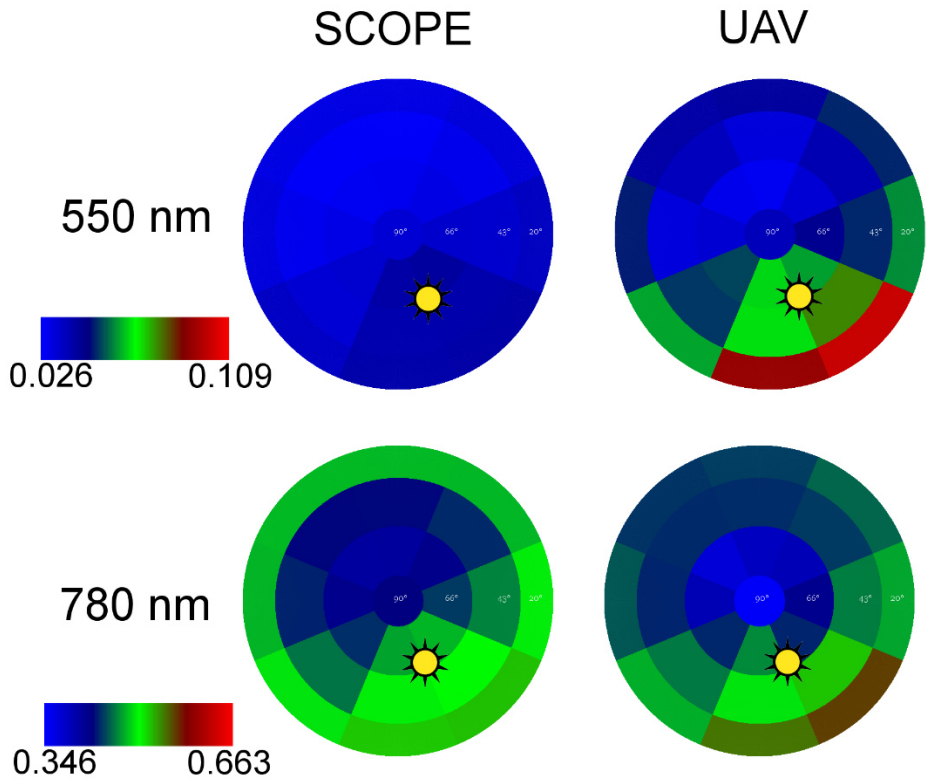

Fig. 10 Comparison of modeled angular reflectance calculated by SCOPE with the values measured by the UAV goniometer. Shown are two exemplary wavelengths, which are scaled to the present range of values.

UAV image time series of barley

To get relevant insights into the development of agricultural crops, not snapshots, but continuous monitoring by time series is necessary. The acquisition of time series of RGB imagery, monitoring the growth of barley on a whole field by using an UAV was tested in this experiment. In the first part the feasibility of the method was investigated within two years of practical work. Acquiring an image of the large 100 plot experiment, required a flying altitude of 100 m, using a wide angle lens with 16 mm focal length. We decided to capture only one image describing the whole experiment. This reduces effects of changing illumination conditions that arise when capturing multiple images and later stitching them together. We further placed color references in the center of the experiment to track differences in light composition or camera parameters over different measurement days. The overall working time for setting up the UAV, the targets and the photography flight itself was 20 minutes. It required only one trained person to perform all the tasks. Overall, the method was simple and no technical problems were encountered over the whole period of two years of measurement flights.

The image quality was assessed in different ways. We first checked the actual resolution that could be achieved from the 16 megapixel camera with the fixed lens. In theory a pixel, from 100 m altitude, has a ground resolution of 3.5 by 2.8 cm. Practically, this resolution is a function of the lens quality and the given illumination conditions that affect ISO and aperture size of the camera. To eliminate motion blur that would otherwise arise from vibration and movements of the UAV, pictures were taken with short shutter times (1/640 s). The camera automatically adapted aperture and ISO to values that ensure a good exposure of the image. If the amount of environmental light is low, the aperture opens up and ISO values become higher. High ISO values mean a binning of multiple pixels to suppress noise and increase sensitivity. Thus, an open aperture lets more light in, but leads to a less accurate focus on individual pixels. Both effects lead to worse images. The majority of images was shot with an aperture of F4 or higher and an ISO of 100. The worst ISO value was at 400. Under favorable conditions, the influence of neighboring pixels is noticeable within two pixels away. Under the worst conditions, present during the images taken in 2014, the pixel blur over 3 neighboring pixels as shown in Fig. 11.

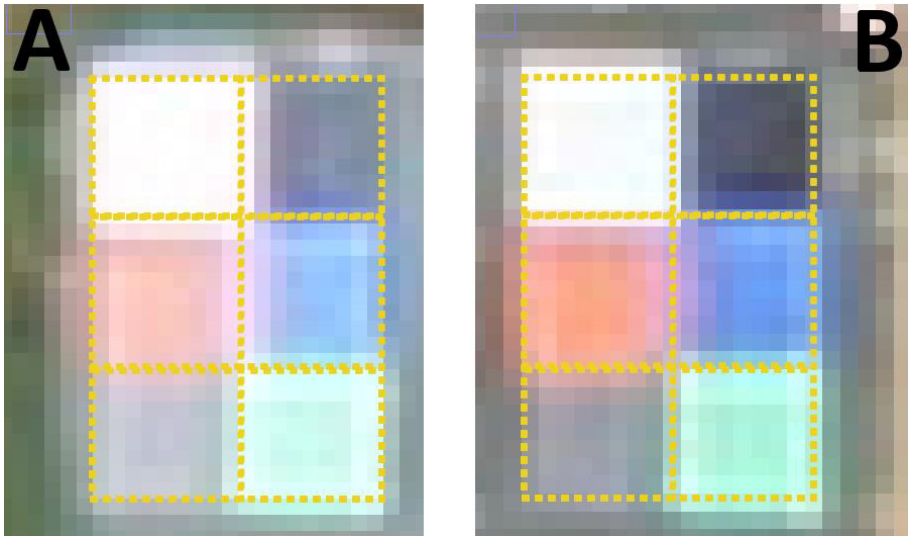

Fig. 11 zoomed images of the color reference targets used in the survey campaign in 2014. The reference targets have six different colors (white, grey, black, red, green, blue) on a 40 cm by 60 cm panel. The UAV imagery was taken from an altitude of 100 m. Image A was imaged under low light conditions (Aperture F4, ISO 320). Image B was taken under favorable high light

conditions (Aperture F5.6, ISO 100). Spreading of color information to neighboring pixels is made visible by the yellow raster, that represents the assumed real shape of the 6 color squares on the reference panel.

Due to the optical path, the overall imaging quality is best in the center of the image and worse in the edges, where vignetting effects and chromatic aberration have the largest impact. In the further analyses we eliminated most of the optical effects by averaging over all pixels of the five repeats of an experimental treatment. As these five plots are randomly spread over the whole experiment and the image, this also minimizes angular effects. These would otherwise change color values retrieved on the edges of the image as compared to the center due to the viewing angle. By applying the GRVI, we further reduced the impact of illumination effects as it mathematically normalizes the overall illumination variation of a scene. We then tested, how the phenological development of the barley experiment is tracked by the GRVI analysis of the UAV image time series. In Fig. 12 the development of 2 different seeding densities is shown, normalized in time to the day after seeding.

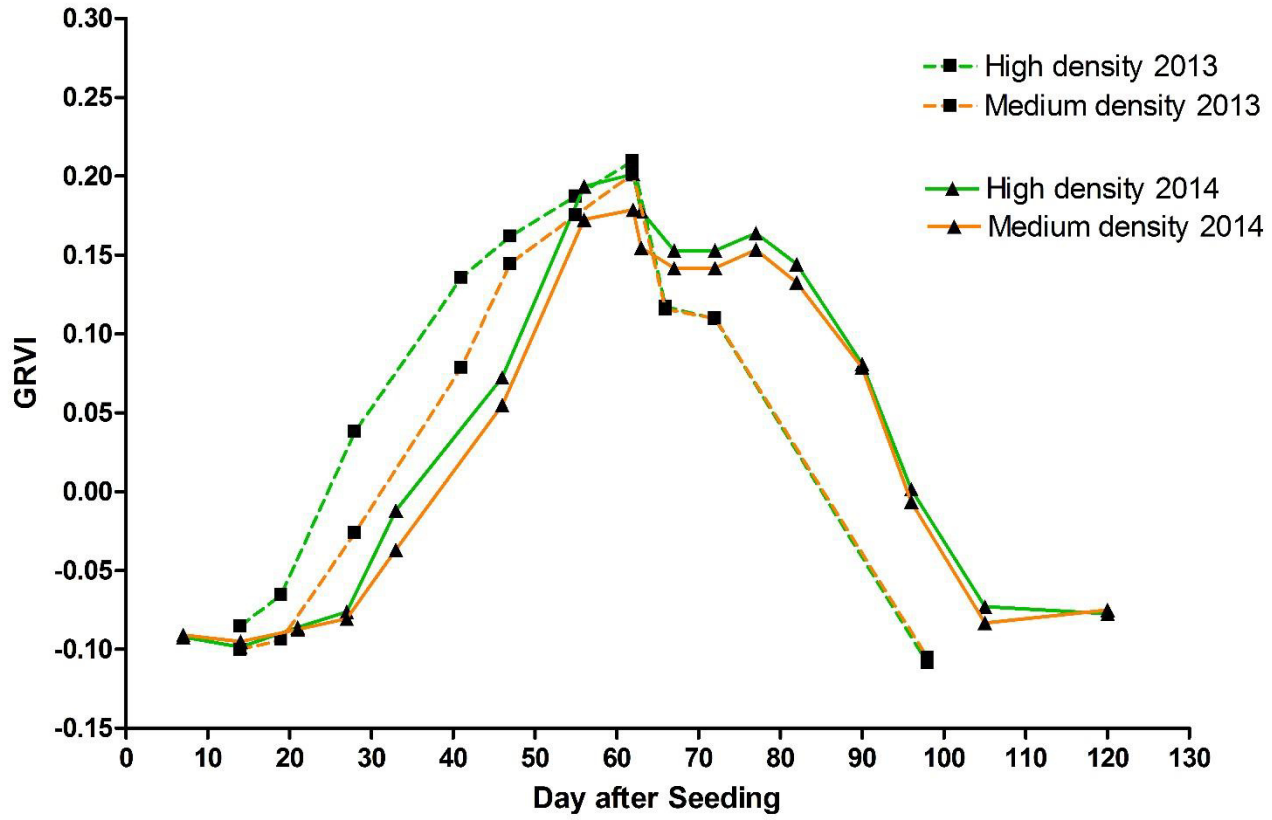

Fig. 12 Development of two different seeding densities (High = green, Medium = orange) as tracked by the GRVI in 2013 (dotted) and 2014 (solid).

The pattern of the GRVI is similar for both years and all densities and genotypes. Plots with low seeding density, however, develop slower compared to the high seeding density. Around day 64, the GRVI plots show a sharp decrease in both years and all treatments. By comparing ground based plant scoring, we identified the event of ear pushing in the plant development that happens at this period of time. We conclude, that a shift of colors induced by ear pushing was the reason for this sudden change in GRVI.

While in 2013 and 2014 different environmental conditions lead to changes in the development of the plants as reflected in the GRVI figures, the day of ear pushing seems to be genetically fixed.

With these first results of our analyses, we could show, that relevant traits of crops can be identified using time series of UAV RGB imagery. With this novel method we achieved a high frequency of images and high spatial resolution, as compared to satellite imagery. We conclude that further analyses of the image data such as heterogeneity distribution, single plant identification, 3D processing using multiple images and detailed color analyses will potentially add relevant results that can be referred to other plant traits. In our example, we investigated barley, but it is likely that similar time series over other crop types, will provide valid information as well. Further work must be done to relate the data of the aerial coverage to the actual processes on the ground and inside the plants.

Outlook on UAV based sensors for precision farming and phenotyping

In the present study, we have adapted a technically mature UAV platform and deployed it as sensor carrier for specific agricultural research questions. Study A1-A3 have shown that placing a sensor above an experimental field, using a flying platform, has become a simple task. Problems, however, arise when information about the plants needs to be derived from the sensors raw data. This led to the main question of the present thesis “Identification of key elements for the retrieval of valid remote sensing data from optical UAV sensors.” We have investigated different aspects of deploying optical UAV sensors over vegetation. In A1 we have placed a spectrometer on an UAV and have optimized the calibration of this flying device. This first copter-based spectrometer with ground reference station, was then used in the following studies as a precise scientific sensor. As different optical sensor equipment may vary in their results, we compared the retrieval of reflectance data by the UAV spectrometer and an RGB camera in [A2]. We have found both sensors to be practical in their specific application. This is spatial analysis with the RGB camera and spectral analysis with the spectrometer. In [A3] we investigated the impact of angular effects on UAV based sensors and have found large influence due to sun to sensor position. We then analyzed a time series of UAV imagery and found good relationships to ground based assessment of plant development. Within this thesis we have shown that most of the practical problems of UAV based sensors can be solved and their usage for agricultural research is feasible. Based on these experiments and the work of other authors, the following description provides an outlook on practical cases for the future of UAVs in precision farming and phenotyping.

The recent development of RGB cameras has led to various possible application scenarios on UAVs. A large number of studies use hundreds of high resolution images, that cover an agricultural field and create a 3D representation of its surface (J. Bendig et al. 2013; Juliane Bendig et al. 2014; Turner, Lucieer, and Watson 2011). This technique is performed rather simple in the field and neither the stability of the UAV nor the quality of the camera must be extremely high to reach a good level of accuracy. The most significant part of the work is done by applying post-processing algorithms that are dependent on different observation positions. This approach provides good correlation between biomass estimation and plant height measurements in barley (Juliane Bendig et al. 2014) and even for orchards (P.J. Zarco-Tejada et al. 2014). These methods have great potential in phenotyping to quickly derive the plant height from UAV generated data. In agriculture this technique can be used to generate input data for plant growth models. These could

characterize the current developmental stage with high spatial resolution, which would then serve for a spatially adapted fertilization plan.

Fig. 13 Storm damage in this experimental field of barley is visible in the top right corner of the image. The stem of the plant might be broken and in this case the harvest of this patch is lost. Due to the lying plant, the reflectance largely changes and is easily discriminated in the picture.

With the same approach of collecting multiple images, a so called ortho-mosaic can be generated. This ortho-mosaic shows the whole field as one single image. Analysis of such an image, however, faces various problems, which were addressed in our studies. Analyzing color values of an ortho-mosaic may produces wrong estimates, as the illumination conditions might change during a flight (Hakala et al. 2013). This can be addressed by either using only one image of the whole area or by placing color references inside the flight path of the UAV. This way the image might be corrected later. Nevertheless, ignoring the color information of a high resolution image, object or path identification can be used for identifying plant traits or disturbances in the field (Herwitz et al. 2004). Counting of single plants have been performed from aerial imagery and sophisticated image analysis (Peña Barragán et al. 2014). Storm damage in barley can be quantified easily by discriminating patches of broken plants against the healthy fields as shown in Fig. 13. But the color of the plants holds far more useful information. The color or reflectance is a representation of the state of the plant and may be altered by infections, drought or other stress (Jackson 1986). Once all problems with sensor calibration, illumination and angular effects are solved, in a way that reproducible measurements can be achieved, meaningful plant traits can be derived. This is further enhanced by using the whole spectrum of the visible and near infrared light by either spectrometer or multispectral frame cameras (Tab. 4). By analyzing narrow spectral bands, detailed information about specific plant traits, can be detected. This way recent studies have used UAV based sensors to directly measure PRI, chlorophyll content, water and nitrogen content (P. J. J. Zarco-Tejada, González-Dugo, and Berni 2011; Baluja et al. 2012; Meggio et al. 2014; J. Berni et al. 2009). However, in most cases the derived signal is a mixture of different plant´s parameters. To untangle this complex mixture of biophysical processes, which are represented in the plants reflection spectrum, two possible ways are currently in the focus. 1) By comparing ground data and airborne data, vegetation indices are identified that have the maximum relation to a single specific plant parameter, but at the same time are not affected by other plant parameters. 2) By modelling the reflectance of plants using known input parameters, the spectral

signature can be calculated. On the other hand, the model can inversely predict the plant´s parameter, using the reflectance spectrum as input. This has been done in SCOPE (Tol et al. 2009) [A3] and highly interesting results from this method are foreseen.

With the steady improvement of spectrometers, it can be expected, that even tiny signals, such as the Sun Induced Fluorescence (SIF) will be measurable from UAVs. Various efforts are undertaken in this direction (P.J. Zarco-Tejada et al. 2009; Malenovsky et al. 2013), but until now the large external influences from sensor, flying platform and scenery, have left the absolute results and their accuracy questionable. With the advent of active SIF references (Burkart et al. 2015), that mimic the emission of SIF, more accurate measurements are expectable.

The development of the flying platforms themselves will go different ways. The so called copters are easy to deploy and a great option for the scientific use over small areas. But their limited payload and endurance largely excludes them from professional use. If a farmer needs timely information about all his fields, a fixed wing UAV with decent speed and endurance is more practical to operate the chosen sensor over a large area. However planes are still limited in payload and endurance and need a runway. A look in the near future raises the need for the continuous survey of agricultural areas, to provide timely information with high temporal and spatial resolution. Satellites are struggling to provide these data, as they are costly, have a limited ground resolution and are highly affected by cloud cover or low overpass frequency. A possible solution for this demand is an UAV at about 1 km altitude that remains airborne for weeks or months. This could be achieved by a helium filled aerostat or zeppelin, which charges itself via solar power and continuously scans the agricultural surface.

The remaining problem is the conversion of sensor data in meaningful products that can finally be delivered to the farmer or breeder. This mainly is a software based problem that must by approached by both, aerial and ground based data. It also must include metadata such as soil and weather conditions, as well as seeding time to correct the plant growth model. The crop model APSIM (Keating et al. 2003) could be used for example to generate the plant parameters that feed the SCOPE radiative transfer model, which then calculates the expected reflectance of a specific crop and growth stage. If a UAV based reflectance sensor measures deviations of the expected reflectance, stress or other factors that influence the growth are detected. The farmer then can adapt its actions accordingly. Once the steps are working in an automated manner, the way is open for a more resource efficient agriculture that only applies what the plant really needs (McBratney et al. 2005).

Conclusion

UAV based sensors are a highly promising tool for the acquisition of relevant data in agriculture. But challenges remain in how to retrieve meaningful results from the sensors, scanning the crops. This led to the primary task of this study “Identification of key elements for the retrieval of valid remote sensing data from optical UAV sensors.” Throughout this work parts of this larger challenge were addressed and we worked out possible solution.

An easy to use octocopter platform (Falcon-8) was introduced. We then developed and implemented a spectrometer system on the UAV to accurately measure reflectance. The correlation of this UAV spectrometer to three other UAV sensors (Sony NEX-5n RGB camera, Canon Powershot modified to infrared sensitivity, MCA6 Tetracam) was investigated. In the spectral domain, the correlation of reflection was moderate between the 4 sensors. But the high spatial resolution of the cameras is beneficial for detailed image analysis of land-cover. The more quality is expected from vegetation measurements, the

more care must be taken to exclude undesired external influences. A major source of this influences are multiangular effects that are caused by the surface architecture and the illumination sensor geometry. Using the UAV equipped with a spectrometer as a huge goniometer, we introduced a novel method for hyperspectral characterization of multiangular effects of vegetation. But UAVs also allow, due to their flexible, fast and easy handling, measurements with a high temporal frequency. This way, the development of a whole experimental field was tracked weekly with high resolution imagery. By the analysis of this imagery, plant developmental stages such as ear pushing could be identified. With the rapid development of UAV platforms and sensors, an exciting future for the use of this systems in agriculture is foreseen. With upcoming long endurance drones such as airships or planes, the screening of farmland on a regular base becomes possible and is going to change the way agriculture is performed. The use of detailed high resolution data will help the breeders to phenotype and identify the best performing crops. At the same time, farmers can optimize their management of resources by applying only what the crop currently needs. With this study, we hope to contribute to a more sustainable agriculture that will be able to feed mankind in the coming decades.

Acknowledgements

Much more people have contributed to this thesis, than could be named within this few pages. But I like to mention some who have helped me a lot in the last three years, and without those, nothing would have happened at all.

Uwe Rascher has not only initiated this thesis but helped out whenever it was necessary. His open supervising gave the freedom to try exciting things, to travel, to fail and to reach aims I did not even know before. I like to acknowledge the great start and comprehensive hyperspectral teaching Anke Schickling gave me, as well as her continuous help throughout the whole thesis. Special thanks go to Francisco Pinto, Mark Müller-Linow, Phillip von Gilhaußen, Vera Hecht and all the people from the ecosys group who helped and contributed ideas, work power or borrowed their experiments to me. A big thank you goes towards Milano Bicocca, where I learned a lot about spectrometers, and without Micol Rossini and Sergio Cogliati all my work about chlorophyll fluorescence would not have been possible. The same goes to Luis Alonso from Valencia who was an always caring remote supervisor and the most critical reviewer one can imagine. I like to acknowledge the priceless help of Tim Malolepszy for the acquisition of material and the field work at the Campus Klein-Altendorf. A huge thank you goes to Thorsten Kraska and all the other people of the Campus Klein Altendorf who did the real hard work on the field experiments. I like to thank Helge Aasen, Thomas Wrobel, Andreas Hueni and Stefanie von Büren for the fun and inspiring working time we spent together at different places of the world.

I acknowledge the various sources of funding that contributed to this thesis. Travel fundings were granted by COST ES0903 EUROSPEC and COST ES1309 OPTIMISE. The author acknowledges the funding of the CROP.SENSe.net project and PhenoCrops in the context of Ziel 2-Programmes NRW 2007–2013 “Regionale Wettbewerbsfähigkeit und Beschäftigung (EFRE)” by the Ministry for Innovation, Science and Research (MIWF) of the state of North Rhine–Westphalia (NRW) and European Union Funds for regional development (EFRE) (FKZ 005-1012-0001).

The warmest thank you goes to my mother Susanne, my father Volker and my brother Thomas who helped me through the time of thesis by helping out whenever it was possible, providing shelter, lecturing help, 3D design services and always listening. My last and biggest thank you is also a wish for a wonderful and

exciting future as a family. During the time of the thesis I felt in love with Anke and our son Emil was born. You both are the light of my day and I am thankful for you being with me.

References

Aasen, H., J. Bendig, A. Bolten, S. Bennertz, M. Willkomm, and G. Bareth. 2014. "Introduction and Preliminary Results of a Calibration for Full-Frame Hyperspectral Cameras to Monitor Agricultural Crops with UAVs." *ISPRS - International Archives of the Photogrammetry, Remote Sensing and Spatial Information Sciences* XL-7 (1). Copernicus Publications: 1–8. doi:10.5194/isprsarchives-XL-7-1-2014.

Anderson, Karen, and Kevin J Gaston. 2013. "Lightweight Unmanned Aerial Vehicles Will Revolutionize Spatial Ecology." *Frontiers in Ecology and the Environment* 11 (3). Ecological Society of America: 138–46. doi:10.1890/120150.

Araus, José Luis, and Jill E Cairns. 2014. "Field High-Throughput Phenotyping: The New Crop Breeding Frontier." *Trends in Plant Science* 19 (1): 52–61. doi:10.1016/j.tplants.2013.09.008.

Asner, Gregory P. 1998. "Biophysical and Biochemical Sources of Variability in Canopy Reflectance." *Remote Sensing of Environment* 64 (3): 234–53. doi:10.1016/S0034-4257(98)00014-5.

Auernhammer, Hermann. 2001. "Precision Farming — the Environmental Challenge." *Computers and Electronics in Agriculture* 30 (1-3): 31–43. doi:10.1016/S0168-1699(00)00153-8.

Baluja, Javier, Maria P. Diago, Pedro Balda, Roberto Zorer, Franco Meggio, Fermin Morales, and Javier Tardaguila. 2012. "Assessment of Vineyard Water Status Variability by Thermal and Multispectral Imagery Using an Unmanned Aerial Vehicle (UAV)." *Irrigation Science* 30 (6): 511–22. doi:10.1007/s00271-012-0382-9.

Bannari, A., D. Morin, F. Bonn, and A. R. Huete. 1995. "A Review of Vegetation Indices." *Remote Sensing Reviews* 13 (1-2). Taylor & Francis Group: 95–120. doi:10.1080/02757259509532298.

Banzi, Massimo. 2008. *Getting Started with Arduino*. First Edit. Sebastpool, US: Make Books. http://books.google.com/books?hl=de&lr=&id=f3xYRaq_4ZYC&pgis=1.

Bayer, B E. 1976. "Color Imaging Array." Google Patents. https://www.google.com/patents/US3971065.

Bendig, J., M. Willkomm, N. Tilly, M. L. Gnyp, S. Bennertz, C. Qiang, Y. Miao, V. I. S. Lenz-Wiedemann, and G. Bareth. 2013. "Very High Resolution Crop Surface Models (CSMs) from UAV-Based Stereo Images for Rice Growth Monitoring In Northeast China." *ISPRS - International Archives of the Photogrammetry, Remote Sensing and Spatial Information Sciences* XL-1/W2 (August): 45–50. doi:10.5194/isprsarchives-XL-1-W2-45-2013.

Bendig, Juliane, Andreas Bolten, Simon Bennertz, Janis Broscheit, Silas Eichfuss, and Georg Bareth. 2014. "Estimating Biomass of Barley Using Crop Surface Models (CSMs) Derived from UAV-Based RGB Imaging." *Remote Sensing* 6 (11). Multidisciplinary Digital Publishing Institute: 10395–412. doi:10.3390/rs61110395.

Berni, J A J, P J Zarco-Tejada, L Surez, V González-Dugo, and E Fereres. 2008. "Remote Sensing of Vegetation from Uav Platforms Using Lightweight Multispectral and Thermal Imaging Sensors." *The International Archives of the Photogrammetry, Remote Sensing and Spatial Information Sciences, XXXVII*.

Berni, J, P J Zarco-Tejada, L Suárez, and E Fereres. 2009. "Thermal and Narrowband Multispectral Remote Sensing for Vegetation Monitoring from an Unmanned Aerial Vehicle." *Geoscience and Remote Sensing, IEEE Transactions on* 47 (3): 722–38.

Birk, R J, and T B McCord. 1994. “Airborne Hyperspectral Sensor Systems.” *Aerospace and Electronic Systems Magazine, IEEE* 9 (10): 26–33.

Blackburn, G. A. 1998. “Spectral Indices for Estimating Photosynthetic Pigment Concentrations: A Test Using Senescent Tree Leaves.” *International Journal of Remote Sensing* 19 (4). Taylor & Francis: 657–75. doi:10.1080/014311698215919.

Bourgeois, C Saskia, Atsumu Ohmura, Karl Schroff, Hans-Jörg Frei, and Pierluigi Calanca. 2006. “IAC ETH Goniospectrometer: A Tool for Hyperspectral HDRF Measurements.” *Journal of Atmospheric and Oceanic Technology* 23 (4). American Meteorological Society: 573–84. doi:10.1175/JTECH1870.1.

Burkart, Andreas, Anke Schickling, Maria Pilar Cendrero Mateo, Thomas Wrobel, Micol Rossini, Sergio Cogliati, Tommaso Julitta, and Uwe Rascher. 2015. “A Method for Uncertainty Assessment of Passive Sun-Induced Chlorophyll Fluorescence Retrieval by Using an Infrared Reference Light.” *IEEE Sensors Journal* PP (99): 1–1. doi:10.1109/JSEN.2015.2422894.

Busetto, Lorenzo, Michele Meroni, G F Crosta, L Guanter, and Roberto Colombo. 2011. “SpecCal: Novel Software for in-Field Spectral Characterization of High-Resolution Spectrometers.” *Computers & Geosciences* 37 (10): 1685–91.

Cassman, K. G. 1999. “Ecological Intensification of Cereal Production Systems: Yield Potential, Soil Quality, and Precision Agriculture.” *Proceedings of the National Academy of Sciences* 96 (11): 5952–59. doi:10.1073/pnas.96.11.5952.

Comar, A., F. Baret, F. Viénot, L. Yan, and B. de Solan. 2012. “Wheat Leaf Bidirectional Reflectance Measurements: Description and Quantification of the Volume, Specular and Hot-Spot Scattering Features.” *Remote Sensing of Environment* 121 (June): 26–35. doi:10.1016/j.rse.2011.01.028.

Eisenbeiss, Henri, and Martin Sauerbier. 2011. “Investigation of Uav Systems and Flight Modes for Photogrammetric Applications.” *The Photogrammetric Record* 26 (136): 400–421. doi:10.1111/j.1477-9730.2011.00657.x.

Evenson, R E, and D Gollin. 2003. “Assessing the Impact of the Green Revolution, 1960 to 2000.” *Science (New York, N.Y.)* 300 (5620): 758–62. doi:10.1126/science.1078710.

Fiorani, Fabio, and Ulrich Schurr. 2013. “Future Scenarios for Plant Phenotyping.” *Annual Review of Plant Biology* 64 (1).

Fischer, R. A., and G. O. Edmeades. 2010. “Breeding and Cereal Yield Progress.” *Crop Science* 50 (Supplement 1): S – 85 – S – 98. doi:10.2135/cropsci2009.10.0564.

Godfray, H Charles J, John R Beddington, Ian R Crute, Lawrence Haddad, David Lawrence, James F Muir, Jules Pretty, Sherman Robinson, Sandy M Thomas, and Camilla Toulmin. 2010. “Food Security: The Challenge of Feeding 9 Billion People.” *Science (New York, N.Y.)* 327 (5967): 812–18. doi:10.1126/science.1185383.

Hakala, T., E. Honkavaara, H. Saari, J. Mäkynen, J. Kaivosoja, L. Pesonen, and I. Pölönen. 2013. “SPECTRAL IMAGING FROM UAVS UNDER VARYING ILLUMINATION CONDITIONS.” *ISPRS - International Archives of the Photogrammetry, Remote Sensing and Spatial Information Sciences* XL-1/W2 (August): 189–94. doi:10.5194/isprsarchives-XL-1-W2-189-2013.

Hautecoeur, Olivier, and Marc Leroy. 1996. “Intercomparison of Several BRDF Models for the Compositing of Spaceborne POLDER Data over Land Surfaces.” In *Geoscience and Remote Sensing Symposium, 1996. IGARSS’96.'Remote Sensing for a Sustainable Future.', International*, 1:204–8. IEEE.

Herwitz, S.R, L.F Johnson, S.E Dunagan, R.G Higgins, D.V Sullivan, J Zheng, B.M Lobitz, et al. 2004. “Imaging from an Unmanned Aerial Vehicle: Agricultural Surveillance and Decision Support.” *Computers and Electronics in Agriculture* 44 (1): 49–61. doi:10.1016/j.compag.2004.02.006.

Israel, M. 2012. “A UAV-BASED ROE DEER FAWN DETECTION SYSTEM.” *ISPRS - International Archives of the Photogrammetry, Remote Sensing and Spatial Information Sciences* XXXVIII-1/ (September): 51–55. doi:10.5194/isprsarchives-XXXVIII-1-C22-51-2011.

Jackson, R D. 1986. “Remote Sensing of Biotic and Abiotic Plant Stress.” *Annual Review of Phytopathology* 24 (1). ANNUAL REVIEWS INC, 4139 EL CAMINO WAY, PO BOX 10139, PALO ALTO, CA 94303-0139: 265–87. doi:10.1146/annurev.py.24.090186.001405.

Jain, H. K. 1986. “Eighty Years of Post-Mendelian Breeding For Crop Yield: Nature of Selection Pressures and Future Potential.” *The Indian Journal of Genetics and Plant Breeding* 46 (1). The Indian Society of Genetics & Plant Breeding New Delhi, India: 30–53. http://www.indianjournals.com/ijor.aspx?target=ijor:ijgpb&volume=46&issue=1&article=003.

Keating, B.A, P.S Carberry, G.L Hammer, M.E Probert, M.J Robertson, D Holzworth, N.I Huth, et al. 2003. “An Overview of APSIM, a Model Designed for Farming Systems Simulation.” *European Journal of Agronomy* 18 (3-4): 267–88. doi:10.1016/S1161-0301(02)00108-9.

Kelcey, Joshua, and Arko Lucieer. 2012. “Sensor Correction of a 6-Band Multispectral Imaging Sensor for UAV Remote Sensing.” *Remote Sensing* 4 (12). Molecular Diversity Preservation International: 1462–93. doi:10.3390/rs4051462.

Knipling, Edward B. 1970. “Physical and Physiological Basis for the Reflectance of Visible and near-Infrared Radiation from Vegetation.” *Remote Sensing of Environment* 1 (3): 155–59. doi:10.1016/S0034-4257(70)80021-9.

Kuusk, Andres. 1991. “The Angular Distribution of Reflectance and Vegetation Indices in Barley and Clover Canopies.” *Remote Sensing of Environment* 37 (2): 143–51.

Kuusk, Andres, Joel Kuusk, and Mait Lang. 2014. “Measured Spectral Bidirectional Reflection Properties of Three Mature Hemiboreal Forests.” *Agricultural and Forest Meteorology* 185 (February). ELSEVIER SCIENCE BV, PO BOX 211, 1000 AE AMSTERDAM, NETHERLANDS: 14–19. doi:10.1016/j.agrformet.2013.10.011.

Kuusk, J. 2011. “Dark Signal Temperature Dependence Correction Method for Miniature Spectrometer Modules.” *Journal of Sensors* 2011.

Lebourgeois, Valentine, Agnès Bégué, Sylvain Labbé, Benjamin Mallavan, Laurent Prévot, and Bruno Roux. 2008. “Can Commercial Digital Cameras Be Used as Multispectral Sensors? A Crop Monitoring Test.” *Sensors* 8 (11). Molecular Diversity Preservation International: 7300–7322. doi:10.3390/s8117300.

Liang, Shunlin, Alan H. Strahler, Michael J. Barnsley, Christoph C. Borel, Siegfried A. W. Gerstl, David J. Diner, Alfred J. Prata, and Charles L. Walthall. 2000. “Multiangle Remote Sensing: Past, Present and Future.” *Remote Sensing Reviews* 18 (2-4). Taylor & Francis Group: 83–102. doi:10.1080/02757250009532386.

Mahlein, A K, T Rumpf, P Welke, H W Dehne, L Plümer, U Steiner, and E C Oerke. 2013. “Development of Spectral Indices for Detecting and Identifying Plant Diseases.” *Remote Sensing of Environment* 128: 21–30.

Malenovsky, Zbynek, Arko Lucieer, Sharon Robinson, Stephen Harwin, Darren Turner, and Tony Veness. 2013. “Monitoring of Antarctic Moss Ecosystems Using a High Spatial Resolution Imaging Spectroscopy.” *EGU General Assembly Conference Abstracts* 15 (April): 7360. http://adsabs.harvard.edu/abs/2013EGUGA..15.7360M.

McBratney, A, B Whelan, T Ancev, and J Bouma. 2005. “Future Directions of Precision Agriculture.” *Precision Agriculture* 6 (1): 7–23.

Meggio, F., P J Zarco-Tejada, J R Miller, P. Martín, M R González, and A. Berjón. 2014. “Row Orientation and Viewing Geometry Effects on Row-Structured Vine Crops for Chlorophyll Content Estimation.” *Canadian Journal of Remote Sensing*, June. Taylor & Francis. http://www.tandfonline.com/doi/abs/10.5589/m08-023#.VP2N5fmG-So.

Meroni, M, and R Colombo. 2006. “Leaf Level Detection of Solar Induced Chlorophyll Fluorescence by Means of a Subnanometer Resolution Spectroradiometer.” *Remote Sensing of Environment* 103 (4): 438–48.

Milton, E J. 1987. “Review Article Principles of Field Spectroscopy.” *Remote Sensing* 8 (12): 1807–27.

Milton, E J, M E Schaepman, K Anderson, M Kneubühler, and N Fox. 2009. “Progress in Field Spectroscopy.” *Remote Sensing of Environment* 113: S92–109.

Mitchell, Jessica J, Nancy F Glenn, Matthew O Anderson, Ryan C Hruska, Anne Halford, Charlie Baun, and Nick Nydegger. 2012. “Unmanned Aerial Vehicle (UAV) Hyperspectral Remote Sensing for Dryland Vegetation Monitoring.”

Motohka, Takeshi, Kenlo Nishida Nasahara, Hiroyuki Oguma, and Satoshi Tsuchida. 2010. “Applicability of Green-Red Vegetation Index for Remote Sensing of Vegetation Phenology.” *Remote Sensing* 2 (10). Molecular Diversity Preservation International: 2369–87. doi:10.3390/rs2102369.

Nicodemus, F E. 1965. “Directional Reflectance and Emissivity of an Opaque Surface.” *Applied Optics* 4 (7): 767–73.

Peña Barragán, José Manuel, Maggi Kelly, Ana Isabel de Castro, and Francisca López Granados. 2014. “Object-Based Approach for Crop Row Characterization in UAV Images for Site-Specific Weed Management.” http://digital.csic.es/handle/10261/98054.

Peñuelas, Josep, and Iolanda Filella. 1998. “Visible and near-Infrared Reflectance Techniques for Diagnosing Plant Physiological Status.” *Trends in Plant Science* 3 (4): 151–56.

Porcar-Castell, Albert, Esa Tyystjärvi, Jon Atherton, Christiaan van der Tol, Jaume Flexas, Erhard E Pfündel, Jose Moreno, Christian Frankenberg, and Joseph A Berry. 2014. “Linking Chlorophyll a Fluorescence to Photosynthesis for Remote Sensing Applications: Mechanisms and Challenges.” *Journal of Experimental Botany* 65 (15): 4065–95. doi:10.1093/jxb/eru191.

Quemada, Miguel, Jose Gabriel, and Pablo Zarco-Tejada. 2014. “Airborne Hyperspectral Images and Ground-Level Optical Sensors As Assessment Tools for Maize Nitrogen Fertilization.” *Remote Sensing* 6 (4). Multidisciplinary Digital Publishing Institute: 2940–62. doi:10.3390/rs6042940.

Reilly, John M, and Keith O Fuglie. 1998. “Future Yield Growth in Field Crops: What Evidence Exists?” *Soil and Tillage Research* 47 (3-4): 275–90. doi:10.1016/S0167-1987(98)00116-0.

Sakamoto, Toshihiro, Anatoly A. Gitelson, Anthony L. Nguy-Robertson, Timothy J. Arkebauer, Brian D. Wardlow, Andrew E. Suyker, Shashi B. Verma, and Michio Shibayama. 2012. “An Alternative Method Using Digital Cameras for Continuous Monitoring of Crop Status.” *Agricultural and Forest Meteorology* 154-155 (March): 113–26. doi:10.1016/j.agrformet.2011.10.014.

Sandmeier, Stefan R, and Klaus I Itten. 1999. “A Field Goniometer System (FIGOS) for Acquisition of Hyperspectral BRDF Data.” *Geoscience and Remote Sensing, IEEE Transactions on* 37 (2): 978–86.

Schaepman, Michael E., and Stefan Dangel. 2000. “Solid Laboratory Calibration of a Nonimaging Spectroradiometer.” *Applied Optics* 39 (21). OSA: 3754. doi:10.1364/AO.39.003754.

Schaepman-Strub, G, M E Schaepman, T H Painter, S Dangel, and J V Martonchik. 2006. “Reflectance Quantities in Optical Remote sensing—Definitions and Case Studies.” *Remote Sensing of Environment* 103 (1): 27–42.

Schlapfer, Daniel, Rudolf Richter, and Tal Feingersh. 2015. “Operational BRDF Effects Correction for Wide-Field-of-View Optical Scanners (BREFCOR).” *IEEE Transactions on Geoscience and Remote Sensing* 53 (4): 1855–64. doi:10.1109/TGRS.2014.2349946.

Siebert, Sebastian, and Jochen Teizer. 2014. “Mobile 3D Mapping for Surveying Earthwork Projects Using an Unmanned Aerial Vehicle (UAV) System.” *Automation in Construction* 41 (May): 1–14. doi:10.1016/j.autcon.2014.01.004.

Sims, Daniel A, and John A Gamon. 2002. “Relationships between Leaf Pigment Content and Spectral Reflectance across a Wide Range of Species, Leaf Structures and Developmental Stages.” *Remote Sensing of Environment* 81 (2-3): 337–54. doi:10.1016/S0034-4257(02)00010-X.

Smith, Geoffrey M., and Edward J. Milton. 1999. “The Use of the Empirical Line Method to Calibrate Remotely Sensed Data to Reflectance.” *International Journal of Remote Sensing* 20 (13). Taylor & Francis Group: 2653–62. doi:10.1080/014311699211994.

Tester, Mark, and Peter Langridge. 2010. “Breeding Technologies to Increase Crop Production in a Changing World.” *Science (New York, N.Y.)* 327 (5967): 818–22. doi:10.1126/science.1183700.

Tol, C, W Verhoef, J Timmermans, Anne Verhoef, and Z Su. 2009. “An Integrated Model of Soil-Canopy Spectral Radiances, Photosynthesis, Fluorescence, Temperature and Energy Balance.” *Biogeosciences* 6 (12): 3109–29.

Turner, DJ, A Lucieer, and CS Watson. 2011. “Development of an Unmanned Aerial Vehicle (UAV) for Hyper-Resolution Vineyard Mapping Based on Visible, Multispectral and Thermal Imagery.” *34th International Symposium on Remote Sensing of Environment*. http://ecite.utas.edu.au/74377.

Verrelst, Jochem, Michael E Schaepman, Benjamin Koetz, and Matthias Kneubühler. 2008. “Angular Sensitivity Analysis of Vegetation Indices Derived from CHRIS/PROBA Data.” *Remote Sensing of Environment* 112 (5): 2341–53.

Wefelscheid, C., R. Hänsch, and O. Hellwich. 2012. “THREE-DIMENSIONAL BUILDING RECONSTRUCTION USING IMAGES OBTAINED BY UNMANNED AERIAL VEHICLES.” *ISPRS - International Archives of the Photogrammetry, Remote Sensing and Spatial Information Sciences* XXXVIII-1/ (September): 183–88. doi:10.5194/isprsarchives-XXXVIII-1-C22-183-2011.

Zarco-Tejada, P J, J A J Berni, L Suárez, G Sepulcre-Cantó, F Morales, and J R Miller. 2009. “Imaging Chlorophyll Fluorescence with an Airborne Narrow-Band Multispectral Camera for Vegetation Stress Detection.” *Remote Sensing of Environment* 113 (6): 1262–75.

Zarco-Tejada, P.J., J.A.J. Berni, L. Suárez, G. Sepulcre-Cantó, F. Morales, and J.R. Miller. 2009. “Imaging Chlorophyll Fluorescence with an Airborne Narrow-Band Multispectral Camera for Vegetation Stress Detection.” *Remote Sensing of Environment* 113 (6): 1262–75. doi:10.1016/j.rse.2009.02.016.

Zarco-Tejada, P.J., R. Diaz-Varela, V. Angileri, and P. Loudjani. 2014. “Tree Height Quantification Using Very High Resolution Imagery Acquired from an Unmanned Aerial Vehicle (UAV) and Automatic 3D Photo-Reconstruction Methods.” *European Journal of Agronomy* 55 (April): 89–99..

Zarco-Tejada, P.J. J, V. González-Dugo, and J.A.J. A J Berni. 2011. “Fluorescence, Temperature and Narrow-Band Indices Acquired from a UAV Platform for Water Stress Detection Using a Micro-Hyperspectral Imager and a Thermal Camera.” *Remote Sensing of Environment* 117: 322–37. doi:10.1016/j.rse.2011.10.007.

Appendix

A1: A novel UAV-based ultra-light weight spectrometer for field spectroscopy

Authors Contribution

Scientific work and development: 100%

Field work and analysis: 90%

Publication work: 80%

A Novel UAV-Based Ultra-Light Weight Spectrometer for Field Spectroscopy

Andreas Burkart, Sergio Cogliati, Anke Schickling, and Uwe Rascher

***Abstract*— A novel hyperspectral measurement system for unmanned aerial vehicles (UAVs) in the visible to near infrared (VIS/NIR) range (350–800 nm) was developed based on the Ocean Optics STS microspectrometer. The ultralight device relies on small open source electronics and weighs a ready-to-fly 216 g. The airborne spectrometer is wirelessly synchronized to a second spectrometer on the ground for simultaneous white reference collection. In this paper, the performance of the system is investigated and specific issues such as dark current correction or second order effects are addressed. Full width at half maximum was between 2.4 and 3.0 nm depending on the spectral band. The functional system was tested in flight at a 10-m altitude against a current field spectroscopy gold standard device Analytical Spectral Devices Field Spec 4 over an agricultural site. A highly significant correlation ($r^2 > 0.99$) was found in reflection comparing both measurement approaches. Furthermore, the aerial measurements have a six times smaller standard deviation than the hand held measurements. Thus, the present spectrometer opens a possibility for low-cost but high-precision field spectroscopy from UAVs.**

***Index Terms*— Hyperspectral sensors, remote sensing, unmanned aerial vehicles, vegetation, calibration.**

I. Introduction

FIELD SPECTROSCOPY as well as hyperspectral remote sensing (RS) are common techniques to gain an insight on land cover beyond the human eye. Handmade ground measurements and on a larger scale air- and spaceborne spectroscopy are common investigation methods in the field of geology, geography and environmental science [1]–[3]. A major field in RS is the investigation of vegetation, which started in the 70th using spectral band indices like the NDVI. Currently RS evolves to a powerful proxy for plant investigation parameters [4]. Present studies show the utility of various parameters derived from hyperspectral data on plants like water [5] and chlorophyll content [6] as well as marker for diseases [7] or even insights in the photosynthetic apparatus by the retrieval of sun induced fluorescence [8]. Thus hyperspectral measurements are of high interest for observation of natural habitats and crop management. For this purpose continuous and automated measurement on single plots [9] and mapping of large areas with a given spatial resolution are needed. For continuous measurements, progress was recently made with the development of an autonomous hyperspectral system measuring the reflection over alpine grassland during a whole vegetation period [10]. On the other side a large number of studies were conducted on spectral imaging of whole agricultural sites with high spatial resolution using manned aircrafts [11]–[13] or different kind of unmanned aerial vehicles (UAV) [14], [15]. With the emerging development of small versatile UAVs their use in RS of vegetation offers simple and affordable observation from the air. Leading the field in spectral imaging of vegetation by UAVs, Zarco-Tejada et al. [16]–[18] demonstrated the feasibility of the technique for plant monitoring. On the technology side progress is expected on the development of miniature sensors to further enhance the performance of unmanned remote sensing platforms [19], [20]. Compared to well-proven field spectroscopy approaches the use of UAV based sensors is tempting due to their great degree of automation and fast throughput. However several issues still remain in the use of the acquired spectral data like Bidirectional Reflection Distribution Function (BRDF) [21], accurate atmospheric correction, adequate calibration procedures and the ease of use under various environmental conditions. Once these issues are solved, it will open up the opportunity to accurate investigation of common and advanced hyperspectral methods. An example is the sun induced fluorescence retrieval, which relies on highly accurate measurements [22] which are based on distinct knowledge about the characteristics of target, sensor and atmosphere.

To address these issues, in this paper we reduced the UAV based hyperspectral measurements to a single point spectrometer to provide a basic tool for the investigation of effects in field spectroscopy and its upscaling to airborne imaging platforms. Development, calibration and validation are described as well as the characterization of the novel Ocean Optics STS microspectrometer and the AscTec Falcon-8 as an airborne platform.

II. Description of the UAV Based Spectrometer

Principle of Measurements: The UAV basedhyperspectral system is able to measure spectral radiance/reflectance over selected targets. It is based on an UAV carried air unit (AIR) and a ground unit (GND) both equipped with a STS-VIS microspectrometer (Ocean Optics, Dunedin, FL, USA).

Manuscript received June 17, 2013; accepted August 11, 2013. Date of publication August 26, 2013; date of current version October 30, 2013. This work was supported by EFRE in the frame of CROP.SENSe.net. The associate editor coordinating the review of this paper and approving it for publication was Dr. David Hecht.

A. Burkart, A. Schickling, and U. Rascher are with the Institute of Bio- and Geosciences, IBG-2: Plant Sciences, Forschungszentrum Jülich GmbH, Jülich 52425, Germany (e-mail: an.burkart@fz-juelich.de; a.schickling@fz-juelich.de; u.rascher@fz-juelich.de).

S. Cogliati is with the Remote Sensing of Environmental Dynamics Laboratory, DISAT, Università degli Studi Milano-Bicocca, Milan 20126, Italy (e-mail: sergio.cogliati@unimib.it).

Color versions of one or more of the figures in this paper are available online at http://ieeexplore.ieee.org.

Digital Object Identifier 10.1109/JSEN.2013.2279720

TABLE I
UAV SPECTROMETER DATASHEET

Spectrometer	Ocean Optics STS-VIS
Spectral Range	338 nm - 824 nm
Dynamic Range	14 bit
Pixels	1024
Field of View	12°
FWHM	3 nm
Integration Time	10 µs - 10 s
Battery life	2 h
Wireless Range	>300 m
Weight (Air Unit)	216 g

Technical details of the spectrometers units are reported in Table I. The AIR unit is placed over the point of interest by the UAV and measures the upwelling radiance while the GND unit acquires the sun irradiance over a white reference. During the technical implementation phase issues with dark current, calibration and a second order effect arose with the spectrometer and were solved before a validation experiment was conducted.

Technical Implementation: Construction of both units was aimed towards simplicity, small weight and low costs. The AIR unit consists of the following components 1. STS microspectrometer; 2. Microcontroller (Seeeduino Stalker, Seeedstudio, Shenzhen, China) for data acquisition and wireless communication (Xbee-Pro, Digi International, Minnetonka, NM, USA); 3. Stable power regulation; 4. Lithium Polymer battery. The microcontroller listens to commands via the wireless interface and controls the spectrometer. Acquired spectra are saved to a micro SD. Due to RAM limitations of the microcontroller, spectra were recorded with a spectral binning of 4 resulting in 256 pixels. The firmware performing the required tasks was written using the open source platform Arduino [23]. The AIR unit itself is fully independent from the UAV and can also be used without the flying platform. Rugged cases for AIR and GND unit were constructed using a 3D printer (Mendel Prusa, www.reprap.org) [24]. The weight of the operational AIR unit including battery is 216 g.

The GND unit establishes the wireless connection to the AIR unit and performs the reference measurements. It consists of: 1. STS microspectrometer 2. Xbee wireless modul. The ground unit is also connected to a field notebook that runs a graphical user interface (GUI) to control the entire system (AIR and GND). The GUI, written in the java based, platform independent, open source language Processing [25], provides simple access to control both spectrometers by mouse or keyboard commands. The software also includes post-processing functions for the output of fully corrected data. During flight the software allows the preliminary visualization of the spectra gathered by both units.

The flying platform used in this study was an AscTecFalcon-8 (Ascending Technologies GmbH, Krailing, Germany) which is an eight motor rotary wing UAV with various stabilization systems. We used a camera adapter originally designed for a thermal camera. This adapter is stabilized to an adjusted angle, which can be specified during flight. It features a small RGB camera streaming a live video to the radio control, which simplifies the accurate aiming of the spectrometer. Furthermore the UAV has the capability to follow navigation points autonomously and to hover over a point of interest to allow for a long spectrometer integration time.

III. DATA PROCESSING-CHAIN

Dark Current (DC) Removal: DC measurements are not possible during flight operations. Moreover STS microspectrometers do not have the "so-called" black pixels, sometimes present in spectrometers, to account for DC without the use of mechanical shutters in front of the instruments foreoptics. As the DC is a function of sensor temperature and integration time (IT) it can substantially change during operation. To correct target spectra during flight we characterised the DC influence in relation to integration time and sensor temperature [26].

DC was recorded in a laboratory considering a range of temperatures between 14 °C to 34 °C which represent the typical temperatures during field measurements. Several levels of integration time from 300 ms to 2000 ms have been selected. Measurements were performed automatically and temperature was detected by the on chip thermometer in the ELIS-1024 linear image photo sensor used in the STS microspectrometer.

Second Order Effect: The STS VIS microspectrometers have a second order effect which introduces an additional stray light signal measured at the double of the real incoming wavelength [13]. Pixels between 676 nm and 823 nm are affected by this stray light due to light measured at the pixels between 338 nm and 412 nm. This effect was characterized using a monochromator (Lambda 950 Spectrophotometer, Perkin Elmer, Waltham, Massachusetts, U.S.) illuminating with a narrow bandwidth of 4 nm and saving the spectra for analysis. The integration time was adapted to prevent the spectrometer from saturation and to compare the strength of the illuminating light and the strength of the stray light induced by the second order effect.

Instrument Calibration: Field spectroscopy techniques aimed at reflectance measurements do not require the absolute spectral and radiometric calibration of spectrometers in physical units. In fact, the reflectance factor is typically determined rationing the target and the white reference measurements collected with the same illumination (i.e. irradiance) and instrumental conditions (i.e. integration time). The UAV system relies on two different spectrometers to collect target and reference measurements. This experimental setup requires a proper spectral/radiometric crosscalibration of the instruments. Factory spectral calibration factors and instruments FWHM were controlled with the SpecCal tool [27] which allows evaluating instruments performances comparing field measurements with radiances simulated by the atmospheric radiative transfer code Modtran5 [28]. Radiometric calibration was inferred comparing STS spectrometers with a well calibrated

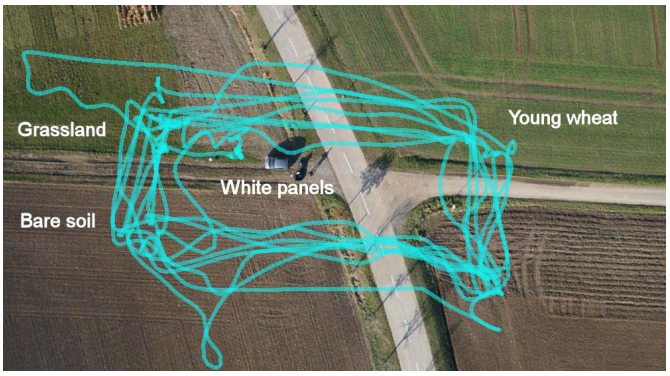

Fig. 1. Experimental site and flight pattern of the Falcon-8 UAV during the hyperspectral measurement collection. Grassland, young wheat and bare soil were observed with the UAV spectrometer and the ASD field spec. White panels were placed in the center as indicated.

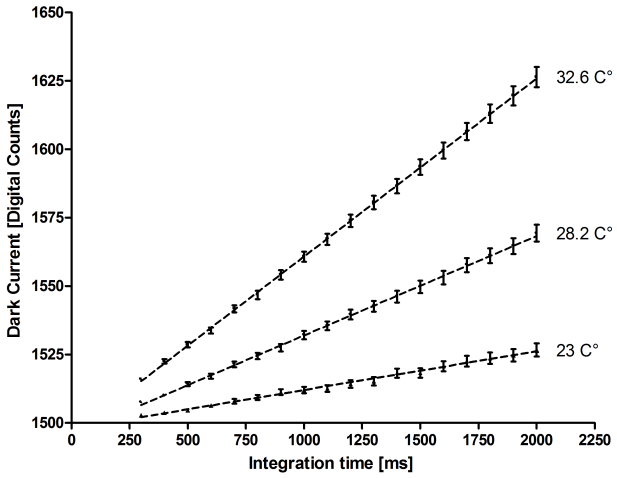

Fig. 2. Linear regression of dark current at three different detector temperatures and changing integration time.Dots and whiskers are mean values and standard deviations respectively for all spectral bands ($n = 256$).

ASD FieldSpec PRO 4 (Analytical Spectral Devices, Inc., Boulder, Colorado, U.S.). Simultaneous measurements were collected in such way that the spectrometer's field of view were totally overlapping on the white reference panel (Spectralon, Labsphere, Inc., North Sutton, NH, U.S.). A number of spectra were collected at different Solar Zenith Angles (SZA) to provide measurements covering different light levels. STS spectra were resampled to the ASD FieldSpec bands, thus a linear relationship between ASD radiance values (L_{ASD}) and STS digital counts at different light levels, normalized for the different instrument integration time (IT), was estimated for the 1024 spectral bands. The slope of the linear models represents the radiometric gain factors at different wavelengths that will successively be used to convert instrument relative values to absolute radiance values (eq. 1).

$$L_{ASD} = \frac{counts}{IT * gains}. \quad (1)$$

IV. Field Measurements

Several test flights were performed to test the technical performance of the spectrometer and the UAV. After those successful preliminary flights a validation experiment was performed on 14 November 2012 over agricultural fields next to the research center of Jülich (lat 50.896312, lon 6.426436). The illumination conditions were low, but because of a cloudless sky stable. Three different homogeneous targets 1. grassland 2. young wheat 3. bare soil were measured with the UAV spectrometer and at the same time with an ASD Field Spec 4 Pro. UAV measurements were conducted between 1:10 pm and 1:23 pm local time and each target was measured 8 times. The ground unit was placed in the center of the three targets. Flight altitude was 10 m over ground according to about 2 m diameter of the viewed spot. The observation angle was at nadir. The UAV was controlled manually and flown in transects over the targets during acquisition (Fig. 1).

Due to the low illumination integration time ranged between 473 and 481 ms and was automatically optimized. The optimization of the dynamic range of the spectrometer was performed by test measurements of the GND unit and adapted to the AIR unit.

ASD measurements were conducted with a pistolgrip about 1 m above the surface. 75 measurements were acquired along a transect over each target. Every 25 measurements irradiance was measured over a white reference panel (Spectralon). ASD data collection took place between 1 pm and 2 pm.

Reflectance was calculated for the ASD data using the average of the white reference measurements recorded for each target. The UAV spectrometer reflectance was calculated using the white reference and upwelling irradiance of each data point after post processing, including dark current correction and calibration. Overall reflectance of the targets was determined for the two datasets with mean and standard deviation.

Statistical analysis was conducted using Excel 2002 (Microsoft Corp., Redmond, WA, U.S.) and Graphpad Prism 4.0 (GraphPad Software Inc., La Jolla, CA, U.S.A.).

V. Results

Dark Current Removal: The DC measured at different integration times and at several stable temperature levels follows a linear function with $R^2 > 0.99$ (Fig. 2). Corresponding measurementswere performed for bothspectrometers (i.e. AIR/GND).

Measurements performed for single pixels with raising temperature (Fig. 3) and divided by integration time after subtraction of the baseline were fitted to an exponential function ($R^2 > 0.95$ for pixel 4 of the air unit). Each pixel showed a different temperature response in dark current leading to an overall $R^2 = 0.91$ for the AIR unit and $R^2 = 0.945$ for the GND unit. With these results the DC for the investigated integration times from 300 ms to 2000 ms and temperature levels from 14 °C to 34 °C could be estimated. With the fitted exponent function for the temperature (T) for each specific spectrometer and pixel (p) and the integration time (IT) the DC can be determined for every single pixel by the formula (2) where A, B and C are the constants of the fitted exponent

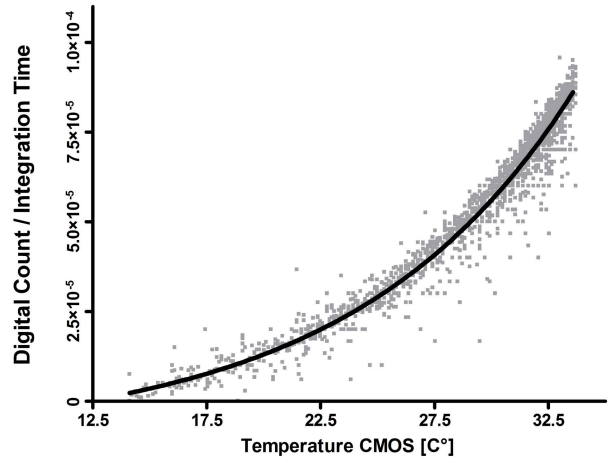

Fig. 3. Exponential regression of dark current dependency to raising detector temperature shown for Pixel 4 of the air units STS microspectrometer ($n = 1854$, $R^2 = 0.9586$). Data was fitted with an exponent function $y = a + b * e^{cx}$).

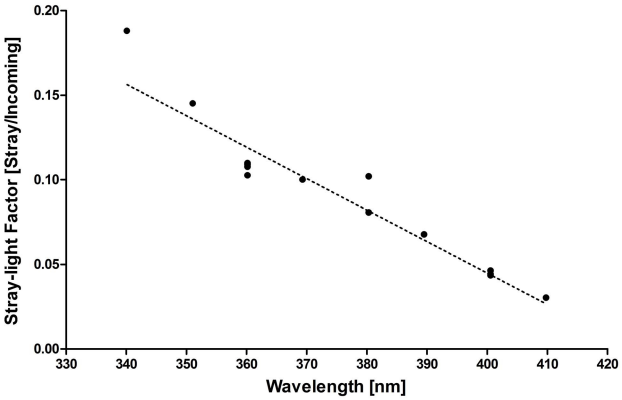

Fig. 4. Linear regression of the measured second order effect and its strength compared to the inducing wavelength ($n = 17$, $R^2 = 0.9149$).

function for each pixel.

$$DC_{[p]} = (A_{[p]} + B_{[p]} * e^{C_{[p]} * T}) * IT \quad (2)$$

To validate the methodology, thisDC correction was applied to additional exemplary measurements at 33 °C. In addition we collected the true DC as measured with closed optics. The deviation from the actual measured DC was in average 2.39 digital counts (air unit) which is less than 0.02 % of the 14 bit dynamic range.

Second Order Effect: The effect of the stray light of the second order was determined for the wavelength from 340 nm to 410 nm of the AIR unit in 10 nm steps. The amount of second order straylight, induced by monochromatic light was determined for the investigated wavelengths (Fig. 4). These factors determining the amplitude of the undesired signal at the double wavelength showed a linear behaviour ($R^2 = 0.9149$).

Instrument Calibration: Investigation of the spectral performance of AIR and GND unit with the SpecCal tool resulted in FHWM less than 3 nm and a small spectral shift as seen in Table II. By comparing the white reference measurements

TABLE II
ACCURACY OF SPECTROMETERS USED IN THIS STUDY

Device	Spectral Range [nm]	Spectral Shift [nm]	FWHM [nm]
ASD	350.00 - 1050.00	-0.05	3.79
GND	337.65 - 824.30	-0.05	2.30
AIR	337.65 - 824.30	0.15	3.00

of the AIR and GND unit with the radiometrically calibrated ASD spectra a transformation vector for each spectrometer was calculated. This vector was used to translate digital count measurements to physical units (eq. 1) and to crosscalibrate GND and AIR.

Field Measurements: Reflection over the 3 different targets (grassland, wheat, soil) was calculated and analyzed for ASD and the UAV spectrometer. Mean reflection spectra of both devices followed the same pattern with minor differences in the beginning and end of the spectra. The most significant difference to the actual reflection was seen in the O_2-A absorption band at 760 nm of the UAV spectrometer. Correlation of the reflection measurements of both systems was highly significant ($R^2 = 0.9912$). The three surfaces showed spatial heterogeneities such as vegetation patches, tire tracks and row seeding. Thestandard deviation of the UAV spectrometer's measurements was smallerthan in ASD data. This was caused by the much larger footprint of the UAV spectrometer. Over grassland ASD data varied with an average standard deviation in reflection of 4.1 % while the standard deviation with an average of 0.59 % of the UAV spectrometer measurements was 6 times smaller (Fig. 5).

VI. DISCUSSION

The calibration and validation experiments performed on the UAV spectrometer have proven that high precision spectroscopic measurements can be performed using the miniaturized spectrometers. The modelled dark current correction showed good results but care must be taken for influence of the second order effect which may cause errors in the NIR. High uncertainties are present in the reflection calculated inside the atmospheric O_2–A absorption feature at 760 nm. This issue will be addressed in future development to enable the spectrometer to accurately retrievethe sun induced fluorescence. The STS microspectrometers performed well regarding their size, but are still outperformed in sensitivity and accuracy by other larger and heavier sensors such as the Ocean Optics HR4000 or the USB2000. Despite this the spectral accuracy is comparable to the VIS of the current gold standard device ASD Field Spec Pro 4. Comparative measurements over agricultural fields have shown a far lower standard deviation in the UAV spectrometer data due to the larger field of view, compared to the ASD Field Spec measurements. Moreover, the very fast acquisition procedure over large sites proves the approach as an useful complement for conventional field spectroscopy. Taking advantage of the system it will be used in upcoming airborne and satellite

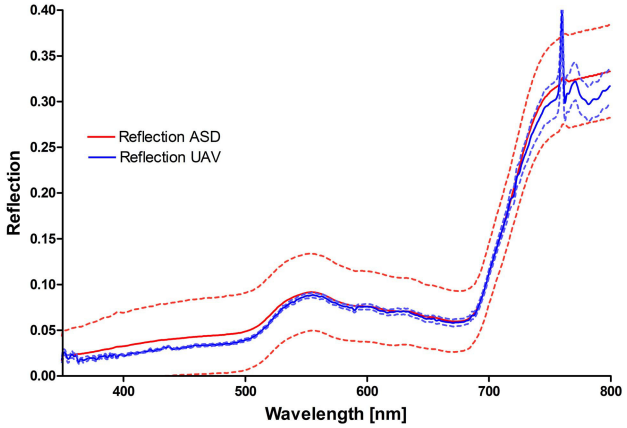

Fig. 5. Reflection over grassland measured by ASD field spec ($n = 75$) and UAV spectrometer ($n = 8$). Standard deviation is indicated by the dotted lines. Standard deviation on the other targets (wheat and soil) was similar high in ASD measurements and low in the UAV measurements.

campaigns such as the new high performance hyperspectral sensor HyPlant, as the UAV allows easy acquisition of reference reflectance measurements over areas difficult to access. The opportunity of changing the angle of the spectrometer during flight also allows the use as a giant flying goniometer for the investigation of BRDF effects [29] especially in forest [30]. The UAV spectrometer without the flying platform is also as a fully autonomous device suitable for the use in constant monitoring. It draws very low energy and has a built-in battery and charge circuit that can be powered by a small solar array.

In the quickly evolving field of UAV based spectral imaging, we took a step towards high-precision field spectroscopy and built a basic tool for hyperspectral research. To lay a base for future experiments the sensor was properly characterized and possible sources of error like the second order effect were identified. With the UAV spectrometer the gap between field spectroscopy and airborne sensors is about to be closed.

ACKNOWLEDGMENT

The author would like to thank T. Burkart for the design and manufacture of the spectrometer cases.

REFERENCES

[1] E. J. Milton, M. E. Schaepman, K. Anderson, M. Kneubühler, and N. Fox, "Progress in field spectroscopy," *Remote Sens. Environ.*, vol. 113, pp. S92–S109, Sep. 2009.

[2] G. Vane and A. F. H. Goetz, "Terrestrial imaging spectrometry: Current status, future trends," *Remote Sens. Environ.*, vol. 44, nos. 2–3, pp. 117–126, 1993.

[3] F. D. van der Meer and S. M. de Jong, *Imaging Spectrometry: Basic Principles and Prospective Applications*, vol. 4. New York, NY, USA: Springer-Verlag, 2011.

[4] A. Bannari, D. Morin, F. Bonn, and A. Huete, "A review of vegetation indices," *Remote Sens. Rev.*, vol. 13, nos. 1–2, pp. 95–120, 1995.

[5] J. Penuelas, J. Pinol, R. Ogaya, and I. Filella, "Estimation of plant water concentration by the reflectance water index WI (R900/R970)," *Int. J. Remote Sens.*, vol. 18, pp. 2869–2875, 1997.

[6] D. Haboudane, J. R. Miller, N. Tremblay, P. J. Zarco-Tejada, and L. Dextraze, "Integrated narrow-band vegetation indices for prediction of crop chlorophyll content for application to precision agriculture," *Remote Sens. Environ.*, vol. 81, no. 13, pp. 416–426, 2002.

[7] A. K. Mahlein, T. Rumpf, P. Welke, H. W. Dehne, L. Plümer, U. Steiner, and E.-C. Oerke, "Development of spectral indices for detecting and identifying plant diseases," *Remote Sens. Environ.*, vol. 128, pp. 21–30, Jan. 2013.

[8] M. Meroni, M. Rossini, L. Guanter, L. Alonso, U. Rascher, R. Colombo, and J. Moreno, "Remote sensing of solar-induced chlorophyll fluorescence: Review of methods and applications," *Remote Sens. Environ.*, vol. 113, no. 10, pp. 2037–2051, 2009.

[9] M. Balzarolo, K. Anderson, C. Nichol, M. Rossini, L. Vescovo, N. Arriga, G. Wohlfahrt, J.-C. Calvet, A. Carrara, S. Cerasoli, S. Cogliati, F. Daumard, L. Eklundh, J. A. Elbers, F. Evrendilek, R. N. Handcock, J. Kaduk, K. Klumpp, B. Longdoz, G. Matteucci, M. Meroni, L. Montagnani, J.-M. Ourcival, E. P. Sánchez-Cañete, J.-Y. Pontailler, R. Juszczak, B. Scholes, and M. P. Martín, "Ground-based optical measurements at European flux sites: A review of methods, instruments and current controversies," *Sensors*, vol. 11, no. 8, pp. 7954–7981, 2011.

[10] M. Meroni, A. Barducci, S. Cogliati, F. Castagnoli, M. Rossini, L. Busetto, M. Migliavacca, E. Cremonese, M. Galvagno, R. Colombo, and U. Morra di Cella, "The hyperspectral irradiometer, a new instrument for long-term and unattended field spectroscopy measurements," *Rev. Sci. Instrum.*, vol. 82, no. 4, pp. 043106-1–043106-9, 2011.

[11] R. Pu, M. Kelly, G. L. Anderson, and P. Gong, "Using CASI hyperspectral imagery to detect mortality and vegetation stress associated with a new hardwood forest disease," *Photogram. Eng. Remote Sens.*, vol. 74, no. 1, p. 65, 2008.

[12] D. Haboudane, J. R. Miller, E. Pattey, P. J. Zarco-Tejada, and I. B. Strachan, "Hyperspectral vegetation indices and novel algorithms for predicting green LAI of crop canopies: Modeling and validation in the context of precision agriculture," *Remote Sens. Environ.*, vol. 90, no. 3, pp. 337–352, 2004.

[13] J. Kuusk and A. Kuusk, "Autonomous lightweight airborne spectrometers for ground reflectance measurements," in *Proc. 2nd Workshop Hyperspect. Image Signal Process., Evol. Remote Sens.*, Jun. 2010, pp. 1–4.

[14] J. J. Mitchell, N. F. Glenn, M. O. Anderson, R. C. Hruska, A. Halford, C. Baun, and N. Nydegger, "Unmanned aerial vehicle (UAV) hyperspectral remote sensing for dryland vegetation monitoring," presented at the Whispers 4th Workshop on Hyperspectral Image and Signal Processing: Evolution in Remote Sensing, Shanghai, China, 2012.

[15] J. Primicerio, S. F. Di Gennaro, E. Fiorillo, L. Genesio, E. Lugato, A. Matese, and F. P. Vaccari, "A flexible unmanned aerial vehicle for precision agriculture," *Precis. Agricult.*, vol. 13, no. 4, pp. 517–523, 2012.

[16] P. Zarco-Tejada, V. González-Dugo, and J. Berni, "Fluorescence, temperature and narrow-band indices acquired from a UAV platform for water stress detection using a micro-hyperspectral imager and a thermal camera," *Remote Sens. Environ.*, vol. 117, pp. 322–337, Feb. 2011.

[17] J. Berni, P. J. Zarco-Tejada, L. Suárez, and E. Fereres, "Thermal and narrowband multispectral remote sensing for vegetation monitoring from an unmanned aerial vehicle," *IEEE Trans. Geosci. Remote Sens.*, vol. 47, no. 3, pp. 722–738, Mar. 2009.

[18] J. Berni, P. Zarco-Tejada, L. Surez, V. González-Dugo, and E. Fereres, "Remote sensing of vegetation from UAV platforms using lightweight multispectral and thermal imaging sensors," in *Proc. 37th Int. Archives Photogram., Remote Sens. Spatial Inf. Sci.*, 2008, pp. 1–6.

[19] G. Rufino and A. Moccia, "Integrated VIS-NIR hyperspectral/thermal-IR electro-optical payload system for a mini-UAV," in *Proc. Infotech Aerosp.*, 2005, pp. 1–9.

[20] H. Saari, V. V. Aallos, A. Akujärvi, T. Antila, C. Holmlund, U. Kantojärvi, J. Mäkynen, and J. Ollila, "Novel miniaturized hyperspectral sensor for UAV and space applications," *Proc. SPIE*, vol. 7474, pp. 1–12, Aug. 2009.

[21] F. E. Nicodemus, "Directional reflectance and emissivity of an opaque surface," *Appl. Opt.*, vol. 4, no. 7, pp. 767–773, 1965.

[22] A. Damm, A. Erler, W. Hillen, M. Meroni, M. E. Schaepman, W. Verhoef, and U. Rascher, "Modeling the impact of spectral sensor configurations on the FLD retrieval accuracy of sun-induced chlorophyll fluorescence," *Remote Sens. Environ.*, vol. 115, no. 8, pp. 1882–1892, 2011.

[23] M. Banzi, *Getting Started with Arduino*. Sebastopol, CA, USA: Make, 2008.
[24] R. Jones, P. Haufe, E. Sells, P. Iravani, V. Olliver, C. Palmer, and A. Bowyer, "RepRap-the replicating rapid prototyper," *Robotica*, vol. 29, pp. 177–191, Jan. 2011.
[25] C. Reas and B. Fry. (2012). *Processing.org (1.5.1)* [Online] Available: http://processing.org
[26] J. Kuusk, "Dark signal temperature dependence correction method for miniature spectrometer modules," *J. Sensors*, vol. 2011, pp. 608157-1–608157-9, Feb. 2011.
[27] M. Meroni, L. Busetto, L. Guanter, S. Cogliati, G. F. Crosta, M. Migliavacca, C. Panigada, M. Rossini, and R. Colombo, "Characterization of fine resolution field spectrometers using solar Fraunhofer lines and atmospheric absorption features," *Appl. Opt.*, vol. 49, no. 15, pp. 2858–2871, 2010.
[28] A. Berk, *et al.*, "MODTRAN5: 2006 update," *Proc. SPIE Algorithms and Technologies for Multispectral, Hyperspectral, and Ultraspectral Imagery XII*, vol. 6233, doi:10.1117/12.665077.
[29] G. J. Grenzdörffer and F. Niemeyer, "UAV based BRDF-measurements of agricultural surfaces with PFIFFikus," presented at the UAV-g, Conf. Unmanned Aerial Vehicle in Geomatics, Zurich, Switzerland, 2011.
[30] F. Fassnacht and B. Koch, "Review of forestry oriented multiangular remote sensing techniques," *Int. Forestry Rev.*, vol. 14, no. 3, pp. 285–298, 2012.

Andreas Burkart is a Ph.D. student with the Research Centre Jülich and the University of Bonn, Bonn, Germany. He received the Diploma degree in biology in bioacoustical studies of neotropical bees. Currently his main field of expertise is plant science based on optical measurements from unmanned airborne platforms with special interest in airships.

Sergio Cogliati received the Ph.D. degree in environmental science from the University of Milano-Bicocca, Milan, Italy. He is currently with the Remote Sensing of Environmental Dynamics Laboratory, University of Milano-Bicocca, continuing studies on hyperspectral remote sensing techniques for the retrieval of vegetation biophysical parameters and vegetation fluorescence.

Anke Schickling is a Post-Doctoral Researcher with the Institute of Bio- and Geosciences, IBG-2: Plant Sciences, Forschungszentrum Jülich, Jülich, Germany. She has broad experience in field and imaging spectroscopy to derive sun induced fluorescence and characterize structural and biochemical properties of vegetation canopies.

Uwe Rascher is leading the research area "Ecosystem Dynamics" with Forschungszentrum Jülich, Jülich, Germany, and is Professor for "Quantitative Physiology of Crops" with Bonn University. He develops and uses high performance remote sensing techniques to extract relevant plant traits from ground and airborne measurements. His main focus is in understanding the spatio-temporal variations in fluorescence that serve as a non-invasive indicator for the functional adaptation of plant function and stress.

A2: Deploying four optical UAV-based sensors over grassland: challenges and limitations

Authors Contribution

Scientific work and development: 50%

Field work and analysis: 50%

Publication work: 50%

Biogeosciences, 12, 163–175, 2015
www.biogeosciences.net/12/163/2015/
doi:10.5194/bg-12-163-2015

Biogeosciences Open Access

Deploying four optical UAV-based sensors over grassland: challenges and limitations

S. K. von Bueren[1,*], A. Burkart[2,*], A. Hueni[3], U. Rascher[2], M. P. Tuohy[1], and I. J. Yule[1]

[1]Institute of Agriculture & Environment, Massey University, Palmerston North, New Zealand
[2]Institute of Bio- and Geosciences, IBG-2: Plant Sciences, Forschungszentrum Jülich GmbH, Jülich, Germany
[3]Remote Sensing Laboratories, University of Zurich, Zurich, Switzerland
[*]These authors contributed equally to this work.

Correspondence to: A. Burkart (an.burkart@fz-juelich.de)

Received: 1 February 2014 – Published in Biogeosciences Discuss.: 7 March 2014
Revised: 25 November 2014 – Accepted: 28 November 2014 – Published: 9 January 2015

Abstract. Unmanned aerial vehicles (UAVs) equipped with lightweight spectral sensors facilitate non-destructive, near-real-time vegetation analysis. In order to guarantee robust scientific analysis, data acquisition protocols and processing methodologies need to be developed and new sensors must be compared with state-of-the-art instruments. Four different types of optical UAV-based sensors (RGB camera, converted near-infrared camera, six-band multispectral camera and high spectral resolution spectrometer) were deployed and compared in order to evaluate their applicability for vegetation monitoring with a focus on precision agricultural applications. Data were collected in New Zealand over ryegrass pastures of various conditions and compared to ground spectral measurements. The UAV STS spectrometer and the multispectral camera MCA6 (Multiple Camera Array) were found to deliver spectral data that can match the spectral measurements of an ASD at ground level when compared over all waypoints (UAV STS: $R^2 = 0.98$; MCA6: $R^2 = 0.92$). Variability was highest in the near-infrared bands for both sensors while the band multispectral camera also overestimated the green peak reflectance. Reflectance factors derived from the RGB ($R^2 = 0.63$) and converted near-infrared ($R^2 = 0.65$) cameras resulted in lower accordance with reference measurements. The UAV spectrometer system is capable of providing narrow-band information for crop and pasture management. The six-band multispectral camera has the potential to be deployed to target specific broad wavebands if shortcomings in radiometric limitations can be addressed. Large-scale imaging of pasture variability can be achieved by either using a true colour or a modified near-infrared camera. Data quality from UAV-based sensors can only be assured, if field protocols are followed and environmental conditions allow for stable platform behaviour and illumination.

1 Introduction

In the last decade, the use of unmanned aerial vehicles (UAVs) as remote sensing platforms has become increasingly popular for a wide range of scientific disciplines and applications. With the development of robust, autonomous and lightweight sensors, UAVs are rapidly evolving into stand-alone remote sensing systems that deliver information of high spatial and temporal resolution in a non-invasive manner. UAV systems are particularly promising for precision agriculture where spatial information needs to be available at high temporal frequency and spatial resolution in order to identify in-field variability (Stafford, 2000; Seelan et al., 2003; Lelong et al., 2008; Nebiker et al., 2008; Link et al., 2013). Zhang and Kovacs (2012) provide a comprehensive review of unmanned aerial systems applied in precision agriculture.

Precision agriculture aims at identifying crop and soil properties in near-real-time (Lebourgeois et al., 2012; Primicerio et al., 2012a) and at delivering results to farmers and decision makers with minimum delay to enable management decisions based on current crop and soil status. The use of input resources such as fertilizers, herbicides or water (Van Alphen and Stoorvogel, 2000; Carrara et al., 2004; Chávez et al., 2010) are matched to the current demand by the crops,

leading to an economical use of resources. The use of UAV-based sensors to detect water stress and quantify biomass and nitrogen content in crops and grasses has been demonstrated (Berni et al., 2008, 2009; Kawamura et al., 2011). Yield forecasting in wheat (Jensen et al., 2007) and rice (Swain et al., 2010), rangeland management (Rango et al., 2009), leaf area index (LAI) and green normalized difference vegetation index (NDVI) estimation in winter wheat (Hunt et al., 2010) and site-specific vineyard management (Turner, 2011; Primicerio et al., 2012b) have been accomplished using unmanned aerial platforms.

Proximal remote sensing methods can be used to detect pasture and crop biophysical parameters such as biomass, dry matter, fibre content, organic matter digestibility and macronutrient availability (nitrogen, phosphorus and potassium). Pasture monitoring approaches capable of measuring biophysical variables over the whole farm at a high spatial resolution allow for site-specific management decisions and optimum nutrient management (Sanches et al., 2012). While vegetation indices have been frequently applied for biomass and dry matter estimation (Mutanga, 2004; Duan et al., 2011; Vescovo et al., 2012), waveband-specific algorithms have been developed to estimate macronutrients (Mutanga and Skidmore, 2007; Pullanagari et al., 2012a, b).

In a pasture management context in New Zealand, where air- and spaceborne remote sensing methods are often limited by frequent cloud cover, UAV-based remote sensing can potentially overcome some of those limitations. Recent developments in commercially available lightweight and small digital cameras and multispectral sensors support precision nutrient management. However, these sensors need to be characterized and validated against state-of-the-art reference instruments. The extraction of quantitative information relies on thorough calibration procedures, good instrument characterization and a high standard of field operation.

Various studies have specifically evaluated multispectral sensors and consumer-grade digital cameras and assessed their potential for vegetation monitoring. The use of a conventional, ground-based broadband digital RGB camera has shown limited success in estimating green biomass on short-grass prairie, suggesting that narrow-band sensors are more promising for application over such complex ecosystems (Vanamburg et al., 2006). An image processing workflow for three consumer digital cameras has been developed by Lebourgeois et al. (2012) and they have suggested that the cameras have a high potential for terrestrial remote sensing of vegetation due to their versatility and multispectral capabilities. Vegetation indices derived from visible and near-infrared imagery acquired by two compact digital cameras were found to generate strong relationships with crop biophysical parameters and to be practical for monitoring of temporal changes in crop growth (Sakamoto et al., 2012). Kelcey and Lucieer (2012) developed a processing chain to improve the imagery acquired with the same six-band multispectral sensor that was used in the current study. They showed that image quality can be improved through application of sensor correction techniques to facilitate subsequent image analysis. A novel, UAV-based lightweight high-resolution spectrometer, which was tested in the field for the first time in the current study, was introduced by Burkart et al. (2013). Nijland et al. (2014) evaluated the use of near-infrared (NIR) and RGB cameras for the use of vegetation monitoring and plant phenology trend detection and found that the NIR-converted cameras were outperformed by standard RGB cameras. Poor band separation and the limited dynamic range of the NIR camera system limited the use of the sensors for vegetation monitoring in a controlled laboratory and in a field experiment.

Studies usually deploy a single UAV sensing system over an area of interest. But because different agricultural applications and environmental frameworks demand specific capabilities of an UAV remote sensing system, the current study uses four different sensors over the same experimental area to evaluate each sensor's suitability for applied grassland monitoring. From preliminary experiments, it was evident that the UAV system, including platform and sensor, need to be specifically matched to the vegetation parameter to be investigated. The present study used two compact digital cameras (RGB and NIR), a six-band multispectral camera (visible/near-infrared – VNIR) and a high-resolution spectrometer (VNIR) mounted on two different UAV platforms to acquire spectral information over dairy pastures in order to characterise each instrument in terms of radiometric quality and accuracy of spectral information obtainable, as compared to a ground reference instrument. Handling and limitations of the UAVs, flight planning, field procedures and the capabilities of the different sensors are discussed as a prospective guideline for upcoming UAV sensor-based research. Results are evaluated with a focus on inter-sensor comparability, aspects of field data collection using UAVs and the sensor's capabilities for monitoring green vegetation.

1.1 Experimental site

The experimental flight campaign was conducted in February 2013 on a Massey University dairy farm near Palmerston North, New Zealand, (No. 1 Dairy, located at lat. −40.376, long. 175.606). No. 1 Dairy is a fully operational dairy farm with an effective area of 119.7 ha. UAV flights were performed over four different paddocks with distinct characteristics from bare soil to dry and irrigated ryegrass pasture. At the time of data acquisition between 11:00 and 15:00 LT no clouds were visible.

1.2 UAV systems

As shown in Table 1, two different UAV systems were used: a QuadKopter (MikroKopter), owned and operated by Massey University, and a Falcon-8 (AscTec (Ascending Technologies), Krailing, Germany), from the Research Centre Jülich,

Table 1. UAV platforms.

Name	QuadKopter	Falcon-8
Manufacturer	MikroKopter	Ascending Technologies
Weight [g]	1900	1800
Max. Payload [g]	1000	500
Power source	LiPo, 4200 mAh, 14.8 V	Lipo, 6400 mAh, 11.1 V
Endurance [min]	12	15
GPS navigation	Ublox LEA 6s GPS chip	Ublox LEA 6T
Features	Open Source Gyro-stabilized camera mount	Stabilized camera mount, live video link, motor redundancy
Sensors	MCA6	UAV STS, RGB, Canon IR

Germany. The Falcon-8 uses the AscTec Autopilot Control V1.68 software. It has two identical exchangeable gimbals manufactured by AscTec, one for the Sony camera the other one for the spectrometer and Canon camera. Both gimbals are dampened and actively stabilized in pitch and roll. The MikroKopter UAV was fitted with an AV130 Standard Gimbal produced by Photo Higher. The gimballed camera mounts levelled out any platform movement to ensure the sensors were pointing in nadir direction to the ground at all times during the flight. The main difference between the Falcon-8 and the MikroKopter platforms is the payload restriction, which precludes the Falcon-8 from lifting sensors heavier than 0.5 kg, thus making it necessary to use the MikroKopter UAV to lift the Mini-MCA6 sensor. Both UAVs with their payloads were intensively tested on multiple flights before the study.

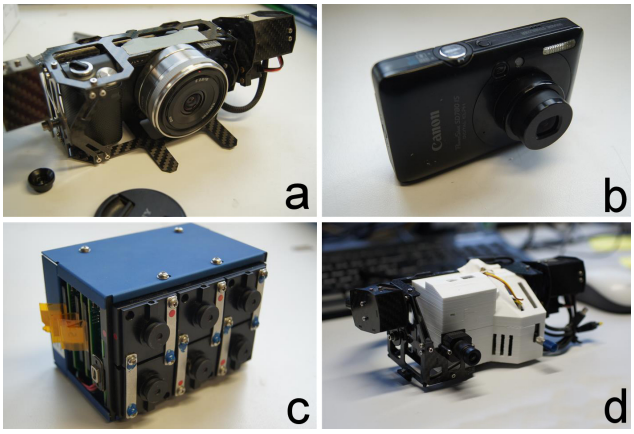

Figure 1. UAV-based sensors: **(a)** Sony Nex5n RGB camera **(b)** Canon PowerShot IR camera **(c)** MCA6 multispectral camera **(d)** Spectrometer (UAV STS).

1.3 UAV sensors

Four UAV sensors (Fig. 1) were tested and compared in terms of their ability to produce reflectance data over pastures. All of the sensors were lighter than 1 kg including batteries and were either modified or specifically designed for use on remotely controlled platforms. The sensors share a spectral range in the VNIR which is considered the most relevant region of the electromagnetic spectrum for agricultural research applications (Lebourgeois et al., 2008). In terms of spatial and spectral resolution (Fig. 2), the sensors differ significantly. Table 2 lists their relevant properties.

Mini-MCA6 (MCA6): the Mini-MCA6 (Multispectral Camera Array) is a six-band multispectral camera (Tetracam, Chatsworth, CA, USA) that can acquire imagery in six discrete wavebands. A camera-specific image alignment file is provided by the manufacturer. Exchangeable filters in the range of 400 to 1100 nm can be fitted to six identical monochromatic cameras. Table 3 lists the filter setup used during the study. The camera firmware allows pre-setting all imaging related parameters such as exposure time, shutter release interval and image format and size. Six two gigabyte CompactFlash memory cards store up to 800 images (10 bit RAW format, full resolution). With an opening angle of 38.3° × 31.0°, the camera has a relatively narrow field of view as opposed to the Canon and Sony cameras. The camera was set to a 2 ms exposure time and was run on a 2 s shutter release interval with images saved in the 10 bit RAW format. Positioning of the camera was achieved by hovering the UAV over the vegetation target for at least 30 s per waypoint.

STS spectrometer (UAV STS): the spectrometer was adapted for UAV-based remote sensing at the Research Centre Jülich. Its design is based on the STS VIS spectrometer (Ocean Optics, Dunedin, FL, USA) with the addition of a micro-controller to enable remote triggering and saving of spectral data. The spectrometer operated on an independent power source and its low weight and fine spectral resolution made it ideal for use on an UAV. The full specifications, calibration efforts and validation of the STS spectrometer are presented in Burkart et al. (2013). An identical spectrometer, on the ground, acquired spectra of incoming radiance every time the airborne sensor was triggered. Spectra were saved on a micro SD card.

Sony RGB camera: a SONY Nex5n (Sony Corporation, Minato, Japan) modified by AscTec was attached to the Falcon-8 using a specially designed camera mount. A live video feed from the camera to the UAV operator and remote triggering were available. Spectral sensitivity was given by

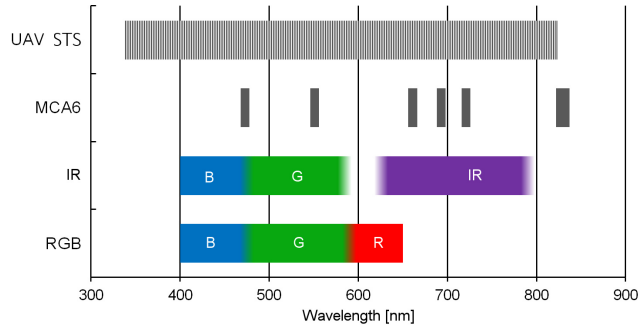

Figure 2. Spectral sensitivity of the four sensors. Spectral bands are indicated by different colours.

the common Bayer matrix (Bayer, 1976; Hirakawa et al., 2007) and hot mirror used in consumer digital cameras.

Canon PowerShot camera: the Canon PowerShot SD780 IS is a consumer digital camera that has been professionally (LDP LLC, Carlstadt, US) converted to acquire near-infrared imagery. The near-infrared filter has been replaced with a red-light-blocking filter. Again, the spectral response of the camera is based on the Bayer pattern colour filter array. Customized CHDK (Canon Hack Development Kit) firmware allows running the camera in a continuous capture mode at specific time intervals (2 s, user defined). Camera acquisition was set to automatic as time constraints and UAV batteries did not allow for accurate manual configuration of white balance, aperture, ISO and shutter speed. Images were saved as JPEGs. A live video link from the UAV's on-board camera enabled precise positioning of the RGB and infrared cameras over the ryegrass pastures. The main difference to the MCA6 is the inability to adjust filter settings and the camera's bandwidths. According to manufacturer information each band has an approximate width of 100 nm.

1.4 Ground-based sensors

ASD HandHeld 2 ground-based reference sensor: ground-based spectral measurements were acquired with an ASD HandHeld 2 portable spectroradiometer (Analytical Spectral Devices, Inc., Boulder, Colorado, US). The device covers a spectral range from 325 nm to 1075 nm which makes it suitable for comparison with all UAV sensors flown in this study. At 700 nm the device has a spectral resolution of 3 nm and the field of view equates to 25°. A Spectralon® panel (Spectralon®, Labsphere, Inc., North Sutton, NH, USA) was used to acquire white reference measurements before each target measurement. Each target was measured 10 times from 1 m distance while moving over the area of interest.

1.5 Flight planning and data acquisition procedure

Taking into account the operational requirements of each sensor and flying platform, a detailed flight plan was developed. Eight sampling locations defined by waypoints were selected from overview images and supported by an in situ visual assessment of the paddock. A focus was put on covering a wide range of pasture qualities from dry to fully irrigated ryegrass pastures. Waypoints were selected in paddock areas with homogeneous pasture cover. This ensured that each waypoint can be considered representative for the area of the paddock it is located in, and it aided dealing with the different sensor footprint sizes (Table 4).

Each sampling location was marked with a tarpaulin square, which was clearly visible in all spectral bands of the aerial images. In order to avoid interference effects of the markers with the UAV STS measurements, they were removed before acquisition of spectra. Next to the first waypoint, a calibration site with coloured tarpaulin squares was set-up and measured with the ASD HandHeld 2.

The sensors were flown over the targets in the following order: (1) RGB camera for an overview shot, (2) IR camera for an overview shot, (3) MCA6 over calibration sites (black, grey, white and red tarpaulins black foam material, bare soil) and waypoints and (4) UAV spectrometer over waypoints. Overview images cover all sampling locations in an area with a single shot from 100 to 150 m flying height. MCA6 images were taken from 25 m above the ground. UAV STS data were collected from a height of 10–15 m, and 15 spectra were taken over each waypoint. During the experiment, the Falcon-8 was flown in semi-autonomous GPS mode. Coordinates of the sampling locations were recorded with a low-accuracy GPS (Legend, HTC, Taoyuan, Taiwan). The Falcon-8 used those coordinates to autonomously reach the marker locations. Over each sampling location, the flight mode was then switched to manual and the UAV was positioned over the target as accurately as possible using a live video link. The UAV STS and the live camera were on the same stabilized gimbal and aligned in a way, that the centre of the FPV camera approximates the UAV STS's field of view. The QuadKopter was flown in manual mode during the entire experiment. In test flights preceding this experiment, it was found that the GPS on board of the MikroKopter was not accurate enough to position the sensor over a waypoint.

Flights were conducted consecutively to minimize variability due to changing illumination and vegetation status. Figure 3 depicts raw data from the imaging sensors before any processing has been applied. Before the flight of the UAV spectrometer, ASD ground reference measurements were taken at each waypoint.

1.6 Data processing

Data from each sensor underwent calibration and correction procedures.

MCA6: a proprietary software package (PixelWrench2 by Tetracam) that was delivered with the Tetracam was used to transfer images from the CompactFlash memory cards to the computer. Each RAW band was processed to a TIFF (Tagged Image File Format) image in order to identify all images that

Table 2. Sensor properties.

Name	Sony Nex5n RGB	Canon Powershot IR	MCA6	STS
Company	Sony – modified	Canon – modified	Tetracam	Ocean Optics – modified
Type	RGB camera integrated	VIS + Infrared camera in the Falcon-8 UAV	Multispectral Imager with 6 bands of 10 nm width	Spectroradiometer with additional electronics for remote control
Field of View	73.7° × 53.1°	57.2° × 40°	38.3° × 31.0°	12°
Spectral bands	3	3	6	256
Spectral range	Blue, Green, Red	Blue, Green, IR	450–1000 nm	338–824 nm
Image size	4912 × 3264	4000 × 3000	1280 × 1024	n/a
Image format	JPEG	JPEG	RAW	n/a
Dynamic Range	8 bit	8 bit	10 bit	14 bit
Weight [g]	500	100	790	216
Handling	Wireless trigger, live view	Interval mode	Interval mode	Wireless trigger, live view

Table 3. MCA6 filter specifications.

	Slave 1	Master	Slave 2	Slave 3	Slave 4	Slave 5
Centre wavelength FWHM (nm)	473	551	661	693	722	831
Bandwidth FWHM (nm)	9.26	9.72	9.73	9.27	9.73	17.81
Peak transmission (%)	64.37	72.54	61.4	66.89	63.63	65.72

show the target area. As a result, between 6 and 15 images per target were found to be suitable for further image processing (total of 109 images) and two images showing the tarpaulin areas and bare soil were selected for reflectance factor calibration. From there, RAW image processing was done in Matlab (The MathWorks Inc., 2011). Both the calibration images and the vegetation target images were noise corrected and vignetting effects were removed for each of the six cameras (Yu, 2004; Olsen et al., 2010; Kelcey and Lucieer, 2012). A sensor correction factor was applied to each filter based on filter sensitivity factory information (Kelcey and Lucieer, 2012).

UAV STS: as described in Burkart et al. (2013) a temperature-based dark current correction (Kuusk, 2011) and an inter-calibration of the air- and ground-based spectrometer were applied before derivation of reflectance factors.

Sony RGB Camera: the red, green and blue bands were calibrated to a reflectance factor with the empirical line method (Smith and Milton, 1999; Baugh and Groeneveld, 2008) relating the ASD reflectance over the coloured reference tarpaulins (Fig. 3) to real reflectance (Aber et al., 2006).

Canon infrared camera: the camera was corrected using the same method as for the RGB camera, but with the centre wavelengths adapted to the infrared sensitive pixels.

The images that show the tarpaulin and the bare soil were selected as calibration images and processed separately. The white and the red tarpaulins were excluded from analysis due to pixel saturation and high specular reflection. For each of the calibration surfaces (black, grey, black foam and bare soil) a subset image area was defined from which the pixel values for the empirical line method were derived.

For each calibration target, ten ASD reference spectra were convolved to the spectral response of the Mini-MCA6 (see Spectral Convolution). The empirical line method was applied to establish band-specific calibration coefficients. Using those coefficients, the empirical line method was applied to each vegetation target image on a pixel-by-pixel basis, thus converting digital numbers of the image pixels to a surface reflectance factor.

In order to extract the footprint area over which ground ASD and UAV spectrometer data had been acquired, the relevant image area was identified and extracted from each image by identifying the markers in the image. Footprints were matched between sensors by defining a 0.3 by 0.3 m area below the waypoint marker as the region of interest. An average reflectance factor was calculated for each footprint resulting in between 6 and 15 values per sample location for the MCA6 images. Standard deviations, mean and median were calculated for each waypoint.

ASD HandHeld 2 ground reference sensor: ASD HandHeld 2 spectral binary files were downloaded and converted to reflectance using the HH2Sync software package (Version 1.30, ASD Inc.). Spectral data were then imported into the spectral database SPECCHIO (Hueni et al., 2009).

Spectral Convolutions: in order to synthesize STS spectrometer data from ground-based ASD data, a discrete spectral convolution was applied (Kenta and Masao, 2012). Each STS band was convolved by applying Eq. (1), using a Gaussian function to represent the spectral response function of each STS band. These spectral response functions (SRFs) were parameterized by the calibrated centre wavelengths of the STS instrument and by a nominal FWHM (full width at half maximum) of 3 nm for all spectral bands. The discrete

Table 4. Optical sensor footprint properties.

	UAV STS	MCA6	Canon IR	Sony RGB	ASD
Footprint shape	Circular	Rectangular	Rectangular	Rectangular	Circular
Footprint size [Sensor height (m)]	Ø 2.1 m [10]	17.3 × 13.9 m [25]	109.0 × 72.8 m [100]	149.9 × 99.9 m [100]	Ø 0.44 m [1]
Number of pixels	n/a	1280 × 1024	4000 × 3000	4912 × 3264	n/a
Ground resolution (m)	n/a	0.0135	0.0273	0.0305	n/a

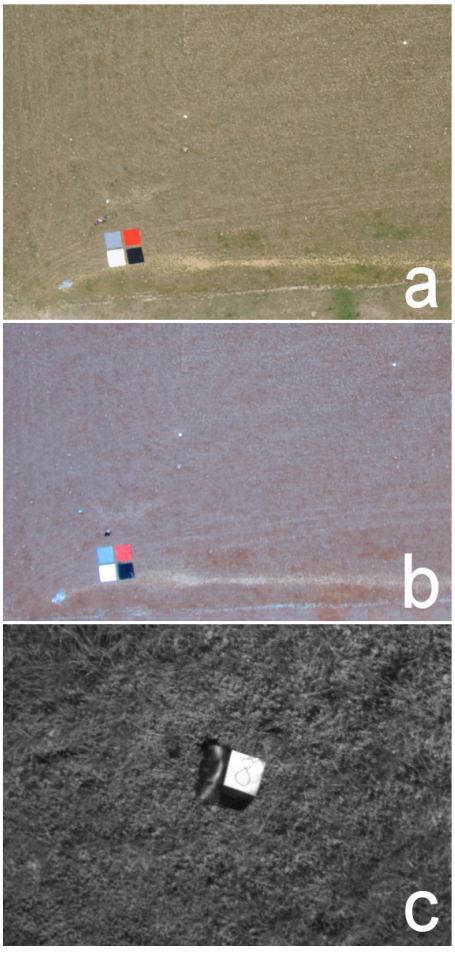

Figure 3. Raw data from the imaging sensors **(a)** RGB camera at 100 m altitude, **(b)** IR camera at 100 m altitude, **(c)** MCA6 at 25 m altitude (red band). The images show the region of interest cropped from a larger image. White points represent the tarpaulin waypoint markers.

convolution range (nm) of each band was based on $\pm 3\sigma$ of the Gaussian function and applied at the wavelength positions where an ASD band occurred, i.e. at every nanometre. It must be noted that the results of this convolution cannot truly emulate the actual system response of the STS as the ASD sampled input spectra are already a discrete representation of the continuous electromagnetic spectrum and are hence already inherently smoothed by the measurement process of the ASD.

In a similar manner, MCA6 bands were simulated, but having replaced the Gaussian assumption of the SRFs with the spectral transmission values (Table 3) digitized from analogue figures supplied by the filter manufacturer (Andover Corporation, Salem, US).

$$R_k = \frac{\sum_{j=n}^{m} c_j R_j}{\sum_{j=n}^{m} c_j}, \quad (1)$$

where R_k = reflectance factor of Ocean Optics band k, R_j = reflectance factor of ASD band j, c_j = weighting coefficient based on the Ocean Optics STS, spectral responsivity at wavelength of ASD band j, $n : m$ = convolution range of Ocean Optics band k.

2 Results

MCA6 and UAV STS: calibrated reflectance factors of the UAV spectrometer and the MCA6 were compared to calculated ASD reflectance values using linear regression analysis. The UAV STS and the ASD HandHeld 2 were compared over the whole STS spectrum, while the MCA6 was compared to the ASD in its six discrete bands.

Figure 4 shows the spectral information derived from both the STS spectrometer and MCA6 in direct comparison with the convolved ASD-derived reflectance spectra for two distinctively different waypoints in terms of ground biomass cover and greenness of vegetation. Waypoint 2 is a recently grazed pasture with a high percentage of dead matter and senescent leaves. Soil background reflectance was high and the paddock was very dry, with no irrigation scheme operating. Pasture at waypoint 8 had not been grazed recently and therefore vegetation cover was dense with a mix of ryegrass pastures and clover. The paddock undergoes daily irrigation and no soil background signal was detectable. The data indicated that the MCA6 estimates higher reflectance factors than the UAV spectrometer and the ASD for the blue, green and the lowest red band. In the far-red and NIR bands, values were consistently lower than those derived from the ASD but still higher than reflectance measured by the UAV STS. While the ASD detected a steep increase in reflectance in the

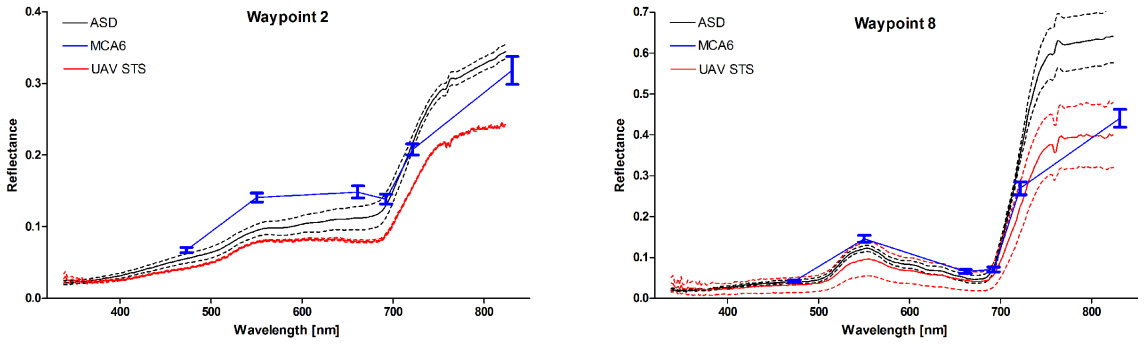

Figure 4. Reflectance of the spectral sensors ASD (black), MCA6 (blue) and UAV STS (red) as measured over the exemplary waypoints 2 and 8. SD in dotted lines for the ASD and UAV STS and with error bars for the 6 bands of the MCA6.

Table 5. Correlation matrix of the optical sensors (R^2). Values were calculated for corresponding bands of each sensor pair over all waypoints. Number of images (n) is given in brackets.

	RGB	IR	MCA6	UAV STS
RGB	1			
IR	0.913 (16)	1		
MCA6	0.377 (16)	0.945 (16)	1	
UAV STS	0.681 (24)	0.891 (24)	0.826 (48)	1
ASD	0.674 (24)	0.647 (24)	0.924 (48)	0.978 (3856)

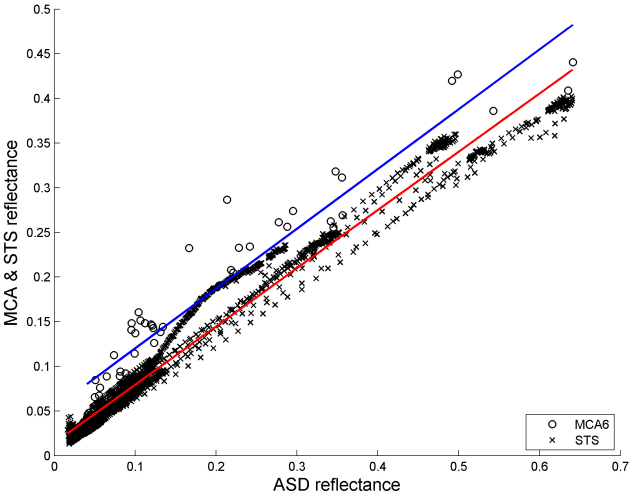

Figure 5. Reflectance comparison of UAV-based sensors to convolved ASD-derived reflectance showing data over all eight sample locations and spectra (MCA6 $n = 48$, STS $n = 120$). MCA6 vs. ASD (blue): $R^2 = 0.92$, slope of linear regression: 0.6691, offset: 0.0533. STS vs. ASD (red): $R^2 = 0.98$, slope of linear regression: 0.6522, offset: 0.0142.

red edge, both UAV sensors detected a lower signal in the same region of the spectrum.

The mean MCA6-derived spectra showed an increase in reflectance in the green peak region of the vegetation spectrum that is approximately 0.05 % higher than in the same region of the UAV spectrometer. The slope between the green and the red bands is positive for both sensors demonstrating the dried, stressed state of the vegetation at waypoint 2. While MCA6 bands show low correlations with the UAV STS and the ASD for the 551 nm and the 661 nm bands, its values are in line with the other sensors in the red-edge region of the spectra.

The MCA6 correlates significantly with ASD-derived reflectance (R^2 0.92, Fig. 5, Table 5) when compared over all eight waypoints and over all six-bands ($n = 48$). Shortcomings of spectral accuracy of the MCA6 are revealed when comparing band reflectance values over different sample locations and per waypoint (Fig. 6). The green band (551 nm) achieves lowest correlations with ASD convolved reflectance values ($R^2 = 0.68$), with MCA6 reflectance factors overestimated for all waypoints. The remaining five bands show correlations with R^2 between 0.70 (722 nm) and 0.97 (661 nm). Overall, the MCA6 overestimates bands below the red edge, while it shows low deviations from the STS- and the ASD-derived reflectance values for the red-edge bands. Due to the low number of waypoints, the blue-, green- and red-band correlations need to be interpreted with caution. With an R^2 of 0.98, the UAV spectrometer strongly correlates to the reflectance derived from the ASD when compared over all waypoints (Table 4). Even though the trend of the spectra is similar to the ASD ground truth, differences are visible in the magnitude of the reflectance mainly in the near-infrared.

RGB and NIR camera: as can be seen in Table 4, the correlation between the RGB and IR cameras results in an R^2 of 0.91, whereas the correlations to the high-resolution spectrometers are as low as 0.65 between the NIR camera and the ASD. The RGB camera and MCA6 are poorly correlated with a R^2 of 0.38.

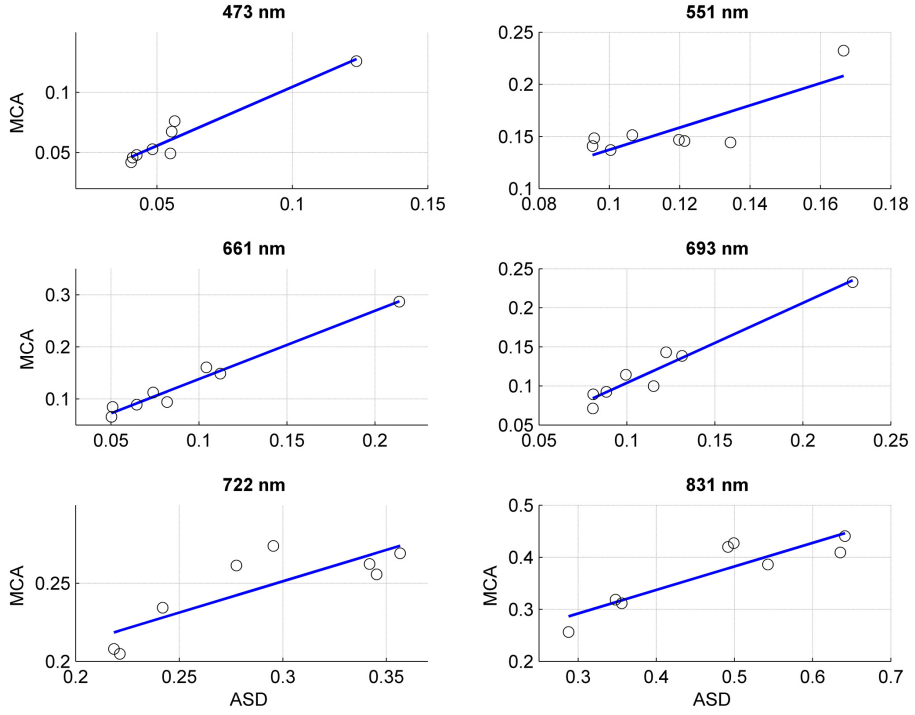

Figure 6. Comparison of reflectance values between MCA6 and convolved ASD reflectance for each MCA6 band. 473 nm: $R^2 = 0.93$, regression slope (RS): 0.9783; 551 nm: $R^2 = 0.68$, RS: 1.0654; 661 nm: $R^2 = 0.97$, RS: 1.311; 693 nm: $R^2 = 0.95$, RS: 1.0225; 722 nm: $R^2 = 0.7$, RS: 0.4009; 831 nm: $R^2 = 0.8$, RS: 0.4516.

3 Discussion

MCA6: when compared to the UAV spectrometer and the ground reference data, the MCA6 filters performed well in the red-edge region of the electromagnetic spectrum. This observation is supported by the CMOS sensor relative sensitivity which is over 90 % in the red-edge and the near-infrared bands according to factory information (Tetracam Inc.). The largest deviations were observed in the green band, where the MCA6 consistently overestimates vegetation reflectance factors. In sample locations with low biomass cover and/or stressed pastures, this results in a negative slope between the red bands. The sensor's performance is further impaired when high soil background reflectance is present, as is the case for the first three waypoints and the bare soil calibration target. While the green peak in the UAV STS and ASD measurements is barely visible over waypoint 2 but pronounced for waypoint 8, the MCA does not pick up on that feature. Green-band reflectance is overestimated for the drier pasture, while deviations from the other sensors' measurements over irrigated, greener pasture are lower. Those differences must be put down to radiometric inconsistencies in the MCA6 and potential calibration issues and it suggests that with the current filter setup, the MCA6 cannot be regarded as suitable for remote sensing of biochemical constituents and fine-scale monitoring of vegetation variability. Another complexity can be seen in the near-infrared regions of the derived spectra. For the UAV STS, MCA6 and the ASD, the variability of measured reflectance factors increases. This discrepancy is likely to arise from a combination of areas of different spatial support in terms of the sensor's field-of view (FOV) and calibration biases (sensor and reflectance calibration). Further investigation into sensor performance over targets with complex spectral behaviour must be conducted in order to evaluate the spectral performance of those bands. The number of waypoints visited was not high enough to fully assess the performance of the four lower MCA6 bands as can be seen in Fig. 6. Due to the statistical distribution of the data points, a definite statement on the performance of those bands is not possible. The empirical line method used for reflectance calibration introduces further errors because only one calibration image was acquired over the entire measurement procedure. Reflectance factor reliability can be improved by more frequent acquisition of calibration images.

UAV STS: the UAV STS-delivered spectra with strong correlations to the ASD measurements. The calculation of narrow-band indices or spectral fitting algorithms is thus possible. However, depending on the status of the vegetation target the ASD-derived reflectance factors can be up to 1.5 times (Fig. 4) higher than the UAV STS measurements. This result, particularly striking in the NIR, is below expectations, as Burkart et al. (2013) compared the Ocean Optics spectrometer (UAV STS) to an ASD Field Spec 4 and reported good agreements between the two instruments. The

main source of discrepancies between the ASD and STS measurements can be attributed to inconsistencies in footprint matching due to using a live feed from a camera that can only approximate the spectrometer's field of view. By choosing homogeneous surfaces and averaging over multiple measurements, parts of the problems arising from footprint were addressed in this study. However the matching of the footprint of two different spectrometers can go beyond comparing circles and rectangles due their optical path as recently shown by MacArthur et al. (2012). A more thorough inter-comparison of the ASD and the particular Ocean Optics device employed on the UAV will be required in the future.

RGB and NIR cameras: an empirical line calibration was used for the reflectance factor estimation of both consumer RGB and infrared-modified cameras. Although correlations between the digital cameras and the high-resolution spectrometers exist, they must be treated with caution. This is due to the unknown radiometric response of the cameras, band overlaps and the inherent differences between simple digital cameras and numerical sensors. Both cameras provide imagery with high on-ground resolution, thus enabling identification of in-field variations. In terms of the NIR camera, the wide bandwidth and limited information on the spectral response call for cautious use and further evaluation if the camera is to be used for quantitative vegetation monitoring. At this stage, this study can only suggest that the sensor might be used for support of visual paddock assessment and broadband vegetation indices. Nevertheless, the results demonstrate the opportunities these low-budget sensors offer for simple assessment of vegetation status over large areas using UAVs. If illumination conditions enable an empirical line calibration, reasonable three-band reflectance results can be calculated. Further improvements of radiometric image quality can be expected from fixed settings of shutter speed, ISO, white balance and aperture, as well as for the use of the RAW format. A calibration of lens distortion and vignetting parameters could further increase the quality, especially in the edges of the image (Yu, 2004). However, operational efficiency increases with automatic camera settings which only varied minimally due to the stable illumination conditions at the time of the study.

The empirical line method that was used for reflectance calibration was based on some simplifications. Variations in illumination and atmospheric conditions require frequent calibration image acquisition in order to produce accurate radiometric calibration results. Due to the conservative management of battery power and thus relatively short flight times, only one MCA6 flight was conducted to acquire an image of the calibration tarpaulins and the bare soil. The same restriction applies to the quality of the radiometric calibration of the RGB and IR camera. The use of colour tarpaulin surfaces as calibration targets has implications on the quality of the achieved reflectance calibration in this study. Although they provide low-cost and easy-to-handle calibration surfaces, they are not as spectrally flat as would be needed for a sensor calibration with minimum errors. Moran et al. (2001, 2003) have investigated the use of chemically treated canvas tarpaulins and painted targets in terms of their suitability as stable reference targets for image calibration to reflectance and introduce measures to ensure optimum calibration results. They concluded that specially painted tarps could provide more suitable calibration targets for agricultural applications.

Discrepancies in measured reflectance factors between the UAV STS, the MCA6 and the ASD arise from a combination of factors. Foremost, inherent differences in their spectral and radiometric properties lead to variations in measured reflectance factors. Deviations in footprint matching between the STS spectrometer and the ground measurements, although kept to a minimum, lead to areas of different spatial support and cannot be fully eliminated. Another dimension to this complexity is added by the UAVs and the camera gimbals. Although platform movements were minimal due to the stable environmental conditions and the compensation of any small platform instabilities by the camera gimbals, a small variability in measured radiant flux must be attributed to uncertainties in sensor viewing directions. For a complete cross-calibration between the UAV-based and ground sensors, these potential error sources need to be quantified. Within the context of evaluating sensors for their usability and potential for in-field monitoring of vegetation, those challenges were not addressed in the current study.

In-field data acquisition and flight procedures, one of the key challenges in accommodating four airborne sensors over the same area of interest is accurate footprint matching and minimizing any errors that are introduced by this complexity. Camera gimbals, on board GPS software, piloting skills and waypoint selection maximized footprint matching between sensors. The Falcon-8 UAV was capable of a very stable hover flight over the area of interest while the MikroKopter UAV required manual piloting to ensure that it hovered over the area of interest. The tarpaulin markers were invaluable as a visual aid both during piloting of the UAVs and during subsequent image processing for identifying the footprint areas in each image. Because of the need to select waypoints that were representative for a large area of the paddock, the stable hovering behaviour of the Falcon-8 ensured that the UAV spectrometer's footprint was comparable to the other sensors' field of view. Although the described measures and precautions enabled confident matching of footprints, they can only be applied when working in homogeneous areas of pasture and vegetation cover. Confounding factors, such as soil background influence, large variations in vegetation cover inside the footprint area and strong winds that destabilise the platform, will compromise accurate footprint matching.

When acquiring data with UAVs, responses to changes in environmental conditions, such as increasing wind speeds and cloud presence, need to be immediate. Although specifications from UAV manufacturers attest that the flying vehicles are able to cope with winds of up to 30 km h^{-1}, in reality

the wind speed at which a flight must be interrupted is considerably lower. Platform stability, altitude control and footprint matching accuracy between sensors are compromised under high winds. The fact that two different UAV platforms had been used potentially introduces more variability that cannot be quantified. However, the aforementioned payload restrictions make the use of two different platforms inevitable. Due to the fast progress in UAV platform development, this intricacy is likely to be irrelevant in the future as platforms become more versatile and adaptable to accommodate various sensor requirements.

Technical specifications of UAVs: both UAVs were powered with lithium polymer (LiPo) batteries. A fully charged battery enabled flying times of approximately 10 min for the payload carried. With only four batteries available for each UAV, this lead to a data acquisition time frame of about 40 min per flying platform. However, because turbulence, unplanned take offs and landings and inaccurate GPS positions frequently required revisiting a waypoint, the total number of sample locations that could be investigated between 11:00 and 15:00 LT when illumination conditions were most favourable, was low. This makes thorough flight planning, marking of waypoints and efficient collection of ground reference data essential. Due to the non-availability of power outlets and the time it takes to fully recharge a LiPo battery, battery life limits the time frame in which airborne data can be collected. At the time of the study, higher powered LiPo batteries were still too heavy, thus neutralizing a gain in flight time due to the high weight of the more powerful battery. Those restrictions can slow down data acquisition considerably and the number of ground sampling locations is limited. In the future, improvements in platform stability and electronics as well as higher powered batteries will enable larger ground coverage by UAVs. Using in-field portable charging options such as powered from car batteries can significantly enhance the endurance of rotary wing UAVs.

The evaluated UAV sensors differ in their suitability for deployment in vegetation monitoring and more specifically pasture management applications. While high spectral accuracy is essential for quantifying parameters such as nutritional status in crops and pastures, the high spatial resolution imaging ability of digital cameras can be used to assess paddocks and fields with regard to spatial variations that may not be visible to a ground observer.

Usability of sensors: the UAV STS spectrometer with its high spectral resolution can be used to derive narrowband vegetation indices such as the PRI (photochemical reflectance index) (Suarez et al., 2009) or TSAVI (transformed soil adjusted vegetation index) (Baret et al., 1989). Furthermore, its narrow bands facilitate identification of wavebands that are relevant for agricultural crop characterization (Thenkabail et al., 2002). Once those centre wavelengths have been identified, a more broadband sensor such as the MCA6 could target crop and pasture characteristics with specific filter setups provided the MCA6 performance can be enhanced in terms of radiometric reliability. The consumer digital cameras seem to be useful for derivation of broadband vegetation indices such as the green NDVI (Gitelson et al., 1996) or the GRVI (Motohka et al., 2010). Identification of wet and dry areas in paddocks and growth variations are further applications that such cameras can cover. Imaging sensors that identify areas in a paddock that need special attention are extremely useful, and although they do not provide the high spectral resolution of the UAV STS spectrometer, they do give a visual indication of vegetation status.

Challenges and limitations: deploying UAVs is a promising new approach to collect vegetation data. As opposed to ground-based proximal sensing methods, UAVs offer non-destructive and efficient data collection and less accessible areas can be imaged relatively easy. Moreover, UAVs can potentially provide remote sensing data when aircraft sensors and satellite imagery are unavailable. However, three main factors can cause radiometric inconsistencies in the measurements: sensors, flying platforms and the environment.

The sensors mounted on the UAVs introduce the largest level of uncertainty in the data. Radiometric aberrations across the camera lenses can be addressed by a flat field-correction of the images.

Further factors are camera settings. In this study, shutter speed, exposure time and ISO were set on automatic because of the clear sky and stable illumination conditions. However, to facilitate extraction of radiance values and quantitative information on the vegetation, these settings need to be fixed for all the flights in order to make the images comparable.

The RAW image format is recommended when attempting to work with absolute levels of radiance as it applies the least alterations to pixel digital numbers.

Furthermore, footprint matching between sensors with different sizes and shapes is challenging. While it is straightforward for imaging cameras with rectangular shaped footprints, matching measurements between the UAV STS, ASD and the imaging sensors can only be approximated. While footprint shape is fixed, the size can be influenced by the flying altitude above ground.

However, it is also important to be aware of any bidirectional effects that are introduced as a result of the camera lens' view angle and illumination direction (Nicodemus, 1965).

Although UAV platforms are equipped with gyro-stabilization mechanisms, GPS chips and camera gimbals, an uncertainty remains of whether the camera is in fact pointing nadir and at the target. Slight winds or a motor imbalance can destabilise the UAV system enough to cause the sensor field of view to be misaligned. For imaging sensors this is less of an issue as it is for numerical sensors such as the UAV STS. The live view will only ever be an approximation of the sensor's actual FOV. Careful setting up of the two systems on the camera gimbal and periodical measurement of known targets to align the spectrometer's FOV to the live view camera can help to minimise deviations between FOVs.

The environment also needs to be considered for the collection of robust radiometric data. Even if all other factors are perfect, winds or wobbling of the platform caused by, e.g., a motor imbalance or a bad GPS position hold can cause the sensor to direct its FOV to the wrong spot. In terms of the imaging cameras this is again simple to check after image download whereas the UAV STS data might possibly not show any deviations in the data.

With a good knowledge of the sensors characteristics and the necessary ground references an UAV operator will be able to acquire satisfying data sets, if the environmental conditions are opportune. Based on a tested UAV with known uncertainties in GPS and gimbal accuracy the data set can be quality flagged and approved for further analysis.

4 Conclusions

UAVs are rapidly evolving into easy-to-use sensor platforms that can be deployed to acquire fine-scale vegetation data over large areas with minimal effort. In this study, four optical sensors, including the first available UAV-based microspectrometer were flown over ryegrass pastures and cross-compared. Overall, the quality of the reflectance measurements of the UAV sensors is dependent on thorough data acquisition processes and accurate calibration procedures. The novel high-resolution STS spectrometer operates reliably in the field and delivers spectra that show high correlations to ground reference measurements. For vegetation analysis, the UAV STS holds potential for feature identification in crops and pastures as well as the derivation of narrow-band vegetation indices. Further investigations and cross-calibrations are needed, mainly with regard to the near-infrared measurements in order to establish a full characterization of the system. It was also demonstrated that the six-band MCA6 camera can be used as a low spectral resolution multispectral sensor with the potential to deliver high-resolution multispectral imagery. In terms of its poor radiometric performance in the green and near-infrared filter regions, it is evident that the sensor needs further testing and correction efforts to eliminate the error sources of these inconsistencies. Over sample locations with low vegetation cover and strong soil background interference, the MCA6 image data needs to be processed with caution. Individual filters must be assessed further, with a focus on the green and NIR regions of the electromagnetic spectrum. Any negative effects that depreciate data quality, such as potentially unsuitable calibration targets (coloured tarpaulins) need to be identified and further examined in order to guarantee high quality data. If those issues can be addressed and the sensor is equipped with relevant filters, the MCA6 can become a useful tool for crop and pasture monitoring. The modified Canon infrared and the RGB Sony camera have proven to be easy-to-use sensors that deliver instant high-resolution imagery covering a large spatial area. No spectral calibration has been performed on those sensors, but factory spectral information allowed converting digital numbers to a ground reflectance factor. Near-real-time assessment of variations in vegetation cover and identification of areas of wetness/dryness as well as calculation of broadband vegetation indices can be achieved using these cameras. A number of issues have been identified during the field experiments and data processing. Exact footprint matching between the sensors was not achieved due to differences in the FOVs of the sensors, instabilities in UAV platforms during hovering and potential inaccuracies in viewing directions of the sensors due to gimbal movements. Although those differences in spatial scale reduce the quality of sensor intercomparison, it must be stated that under field conditions a complete match of footprints between sensors is not achievable. For the empirical line calibration method that was applied to the MCA6 and the digital cameras, we propose the use of spectrally flat painted panels for radiometric calibration rather than tarpaulin surfaces. To reduce complexity of the experiment and keep the focus on the practicality of deploying multiple sensors on UAVs, the influence of directional effects has been neglected.

The field protocols developed allow for straightforward field procedures and timely coordination of multiple UAV-based sensors as well as ground reference instruments. The more autonomously the UAV can fly, the more focus can be put on data acquisition. Piloting UAVs in a field where obstacles such as power lines and trees are present requires the full concentration of the pilot and at least one support person to observe the flying area. Due to technical restrictions, the total area that can be covered by rotary wing UAVs is still relatively small, resulting in a point sampling strategy. Higher powered, lightweight batteries on UAVs can allow for more frequent calibration image acquisition and the coverage of natural calibration targets, thus improving the radiometric calibration. Differences in UAV specifications and capabilities lead to the UAVs having a specific range of applications that they can undertake reliably.

As shown in this study even after calibration efforts, biases and uncertainties remain and must be carefully evaluated in terms of their effects on data accuracy and reliability. Restrictions and limitations imposed by flight equipment must be carefully balanced with scientific data acquisition protocols. The different UAV platforms and sensors each have their strengths and limitations that have to be managed by matching platform and sensor specifications and limitations to data acquisition requirements. UAV-based sensors can be quickly deployed in suitable environmental conditions and thus enable the timely collection of remote sensing data. The specific applications that can be covered by the presented UAV sensors range from broad visual identification of paddock areas that require increased attention to the identification of waveband-specific biochemical crop and pasture properties on a fine spatial scale. With the development of sensor-specific data processing chains, it is possible to generate data sets for agricultural decision making within a few

hours of data acquisition and thus enable the adjustment of management strategies based on highly current information.

Acknowledgements. The research was supported by a Massey University doctoral scholarship granted to S. von Bueren and a travel grant from COST ES0903 EUROSPEC to A. Burkart. The authors acknowledge the funding of the CROP.SENSe.net project in the context of Ziel 2-Programmes NRW 2007–2013 "Regionale Wettbewerbsfähigkeit und Beschäftigung (EFRE)" by the Ministry for Innovation, Science and Research (MIWF) of the state of North Rhine–Westphalia (NRW) and European Union Funds for regional development (EFRE) (FKZ 005-1012-0001) while collaborating on the preparation of the manuscript.

All of us were shocked and saddened by the tragic death of Stefanie von Bueren on 25 August. We remember her as an enthusiastic adventurer and aspiring researcher.

Edited by: M. Rossini

This publication is supported by COST – www.cost.eu

References

Aber, J. S., Aber, S. W., Pavri, F., Volkova, E., and Penner II, R. L.: Small-format aerial photography for assessing change in wetland vegetation, Cheyenne Bottoms, Kansas, Transactions of the Kansas Academy of Science, 109, 47–57, doi:10.1660/0022-8443(2006)109[47:sapfac]2.0.co;2, 2006.

Baret, F., Guyot, G., and Major, D. J.: TSAVI: A Vegetation Index Which Minimizes Soil Brightness Effects On LAI And APAR Estimation, Geoscience and Remote Sensing Symposium, 1989, IGARSS'89, 12th Canadian Symposium on Remote Sensing, International, 1355–1358, 1989.

Baugh, W. M. and Groeneveld, D. P.: Empirical proof of the empirical line, Int. J. Remote Sens., 29, 665–672, doi:10.1080/01431160701352162, 2008.

Bayer, B. E.: Color imaging array, 1976.

Berni, J., Zarco-Tejada, P., Surez, L., González-Dugo, V., and Fereres, E.: Remote sensing of vegetation from uav platforms using lightweight multispectral and thermal imaging sensors, The International Archives of the Photogrammetry, Remote Sensing and Spatial Information Sciences, XXXVII, 2008.

Berni, J. A. J., Zarco-Tejada, P. J., Suarez, L., and Fereres, E.: Thermal and Narrowband Multispectral Remote Sensing for Vegetation Monitoring From an Unmanned Aerial Vehicle, Ieee T. Geosci. Remote, 47, 722–738, doi:10.1109/Tgrs.2008.2010457, 2009.

Burkart, A., Cogliati, S., Schickling, A., and Rascher, U.: A novel UAV-based ultra-light weight spectrometer for field spectroscopy, Sensors Journal, IEEE, 14, 62–67, doi:10.1109/jsen.2013.2279720, 2013.

Carrara, M., Comparetti, A., Febo, P., and Orlando, S.: Spatially variable rate herbicide application on durum wheat in Sicily, Biosys. Eng., 87, 387–392, 2004.

Chávez, J. L., Pierce, F. J., Elliott, T. V., Evans, R. G., Kim, Y., and Iversen, W. M.: A remote irrigation monitoring and control system (RIMCS) for continuous move systems. Part B: Field testing and results, Precis. Agric., 11, 11–26, 2010.

Duan, M., Gao, Q., Wan, Y., Li, Y., Guo, Y., Ganzhu, Z., Liu, Y., and Qin, X.: Biomass estimation of alpine grasslands under different grazing intensities using spectral vegetation indices, Can. J. Remote Sens., 37, 413–421, 2011.

Gitelson, A. A., Kaufman, Y. J., and Merzlyak, M. N.: Use of a green channel in remote sensing of global vegetation from EOS-MODIS, Remote Sens. Environ., 58, 289–298, 1996.

Hirakawa, K., Wolfe, P. J., and Ieee: Spatio-spectral color filter array design for enhanced image fidelity, in: 2007 Ieee International Conference on Image Processing, Vols 1–7, IEEE International Conference on Image Processing ICIP, 645–648, 2007.

Hueni, A., Nieke, J., Schopfer, J., Kneubühler, M., and Itten, K. I.: The spectral database SPECCHIO for improved long-term usability and data sharing, Comput. Geosci., 35, 557–565, doi:10.1016/j.cageo.2008.03.015, 2009.

Hunt, E. R., Hively, W. D., Fujikawa, S. J., Linden, D. S., Daughtry, C. S. T., and McCarty, G. W.: Acquisition of NIR-Green-Blue Digital Photographs from Unmanned Aircraft for Crop Monitoring, Remote Sens., 2, 290–305, doi:10.3390/Rs2010290, 2010.

Jensen, T., Apan, A., Young, F., and Zeller, L.: Detecting the attributes of a wheat crop using digital imagery acquired from a low-altitude platform, Comput. Electron. Agr., 59, 66–77, doi:10.1016/j.compag.2007.05.004, 2007.

Kawamura, K., Sakuno, Y., Tanaka, Y., Lee, H.-J., Lim, J., Kurokawa, Y., and Watanabe, N.: Mapping herbage biomass and nitrogen status in an Italian ryegrass (Lolium multiflorum L.) field using a digital video camera with balloon system, J. Appl. Remote Sens., 5, 053562, doi:10.1117/1.3659893, 2011.

Kelcey, J. and Lucieer, A.: Sensor Correction of a 6-Band Multispectral Imaging Sensor for UAV Remote Sensing, Remote Sens., 4, 1462–1493, 2012.

Kenta, T. and Masao, M.: Radiometric calibration method of the general purpose digital camera and its application for the vegetation monitoring, Land Surf. Remote Sens., 8524, doi:10.1117/12.977211, 2012.

Kuusk, J.: Dark Signal Temperature Dependence Correction Method for Miniature Spectrometer Modules, J. Sens., 2011, 608157, 2011.

Lebourgeois, V., Bégué, A., Labbé, S., Mallavan, B., Prévot, L., and Roux, B.: Can commercial digital cameras be used as multispectral sensors? A crop monitoring test, Sensors, 8, 7300–7322, 2008.

Lebourgeois, V., Begue, A., Labbe, S., Houles, M., and Martine, J. F.: A light-weight multi-spectral aerial imaging system for nitrogen crop monitoring, Precis. Agric., 13, 525–541, doi:10.1007/s11119-012-9262-9, 2012.

Lelong, C. C. D., Burger, P., Jubelin, G., Roux, B., Labbe, S., and Baret, F.: Assessment of unmanned aerial vehicles imagery for quantitative monitoring of wheat crop in small plots, Sensors, 8, 3557–3585, doi:10.3390/S8053557, 2008.

Link, J., Senner, D., and Claupein, W.: Developing and evaluating an aerial sensor platform (ASP) to collect multispectral data for deriving management decisions in precision farming, Comput. Electron. Agr., 94, 20–28, doi:10.1016/j.compag.2013.03.003, 2013.

MacArthur, A., MacLellan, C. J., and Malthus, T.: The fields of view and directional response functions of two field spectroradiometers, IEEE Geosci. Remote Sens., 50, 3892–3907, 2012.

Moran, M. S., Bryant, R. B., Clarke, T. R., and Qi, J. G.: Deployment and calibration of reference reflectance tarps for use with airborne imaging sensors, Photogram. Eng. Rem. S., 67, 273–286, 2001.

Moran, S., Fitzgerald, G., Rango, A., Walthall, C., Barnes, E., Bausch, W., Clarke, T., Daughtry, C., Everitt, J., Escobar, D., Hatfield, J., Havstad, K., Jackson, T., Kitchen, N., Kustas, W., McGuire, M., Pinter, P., Sudduth, K., Schepers, J., Schmugge, T., Starks, P., and Upchurch, D.: Sensor development and radiometric correction for agricultural applications, Photogram. Eng. Rem. S., 69, 705–718, 2003.

Motohka, T., Nasahara, K. N., Oguma, H., and Tsuchida, S.: Applicability of green-red vegetation index for remote sensing of vegetation phenology, Remote Sensing, 2, 2369–2387, 2010.

Mutanga, O.: Hyperspectral remote sensing of tropical grass quality and quantity, Hyperspectral remote sensing of tropical grass quality and quantity, x + 195 pp.-x + 195 pp., 2004.

Mutanga, O. and Skidmore, A. K.: Red edge shift and biochemical content in grass canopies, ISPRS J. Photogram., 62, 34–42, doi:10.1016/j.isprsjprs.2007.02.001, 2007.

Nebiker, S., Annen, A., Scherrer, M., and Oesch, D.: A Lightweight Multispectral Sensor for Micro UAV – Opportunities for Very High Resolution Airborne Remote Sensing, XXI ISPRS Congress. Beijing, China, 2008.

Nijland, W., de Jong, R., de Jong, S. M., Wulder, M. A., Bater, C. W., and Coops, N. C.: Monitoring plant condition and phenology using infrared sensitive consumer grade digital cameras, Agr. Forest Meteorol., 184, 98–106, doi:10.1016/j.agrformet.2013.09.007, 2014.

Olsen, D., Dou, C., Zhang, X., Hu, L., Kim, H., and Hildum, E.: Radiometric Calibration for AgCam, Remote Sens., 2, 464–477, doi:10.3390/rs2020464, 2010.

Primicerio, J., Di Gennaro, S. F., Fiorillo, E., Genesio, L., Lugato, E., Matese, A., and Vaccari, F. P.: A flexible unmanned aerial vehicle for precision agriculture, Precis. Agric., 13, 517–523, doi:10.1007/s11119-012-9257-6, 2012a.

Primicerio, J., Di Gennaro, S. F., Fiorillo, E., Genesio, L., Lugato, E., Matese, A., and Vaccari, F. P.: A flexible unmanned aerial vehicle for precision agriculture, Precis. Agric., 13, 1–7, 2012b.

Pullanagari, R. R., Yule, I. J., Hedley, M. J., Tuohy, M. P., Dynes, R. A., and King, W. M.: Multi-spectral radiometry to estimate pasture quality components, Precis. Agric., 13, 442–456, doi:10.1007/s11119-012-9260-y, 2012a.

Pullanagari, R. R., Yule, I. J., Tuohy, M. P., Hedley, M. J., Dynes, R. A., and King, W. M.: In-field hyperspectral proximal sensing for estimating quality parameters of mixed pasture, Precis. Agric., 13, 351–369, doi:10.1007/s11119-011-9251-4, 2012b.

Rango, A., Laliberte, A., Herrick, J. E., Winters, C., Havstad, K., Steele, C., and Browning, D.: Unmanned aerial vehicle-based remote sensing for rangeland assessment, monitoring, and management, J. Appl. Remote Sens., 3, 033542, doi:10.1117/1.3216822, 2009.

Sakamoto, T., Gitelson, A. A., Nguy-Robertson, A. L., Arkebauer, T. J., Wardlow, B. D., Suyker, A. E., Verma, S. B., and Shibayama, M.: An alternative method using digital cameras for continuous monitoring of crop status, Agr. Forest Meteorol., 154, 113–126, doi:10.1016/j.agrformet.2011.10.014, 2012.

Sanches, I. D., Tuohy, M. P., Hedley, M. J., and Mackay, A. D.: Seasonal prediction of in situ pasture macronutrients in New Zealand pastoral systems using hyperspectral data, Int. J. Remote Sens., 34, 276–302, doi:10.1080/01431161.2012.713528, 2012.

Seelan, S. K., Laguette, S., Casady, G. M., and Seielstad, G. A.: Remote sensing applications for precision agriculture: A learning community approach, Remote Sens. Environ., 88, 157–169, 2003.

Smith, G. M. and Milton, E. J.: The use of the empirical line method to calibrate remotely sensed data to reflectance, Int. J. Remote Sens., 20, 2653–2662, doi:10.1080/014311699211994, 1999.

Stafford, J. V.: Implementing precision agriculture in the 21st century, J. Agr. Eng. Res., 76, 267–275, 2000.

Suarez, L., Zarco-Tejada, P. J., Berni, J. A. J., Gonzalez-Dugo, V., and Fereres, E.: Modelling PRI for water stress detection using radiative transfer models, Remote Sens. Environ., 113, 730–744, doi:10.1016/j.rse.2008.12.001, 2009.

Swain, K. C., Thomson, S. J., and Jayasuriya, H. P. W.: Adaption of an unmanned helicopter for low altitude remote sensing to estimate yield and total biomass of a rice crop, Trans. ASABE, 53, 21–27, 2010.

Thenkabail, P. S., Smith, R. B., and De Pauw, E.: Evaluation of narrowband and broadband vegetation indices for determining optimal hyperspectral wavebands for agricultural crop characterization, Photogram. Eng. Rem. S., 68, 607–621, 2002.

Turner, D. J.: Development of an Unmanned Aerial Vehicle (UAV) for hyper-resolution vineyard mapping based on visible, multispectral and thermal imagery, School of Geography & Environmental Studies Conference 2011, 2011.

Van Alphen, B. and Stoorvogel, J.: A methodology for precision nitrogen fertilization in high-input farming systems, Precis. Agric., 2, 319–332, 2000.

Vanamburg, L. K., Trlica, M. J., Hoffer, R. M., and Weltz, M. A.: Ground based digital imagery for grassland biomass estimation, Int. J. Remote Sens., 27, 939–950, doi:10.1080/01431160500114789, 2006.

Vescovo, L., Wohlfahrt, G., Balzarolo, M., Pilloni, S., Sottocornola, M., Rodeghiero, M., and Gianelle, D.: New spectral vegetation indices based on the near-infrared shoulder wavelengths for remote detection of grassland phytomass, Int. J. Remote Sens., 33, 2178–2195, doi:10.1080/01431161.2011.607195, 2012.

Yu, W.: Practical anti-vignetting methods for digital cameras, IEEE Transactions on Consumer Electronics, 50, 975–983, 2004.

Zhang, C. and Kovacs, J. M.: The application of small unmanned aerial systems for precision agriculture: a review, Precis. Agric., 13, 693–712, doi:10.1007/s11119-012-9274-5, 2012.

A3: Angular dependency of hyperspectral measurements over wheat characterized by a novel UAV based goniometer

Authors Contribution

Scientific work and development: 100%

Field work and analysis: 70%

Publication work: 70%

Remote Sens. **2015**, *7*, 725-746; doi:10.3390/rs70100725

OPEN ACCESS

remote sensing

ISSN 2072-4292

www.mdpi.com/journal/remotesensing

Article

Angular Dependency of Hyperspectral Measurements over Wheat Characterized by a Novel UAV Based Goniometer

Andreas Burkart [1,*,†], Helge Aasen [2,†], Luis Alonso [3], Gunter Menz [4,5], Georg Bareth [2] and Uwe Rascher [1]

[1] Research Center Jülich, Institute of Bio- and Geosciences, IBG-2: Plant Sciences, 52428 Jülich, Germany; E-Mail: u.rascher@fz-juelich.de

[2] Department of Geoscience, Working Group GIS and Remote Sensing, University of Cologne, 50923 Cologne, Germany; E-Mails: helge.aasen@uni-koeln.de (H.A.); g.bareth@uni-koeln.de (G.B.)

[3] Laboratory of image processing, University of Valencia, 46980 Paterna, Spain; E-Mail: luis.alonso@uv.es

[4] Department of Geography, Remote Sensing Research Group, University of Bonn, 53001 Bonn, Germany; E-Mail: g.menz@uni-bonn.de,

[5] Center for Remote Sensing for Land Surfaces, University of Bonn, 53113 Bonn, Germany

[†] These authors contributed equally to this work.

[*] Author to whom correspondence should be addressed; E-Mail: an.burkart@fz-juelich.de; Tel.: +49-2461-61-8084.

Academic Editors: Arko Lucieer and Prasad S. Thenkabail

Received: 27 October 2014 / Accepted: 4 January 2015 / Published: 12 January 2015

Abstract: In this study we present a hyperspectral flying goniometer system, based on a rotary-wing unmanned aerial vehicle (UAV) equipped with a spectrometer mounted on an active gimbal. We show that this approach may be used to collect multiangular hyperspectral data over vegetated environments. The pointing and positioning accuracy are assessed using structure from motion and vary from σ = 1° to 8° in pointing and σ = 0.7 to 0.8 m in positioning. We use a wheat dataset to investigate the influence of angular effects on the NDVI, TCARI and REIP vegetation indices. Angular effects caused significant variations on the indices: NDVI = 0.83–0.95; TCARI = 0.04–0.116; REIP = 729–735 nm. Our analysis highlights the necessity to consider angular effects in optical sensors when observing vegetation. We compare the measurements of the UAV goniometer to the angular modules of the SCOPE radiative transfer model. Model and measurements are in high accordance

(r^2 = 0.88) in the infrared region at angles close to nadir; in contrast the comparison show discrepancies at low tilt angles (r^2 = 0.25). This study demonstrates that the UAV goniometer is a promising approach for the fast and flexible assessment of angular effects.

Keywords: hyperspectral; unmanned aerial vehicle (UAV); vegetation; bidirectional reflectance distribution function (BRDF); goniometer; vegetation indices

1. Introduction

Spectral radiometers (spectrometers) reach beyond the capabilities of human vision and enable scientists to retrieve diverse information from reflected light. Field spectroscopic measurements have a long history [1] and are nowadays a common investigative tool in various research areas. Moreover, spectral vegetation analysis from air- or spaceborne platforms is a mature technology, and is commonly used for the accurate derivation of land cover classes [2]. Hyperspectral measurements, which consist of continuous narrow spectral bands, help to retrieve information about the biophysical and biochemical components of vegetation [3–5] and may be used to discriminate healthy or stressed plants [6,7].

With their synoptic view, airborne and spaceborne imaging sensors typically capture a large swath. Discrete image elements (pixels) located in the geometric center of an image are commonly acquired from a nadir view angle, whereas pixels at image edges are recorded from oblique angles. Off-nadir view geometry depends on the field of view (FOV) specifications and measurement methodology and varies among sensor systems; MODIS, for example is imaging ±55° off nadir [8].

The bidirectional reflectance distribution function (BRDF) is the conceptual framework that explains changes in reflectance that result from view angle changes dependent on surface property and illumination [9,10]. BRDF influence is not desirable in a nadir image, as it impacts reflectance values recorded by the sensor and complicates the compositing of multiple images or flight lines. However, angular or off-nadir imaging can complement nadir image data by integrating additional spectral information. In forest environments, for example, an oblique view will—depending on the stand density—detect less reflectance from tree crowns and more from tree trunks [11,12]. Lack of knowledge in effects created from different sun-sensor geometries throughout the vegetation season have for instance led to incorrect greening estimates from satellite data in the Amazon rainforest, as recently shown by Morton *et al.* [13].

The need for BRDF correction, along with an interest in angular characteristics, has led to the development of various goniometric measurement approaches. These are able to exploit a center point from multiple view angles. The most common approach utilizes a semi-automated goniometer equipped with a point spectrometer with a radius of one meter or larger [14–16]. On larger scales the POLDER and MISR instruments and the orbiting sensor Chris/Proba are capable of retrieving spectral data of the same area from different angles during one or multiple overpasses [17,18]. On a smaller scale Comar *et al.* [19] used a conoscope to assess the BRDF of wheat at leaf surface level. This technique allows characterizing the reflectance of small leaf structures, such as veins. Such multiangular measurements are necessary to accumulate knowledge regarding vegetation cover BRDF characteristics.

The fundamental goal of these research efforts is to develop a model capable of predicting the BRDF of a known vegetation cover type as well as the other way round, to derive knowledge about unidentified vegetation cover from multiangular measurements. Various models have been introduced in the past to estimate BRDF on a mathematical or empirical basis [20,21], or to compute the aggregate energy balance of a vegetation canopy including radiative transfer, as done in the SCOPE (Soil-Canopy-Observation of Photosynthesis and the Energy balance) model [22].

Using these methods, an effective theoretical understanding of the BDRF was developed for flat and accessible land cover like snow or soil [23]. The small size of common goniometers along with their small FOV made the BRDF characterization of other important land cover types (including forest or agriculture) difficult [24] or impossible. Forest and agriculture land covers are of particular significant scientific and economic interest, and alternative analytic approaches are necessary to allow BRDF measurements on larger scales and within inaccessible areas.

Some recent studies have investigated UAVs as a novel platform for goniometric measurements. Burkhart *et al.* [25] performed a survey over ice fields using a fixed-wing UAV equipped with an on-board spectrometer. Principally due to maneuvering and incident wind, the flight patterns of this platform introduced banking levels of up to ±30°, causing the spectrometer to collect multiangular hyperspectral measurements of numerous points that were overflown. A more defined method was presented by Hakala *et al.* [26] and Honkavaara *et al.* [27], who deployed a rotary-wing UAV equipped with a stabilized gimbal mounting RGB and multispectral camera, respectively. Utilizing specific flight patterns, multiangular information could be derived in the bands of the given camera.

To fully understand the BRDF effects of vegetation, we suggest that an optimized dataset providing a comprehensive understanding of multiple agricultural sites would consist of frequent multiangular hyperspectral measurements acquired at a number of different locations throughout a complete vegetation phenological cycle. Only airborne platforms can fulfill these requirements without disturbing crop growth by physically stepping through the field or casting shadows within the sensor FOV. With their recent development and improving utility and stability, UAVs can be employed as platforms for multi-angular remote data collection.

The main focus of this study is to introduce a way of collecting multiangular hyperspectral data over almost every kind of terrain and scale with a flying spectrometer. The approach combines the benefits of goniometers equipped with a high-resolution spectrometer and the flexibility of UAV platforms. We then demonstrate the acquisition and analysis of a datasets to explore BRDF effects over wheat. The angular dependency of reflectance as measured with the UAV goniometer was also compared to the reflectance modeled by SCOPE.

2. Material and Methods

The Falcon-8 octocopter UAV (Ascending Technology, Krailing, Germany) was used in this study. This platform was chosen due to its accurate flight controls and inherent stability. A hyperspectral measurement system was integrated on the UAV [28]. This instrument was recently developed at the interdisciplinary Research Center Jülich (Forschungszentrum Jülich GmbH) and is based on the STS-VIS spectrometer (Ocean Optics Inc. Dunedin, USA). The FOV of this spectrometer is

approximately 12°; spectral resolution was at a full width at half maximum (FWHM) of 3 nm, with 256 spectral bands (4 pixel spectrally binned) within the range of 338 to 823 nm.

The Falcon-8 was originally designed as a camera platform for photographers and video production. It is equipped with a camera mount whose angle can be set during flight within 1° increments. The vertical angle (tilt) is defined by the camera mount, while the horizontal angle (heading) is determined by UAV orientation. The position and navigation is done by combining the GPS information from a navigation grade GPS (Ublox LEA 6T) and the information of the orientation information of the sensors onboard the UAV. Wind gusts during the flight are counteracted by an active system, which stabilizes the camera by pitch and roll. The spectrometer is also equipped with a RGB camera, which feeds a live video stream to the operator to facilitate operation and allow proper aiming of the system.

Airborne hyperspectral target reflectance measurements were performed with the UAV spectrometer wirelessly synchronized with a second spectrometer on the ground. Latter measured a white reference (Spectralon®) to adapt to changing illumination. A thorough calibration of the hyperspectral system was performed following the procedure described by Burkart, *et al.* [28]. This process included dark current correction [29], spectral shift, dual spectrometer cross-calibration and additional quality checks using the SpecCal tool [30]. Our approach allows to compute the ratio of light reflected by the target surface to the hemispherical illumination (diffuse-, ambient-, and direct-sunlight) as reflected by the white reference and is termed a hemispherical/conical reflectance factor. The actual BRDF is thus only approximated by this approach. Schaepman-Strub *et al.* [10] provide a comprehensive BRDF description and nomenclature.

2.1. Flight Pattern

Grenzdörffer and Niemeyer [31] demonstrated that a distinct hemispherical flight pattern is necessary to enable goniometric measurements using an UAV-based airborne RGB camera. The flight pattern accurately defines the position of the UAV as well as the aiming of the camera. The flight path of the UAV is selected to follow waypoints (WP) in a hemisphere and the angle and heading of the spectrometer is set to continuously point towards the center of the hemisphere. In this manner the center of the hemisphere is measured from different viewing angles.

To quickly compute such flight patterns for UAVs, we developed the software mAngle. It was written in the platform independent open source language “Processing” and is freely available as source code and compiled versions [32]. mAngle calculates the desired WP around a given center GPS coordinate. Placement of the WP are optimized for speed, as the UAV can quickly change horizontal position but requires more time to climb vertically to a different altitude. Flight pattern parameters including number of WP, initial angle, and hemisphere diameter can be set as desired (Figure 1). A designated flight pattern can be exported as a *.kml file to Google Earth (Google Inc., Mountain View, CA, USA) for visualization. The flight pattern can also be exported as a *.csv file, the format used by the Falcon-8 flight planning software (AscTec Autopilot Control V1.68). Such a hemispheric flight pattern is also useful to acquire pictures around a center object of interest for 3D reconstruction.

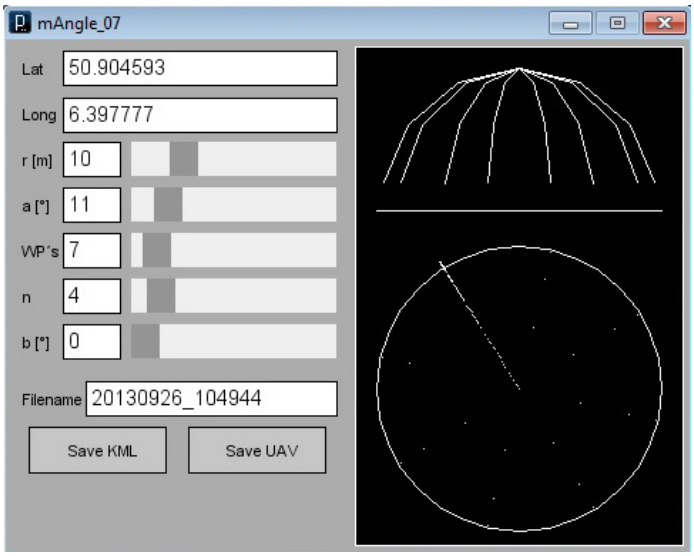

Figure 1. Graphical user interface of the *mAngle* software with input fields for the desired waypoint pattern. By setting radius, number of desired waypoints as well as starting angle and other parameters, a distinct goniometric flight pattern can be generated. A draft of the waypoint pattern is visualized in the right box of the program window.

2.2. Accuracy of the Unmanned Aerial Vehicle (UAV) Goniometer

To assess the positioning and pointing accuracy of the UAV goniometer the spectrometer was replaced by a high resolution RGB camera (NEX 5n, Sony, 16 mm lens) mounted on a similar active stabilized gimbal. In this configuration the UAV was flown following the same waypoint pattern as was used for a multi-angular spectrometer flight. In operation, the airborne spectrometer is triggered three times at each WP. The RGB camera also acquired three digital images at each WP (84 in total). Eleven ground control points (GCPs) were distributed within the covered area and registered using a differential GPS (Topcon HiPer Pro, Topcon). 3D reconstruction software (Agisoft Photoscan, version 1.0.4) was used to structure the spatial arrangement of the scene and georeference it with the GCPs. This rendering was calculated with a resolution of 3.53 mm/pixel and an average error of 1.46 pixels. The camera position and view angles for each individual image were exported and served as an estimator for the spatial accuracy of the UAV under operational conditions.

2.3. Field Campaign

Two multiangular flights (referred to as MERZ1, MERZ2) were conducted over farmland (Lat 50.93039, Lon 6.29689) on 18 June 2013 during the ESA-HyFlex campaign in Merzenhausen, Germany. The two flights were performed under cloud-free moderate wind (1.6–5.5 m/s) conditions with an interval of two hours—one hour before and one hour after solar noon (Table 1). At the time of the study, the field contained mature wheat, with fully developed but still green ears (Figure 2). The centroid of the hemispherical waypoint pattern was located within the field in an area of uniform cover, avoiding farm equipment tracks and trails. The center point was defined using aerial imagery, in order to avoid disturbing measurements by walking into the area of interest. The two datasets produced

in this campaign are freely available via SPECCHIO [33] at the server of the University of Zuerich under the campaign name "Merzen".

Figure 2. Wheat (*Triticum aestivum*) at the study site Merzenhausen, Germany, at the time of the multiangular flights, 18 June 2013. Ears were fully developed but still green.

Table 1. Local time and duration with the corresponding sun angle parameters for the two hyperspectral flights performed over wheat field in Merzenhausen, Germany.

Flight	Start Time	Duration	Sun Azimuth	Sun Elevation
MERZ1	12:43	09 min	155°	61°
MERZ2	14:47	11 min	213°	59°

For these flights a hemisphere with a radius of 16 m was specified. The spectrometer has a FOV of 12°. The areal coverage of each measurement is a function of sensor tilt angle, encompassing here 9 m^2 at nadir up to 30 m^2 with 20° tilt. WPs around the hemisphere were set to cover vertical tilt angles of 90° (nadir), 66°, 43° and 20°, at 8 equally distributed heading angles, potentially producing a total of 28 WPs. However, nadir measurements were only acquired at four different headings, which were then merged into a single WP, leading to a total of 25 WPs included in the analysis. In the following individual WPs will be identified as WP (tilt degree, heading degree). The spectrometer was activated three times at each WP to allow averaging and assessment of response variance. MERZ1 required a flight time of nine minutes, and MERZ2 required eleven minutes to consecutively measure the WP pattern. An additional UAV flight was conducted over the target using an RGB camera (NEX 5n, Sony Corporation, Minato, Japan, 16 mm lens) to image each WPs (Figure 3).

2.4. Data Preprocessing

Each spectrum captured from the UAV was transformed to reflectance using the reference spectra simultaneously measured by the ground spectrometer. Then, for each WP, the mean, standard deviation and coefficient of variation were calculated from the three measured spectra. All further analyses were based on the mean spectra. To analyze the data with regard to the tilt and heading angle, averaged values were calculated depending on the parameter of interest. Additionally, to analyze relative changes in reflectance, spectra from all measurement positions were normalized using the nadir spectra response

values [34]. The resulting normalized nadir anisotropy factor ($ANIF_{band}$) produces a coefficient for each band, which individually adjusts (increases or decreases) reflectance factor values for each spectral band in relation to those recorded at nadir (Equation A). Thus, an ANIF factor of one describes an identical reflectance as recorded for a given band at nadir, while values above or below one describe higher or lower reflectance than the nadir value.

$$ANIF_{band} = \frac{Reflectance(tilt, heading)_{band}}{Reflectance(NADIR)_{band}} \quad \text{(A)}$$

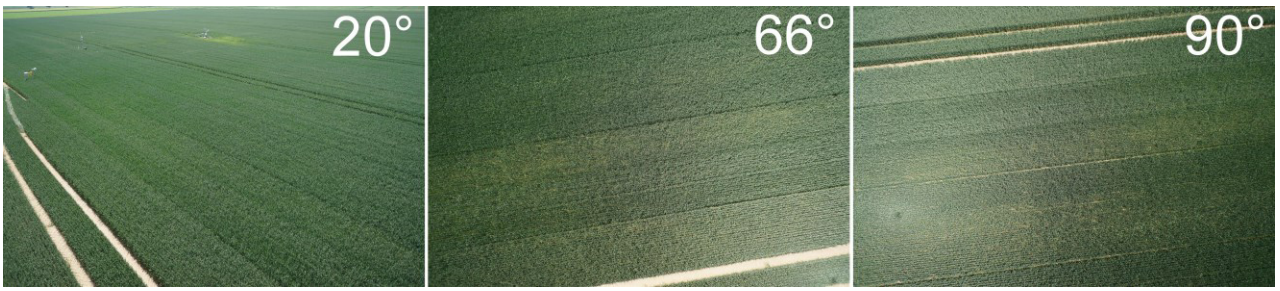

Figure 3. Example Red-Green-Blue (RGB) images with tilt angles of 20°, 66° and 90°. These images were acquired at the Merzenhausen site at approximately 13:30 following a multiangular flight path identical to the spectrometer flights. The Field-Of-View (FOV) of the RGB camera is 73.7° × 53.1° (compared to the 12° FOV of the airborne spectrometer) and allows observing multiangular effects within a single image–the bright hotspot with the shadow of the unmanned aerial vehicle in the center, located in the lower left corner of the 90° image is an example.

2.5. Vegetation Indices

Broadband vegetation indices (VIs) have an extensive history in remote sensing. Together with their hyperspectral counterparts they are still widely used in vegetation studies [35,36]. VIs commonly ratio near-infrared (NIR) and red band reflectance values in order to compensate for influences of different illumination conditions or background materials. To investigate the effect of the BRDF we examined three common Vis (Table 2) and calculated their values for all WPs. The Normalized Difference Vegetation Index (NDVI) uses two wavelengths in the red and NIR domain and has been widely used in a diverse range of applications. In our study we used the NDVI as proposed by Blackburn *et al.* [37]. As a second index we used the Transformed Chlorophyll Absorption in Reflectance Index (TCARI) developed by Haboudane *et al.* [38]. TCARI was developed to predict chlorophyll absorption and uses wavelengths in the green, red and NIR spectral regions. The last index used in this study is the Red Edge Inflection Point (REIP). Originally introduced by Guyot *et al.* [39] it characterizes the inflection in the spectral red edge by calculating the wavelength with maximum slope. It has been used to quantify leaf chlorophyll content [40].

Table 2. Vegetation indices used in this study and their underlying formulas.

Index	Formula	Reference
NDVI	(R800 − R680)/(R800 + R680)	Blackburn *et al.* 1998
TCARI	3 × ((R700 – R760) – 0.2 × (R700 – R550) × (R700/R670))	Haboudane *et al.* 2002
REIP	700 + 40 × (((R667 + R782)/2) – R702)/(R738 – R702))	Guyot *et al.* 1988

2.6. Data Visualization

Several different visualizations or graphics were used in this study to focus on specific features under investigation. An effective method for assessing multiangular measurements includes the use of a segmented circular display known as a "polar plot". The polar plot shown here in Figure 4 represents the UAV headings and sensor tilt angles within a circular matrix and illustrates the intensity of the measurement values by applying a color to each segment. To provide an useful overview of the dataset of this study and to include as well a comparison of the reflectance in the spectral domain, multiple plots are necessary.

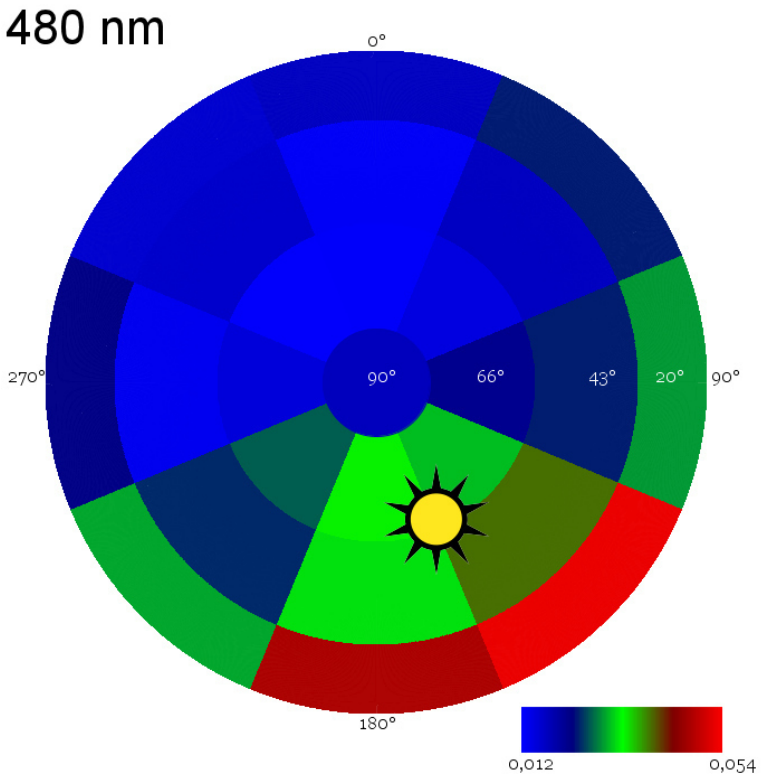

Figure 4. Reflectance of wheat at 480 nm measured at all 25 waypoints shown as a circular graph, or polar plot. Each "slice" represents a heading while each ring represents a sensor tilt angle. Spectral reflectance magnitude is color coded from low values of light blue, to high values in bright red. The angular position of the sun is depicted by the sun-symbol. In this figure no interpolation between waypoints is performed.

2.7. Radiative Transfer Model Comparison

To compare the multiangular UAV measurements to modeled data, the SCOPE radiative transfer model was tested. The model generates the spectrum of outgoing radiation in the viewing direction as a function of vegetation structure [22]. SCOPE input parameters were derived through comparison of the MERZ1 nadir spectrum with a lookup table of SCOPE spectra generated using a permutation of input parameters that were expected from wheat at the present phenological state. The resulting best-fit parameters are shown in Table 3.

Table 3. Soil-Canopy-Observation of Photosynthesis and the Energy balance model (SCOPE) input parameters: Leaf Area Index (LAI), Leaf Inclination (LIDFa), Chorophyll A/B (Cab) content in µg/cm^2, Leaf Thickness Parameter (N), Leaf water equivalent layer (Cw) in cm, Dry matter content (Cdm) in g/cm^2, Senescent material fraction (Cs), Variation in leaf inclination (LIDFb). Default values were used for all other SCOPE input parameters.

Fitted Parameters				Constant Parameters			
LAI	LIDFa	Cab	N	Cw	Cdm	Cs	LIDFb
3.5	−0.35	95	1.5	0.004	0.005	0.15	−0.15

Using the input parameters above, the angular module of SCOPE was run to estimate the reflectance spectra at identical angles as those measured with the UAV goniometer. Sun azimuth and zenith angles were set to match the values present at the time of the MERZ1 measurements.

3. Results

In this section we first present the results of the accuracy assessment of the UAV goniometer. We then summarize the results of the analysis of the MERZ1 dataset and the influence of the BRDF on the full hyperspectral data as well as on the vegetation indices. Then the BRDF effects of MERZ1 are compared to the MERZ2 dataset. Finally, we compare the data derived from the UAV goniometer with results of the SCOPE radiative transfer model.

3.1. Accuracy Assessment of the Unmanned Aerial Vehicle (UAV) Goniometer

Table 4 shows the deviation of the UAVs actual position from the planned position. Definitions of altitude and position in X and Y dimensions are commonly accepted. However, to describe the functions of vehicle and sensor heading and tilt angle, several different definitions exist. Figure 5 shows how heading and tilt angles were used in this study with the UAV and its spectrometer system. The average deviation in heading and tilt may differ slightly from the actual UAV spectrometer pointing error, as a small error may have been introduced during the process of replacing the spectrometer with the RGB camera in the gimbal mount using a tripod screw.

Table 4. Accuracy of the unmanned aerial vehicle (UAV) heading and spatial positioning calculated by structure from motion using 75 high-resolution images. Nine images were unusable due to motion induced "blur" and excluded from processing. Heading and tilt columns represent the deviation of the cameras actual pointing direction to the programmed angle. Altitude, X- and Y-position describe the deviation of the UAVs position as calculated from the differential-Global-Positioning-System ground-referenced structure from motion approach compared to the programmed waypoints.

Deviation of:	Heading (°)	Camera Tilt (°)	Altitude (m)	Position X (m)	Position Y (m)
Average	0.11	6.07	0.03	−1.15	−2.22
SD	8.67	1.22	0.70	0.68	0.82
Max	26.20	9.74	1.44	0.67	−0.39
Min	−17.99	3.68	−1.09	−2.79	−4.60

Movements of the airborne platform cause slight variations in the footprint of the spectrometer and introduce minor differences in the individual measurements at each waypoint. Figure 6 shows the average coefficient of variation (CV) of the spectral measurements acquired at all WP during the MERZ1 flight. CV values within the blue and red regions of the spectrum are between 5% and 6%; in the green portion the value is approximately 4%. The CV in the NIR is less than 1.5%.

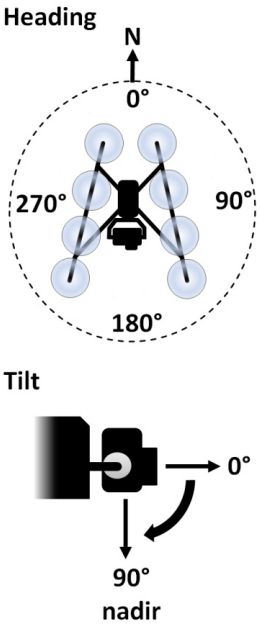

Figure 5. Camera orientation: Heading (azimuth) of the spectral measurements expressed in angular degrees from north. To assume a view angle of 0°, the Unmanned Aerial Vehicle *(*UAV*)* will hover north of the centeroid and aim the spectrometer at 180°. Tilt: 0° = horizontal and 90° = nadir view.

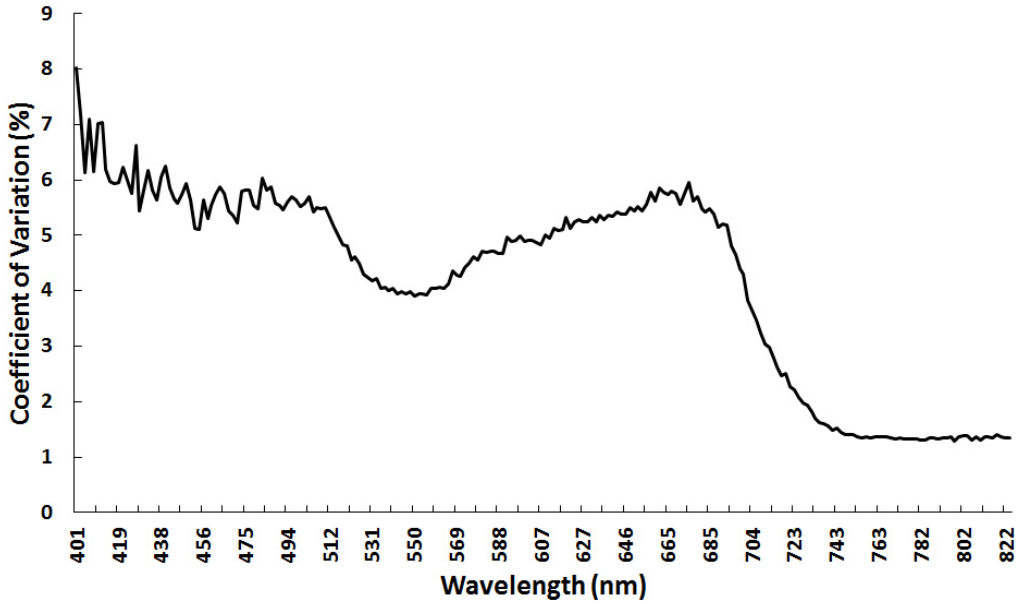

Figure 6. The spectrometer of the unmanned aerial vehicle goniometer was triggered three times at each waypoint. This figure shows the overall variation of the three spectra measured at each waypoint as average for the MERZ1 dataset.

3.2. Full Spectrum Analysis

In Figure 7 the ANIF for the MERZ1 dataset is shown for a tilt of 66°. All spectral measurements acquired at headings between 90° and 225° exceed nadir values, with the largest increases seen in measurements taken within the blue spectral region. When heading parameters are examined, the 180° heading shows an increase of approximately 95% (the highest). The 90° measurement shows the lowest increase at approximately 25%. Deviation for these headings show a gradual decrease until the red edge position where values for 135°, 180° and 225° headings drop to range between 25% and 30%. For all these WP, the deviation decreases in the green spectral region. At headings of 0°, 45°, 270° and 315° reflectance measurements are 10% to 30% lower than nadir within the blue spectra. Until the red edge spectral region is reached, reflectance values decrease from 20% to 40% below the nadir measurement. In the red edge region the reflectance increases to approximately 10% above that of the nadir measurement.

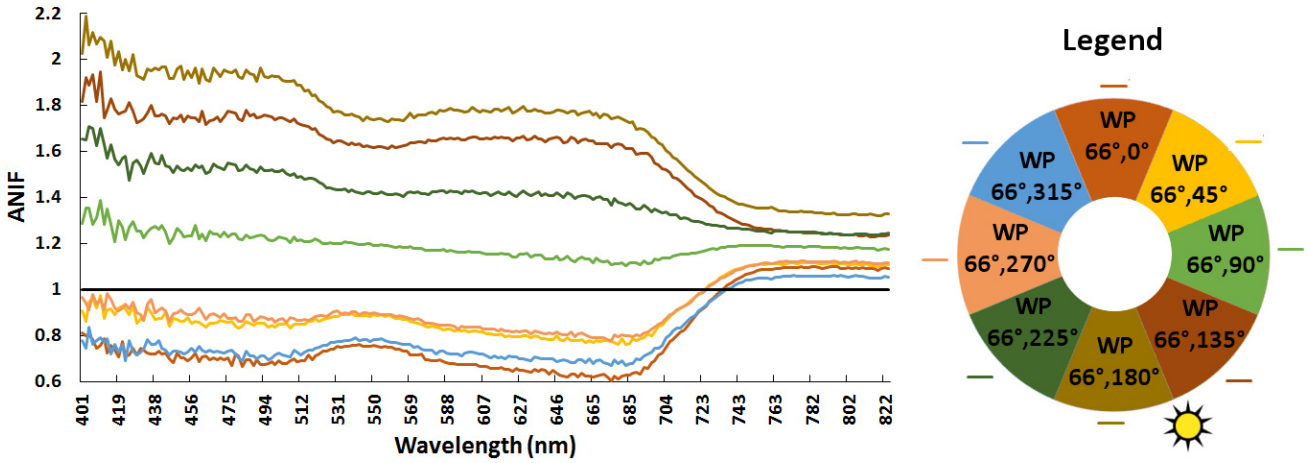

Figure 7. To present the angular influence at different waypoints on the full spectrum the normalized nadir anisotropy factor (ANIF) of 66° tilt for all headings at MERZ1 from 400 to 823 nm is plotted as example. By using the ANIF notation spectral deviation of single waypoints is referred to the nadir waypoint and thus can be relatively compared. A waypoint with the same spectrum as nadir would remain at an ANIF of 1 throughout all wavelengths. The legend on the right represents the color of each ANIF curve and depicts their respective heading angle. The azimuth position of the sun (155°) is visualized by the sun symbol.

This shape of the ANIF which was observed for the 66° sensor tilt angle can also be found for the other tilt angles used in the overflights. Figure 8 shows the ANIF for five regions of the spectrum for all investigated tilt and heading angles. For all wavelengths the ANIF decreases with increase of the tilt angle. Only for most of the VIS region with heading from 180° to 270° the ANIF is smaller in the 43° tilt than in the 66°. On average the reflectance of the 135° and 180° show the highest increase from nadir with 191% and 181%, respectively. Lower reflectance values than in nadir are seen in the VIS spectral region with headings of 0°, 45°, 270° and 315°. At 0° and 315° even the average of all tilt reflection values is lower than in nadir.

		heading								
tilt	nm	0°	45°	90°	135°	180°	225°	270°	315°	average
20°	481	0.98	1.36	1.66	3.02	2.71	1.69	1.26	0.91	1.70
43°	481	0.72	0.98	1.36	2.24	1.83	1.39	0.76	0.93	1.28
66°	481	0.71	0.83	1.22	1.74	1.93	1.52	0.86	0.70	1.19
20°	550	1.12	1.35	1.58	2.71	2.49	1.63	1.32	1.09	1.66
43°	550	0.86	1.04	1.35	2.09	1.76	1.39	0.85	0.99	1.29
66°	550	0.76	0.89	1.19	1.62	1.74	1.42	0.90	0.78	1.16
20°	681	0.74	1.08	1.32	2.51	2.31	1.33	0.98	0.70	1.37
43°	681	0.59	0.81	1.15	1.96	1.56	1.21	0.60	0.77	1.08
66°	681	0.63	0.79	1.12	1.63	1.74	1.38	0.81	0.69	1.10
20°	733	1.27	1.34	1.43	1.89	1.81	1.44	1.34	1.26	1.47
43°	733	1.17	1.22	1.35	1.64	1.52	1.35	1.13	1.18	1.32
66°	733	0.99	1.05	1.18	1.33	1.41	1.27	1.05	0.98	1.16
20°	780	1.27	1.30	1.36	1.61	1.56	1.37	1.29	1.26	1.38
43°	780	1.25	1.27	1.33	1.49	1.42	1.32	1.25	1.25	1.32
66°	780	1.10	1.11	1.19	1.25	1.34	1.25	1.12	1.06	1.18
	average	0.94	1.09	1.32	1.91	1.81	1.40	1.03	0.97	

Figure 8. Normalized nadir anisotropy factor (ANIF) values for five characteristic wavelengths in the blue (480 nm), green (550 nm), red (680 nm) spectral bands; red-edge-inflection-point (REIP) (733 nm) and near-infrared (NIR) (780 nm) for 20°, 43° and 66° tilt, as well as all headings together with their average values. Values greater than 1 (blue bar) represent spectral reflectance measurements greater than nadir; values below 1 (red bar) represent measurements less than nadir. The suns azimuth was 155° and elevation 66°.

3.3. Vegetation Indices

NDVI values range from 0.83 (WP 20°, 135°) to 0.95 (WP 43°, 0°), compared to the nadir value of 0.89. Values decrease for each tilt angle as the 135° heading is approached and generally increase toward the 0° heading, with an increase seen only at the WP (43°, 270°). On average, the 43° tilt yields the highest NDVI value with 0.92 (within a range of 0.86–0.95) while the 20° and 66° tilt parameters show an average NDVI of 0.9 (0.83–0.94, and 0.86–0.94, respectively). Relative differences from nadir NDVI range between −6.5% and 6.2%. The relative mean absolute difference is 3.3 percent. The 90° and the 225° headings show the smallest differences from the nadir NDVI. Aside from the 135° and 180° headings, all WPs return higher NDVI values when compared with the nadir position. The tilt angle has only a minor influence on the relative difference (Figure 9).

TCARI values vary with UAV heading, ranging from 0.04 (WP 66°, 315°) to 0.116 (WP 20°, 135°), against a nadir value of 0.046. This pattern is opposite as observed for NDVI. Vehicle heading values vary systematically, increasing (for all tilt angles) towards 135° and decreasing as the 0° heading is approached. As seen for the NDVI, WP (43°, 270°) poses an exception with a lower TCARI value.

Sensor tilt parameter variability can be briefly summarized. The 20° tilt setting shows the highest mean TCARI value of 0.078 (within a range of 0.06–0.116); the 43° setting yields a mean TCARI value of 0.062 (with a range of 0.046–0.090) and the 66° tilt shows mean TCARI of 0.053 (range 0.038–0.074). In relative terms, the differences from the nadir TCARI range from −16.8% to

153.2%. The relative mean absolute difference is 40%. Most WPs greatly surpass the nadir TCARI value; at a sensor tilt of 20° no TCARI value is smaller than the nadir value at 43° only a single value is smaller and at tilt = 66° four values are smaller than the nadir value. The tilt parameter is shown to have a significant influence on the relative difference. From 20° to 60° the relative mean absolute difference decreases from 69% to 25% (Figure 9 bottom).

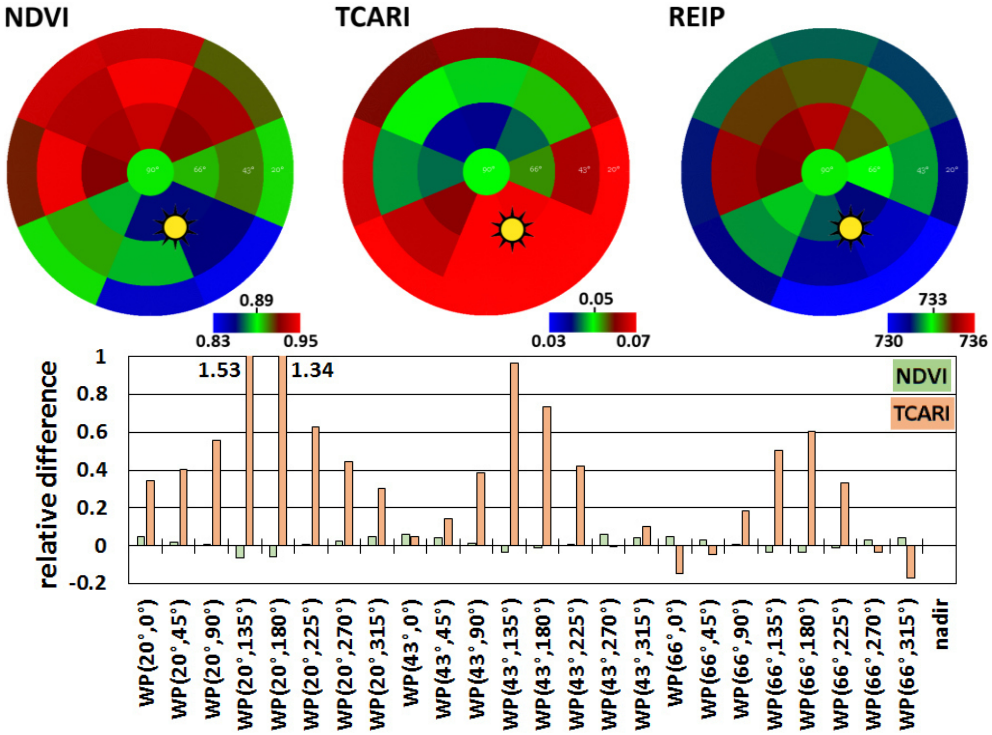

Figure 9. (**Top**) Absolute values for the NDVI, TCARI and REIP compared to the nadir value (center of the polar plot) for all waypoints of MERZ1. The range of values is chosen with nadir as center value, respectively, for each plot. Figure 5 details the angular arrangement depicted here. (**Bottom**) Relative differences for NDVI and TCARI compared to the nadir value.

The Red Edge Inflection Point (REIP) was also analyzed in this study (Figure 9). For nadir spectral measurements the REIP is approximately 733 nm. WP (20°, 135°) shows the lowest REIP (approximately 729 nm) while WP (66°, 0°) shows the highest REIP (735 nm). The average REIP value was slightly lower than the nadir value with 732.5 nm. At all WPs, measurements acquired at a heading of 135° show the lowest values; these increase towards the 0° heading. All the WPs measured with a sensor tilt angle of 20° surpass the nadir REIP. Measurements acquired at tilts of 43° and 66° produced two, respectively, 4 values that are smaller than the nadir value. The overall mean absolute difference was less than 0.2%, decreasing from approximately 0.3% at 20° tilt to 0.15% at 66° tilt.

3.4. Diurnal Variations of Angular Effects

Ideal clear weather conditions were present over the Merzenhausen study area throughout 18 June 2013. Sequencing a pair of overflights enabled us to compare these two datasets and analyze how the change in sun illumination affects multiangular sensor response (Figure 10). Nadir measurements remained consistent during the day. However, significant changes in target response

(including hotspot and backscattering features) were observed at lower sensor tilt angles, dependent on sun position (Table 1). These features show distinct spectral differences within the five different wavelengths (Figures 7 and 8). The hotspot feature is clearly visible and is characterized by higher spectral reflectance values within the shorter blue and green wavelengths. These spectral differences are less apparent in the infrared wavelengths.

Figure 10 shows the angular distribution of reflectance in five selected wavelengths of interest: 480 nm (blue), 550 nm (green), 680 nm (red), 733 nm (Red-REIP) and 780 nm (NIR). All bands show the directional effect of increased reflectance values as heading angles approach 180°, and decreased reflectance with the opposite orientation. This effect is most pronounced in the shorter spectral wavelengths (up to 680 nm) and is less characteristic in the NIR region. Angular distribution differs in MERZ1 and MERZ2. Elevated reflectance values cluster between 135° and 180° headings in the MERZ1 dataset, while in MERZ2 this phenomena is oriented to heading angles between 180° and 225°.

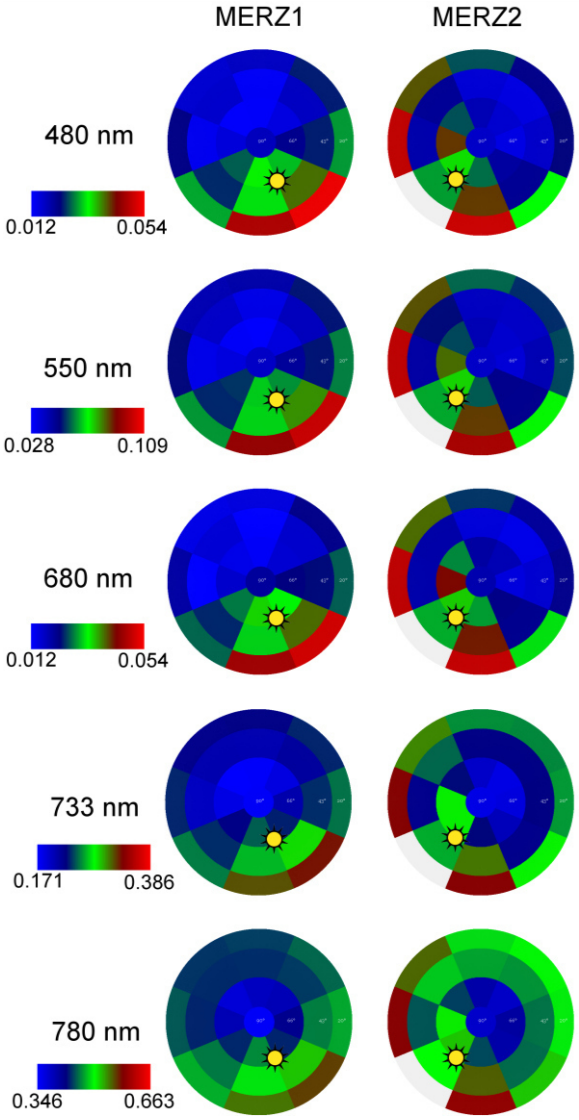

Figure 10. Reflection of MERZ1 and MERZ2 for 5 wavelengths of interest. The color legend of reflection for each horizontal pair was scaled to the occurring reflectance wavelength range. Figure 5 details the angular arrangement depicted here. Waypoint (20°, 225°) is missing in MERZ2 and coded in this graphic in grey.

3.5. Flying Goniometer vs. Radiative Transfer Model

Results of the comparison between the scope model and the flying spectrometer measurements are shown in Figure 11 for exemplary wavelengths of 550 nm and 780 nm.

Correlation of angular measurements with modeled data show clear differences in wavelengths and tilt angles. To test this hypothesis, ANIF values were calculated for both datasets. Our comparison included sensor tilt angles of 66°, 43° and 20° and wavelengths at 480 nm, 570 nm, 680 nm and 750 nm. Correlation statistics (r^2) were calculated for the linear regression of UAV-ANIF against SCOPE-ANIF. While SCOPE produces results similar to UAV measurements at high tilt angles, r^2 is low at the 20° angle (Table 5).

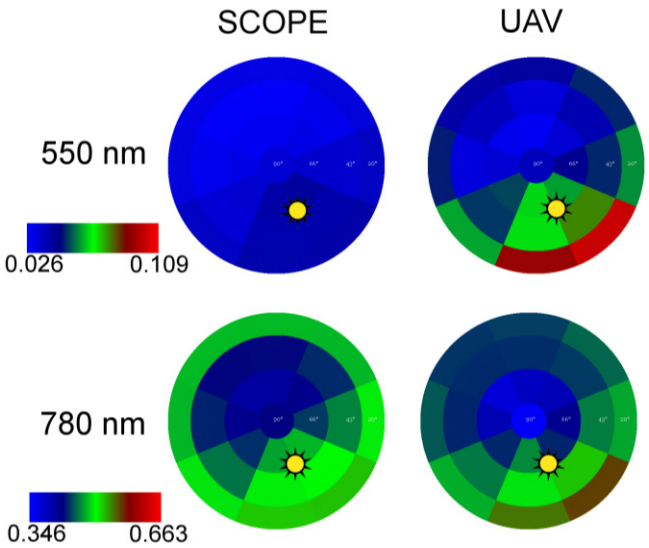

Figure 11. Comparison of modeled angular reflectance Soil-Canopy-Observation of Photosynthesis and the Energy balance (SCOPE) with the unmanned aerial vehicle (UAV) measured values for MERZ1. Shown are two exemplary wavelengths, which are scaled to the present range of values.

Table 5. Correlation of modeled data with measured data for different tilt angles.

Tilt	20°	43°	66°
Correlation (r^2)	0.2504	0.7484	0.8819

In the spectral domain the maximum UAV reflectance/SCOPE model r^2 was found in the NIR (750 nm); the lowest correlation value was derived for the 680 nm spectral wavelength (Table 6).

Table 6. Correlation of modeled data with measured data for all tilt angles at specific wavelengths.

Wavelength	480 nm	570 nm	680 nm	750 nm
Correlation (r^2)	0.4298	0.5685	0.3605	0.815

4. Discussion

In this study, a new goniometer approach for large-scale measurement of BRDF is presented and an initial hyperspectral dataset is analyzed. By deploying the spectrometer on a rotary-wing UAV there is no longer a need to mount the instrument on large ground-based positioning structures. The large FOV has the advantage of averaging out small variations, which are part of the canopies variability. As the device is flying, surfaces can be investigated with desired measurement patterns even over areas inaccessible by land and without disturbing the eventual surface cover like vegetation. Until now these areas had to be approached using satellites or by modeling [41]. In remote sensing applications, where goniometers cannot be deployed, angular effects are currently minimized or correction approaches are applied: Field-spectrometer measurements are carried out around the same time (noon) and from nadir view [5]. Thus the sun-object-sensor geometry is almost stable. For UAV-, air- and spaceborne systems a number of correction methods have been developed. These include the use of image statistic based methods for flat terrain [42] and physical or semi-empirical models such as for the processing of MODIS data [43]. Lately, a more generic BRDF correction method was introduced, which builds on a surface cover characterization [44]. Since physical and empirical models are based on the current knowledge and BRDF effects depend on many factors, the flying goniometer could help to evaluate and eventually improve the correction methods.

We assessed the pointing accuracy of the UAV system and found it to be of acceptable accuracy for a GPS-aided flying system, although it is still not as precise as ground-based instrumentation [34,45]. Parameters of altitude, X/Y position and sensor tilt angle are highly accurate within the navigation grade GPS specifications. Additionally, the remounting of the RGB camera described in Section 2.2 might have introduced an artificial error. The relative position as described by the low standard deviation demonstrates the precision of the system (Table 4). However, the vehicle heading parameters are less accurate. Relative heading inaccuracies may be ascribed to the Falcon-8 flight control system, which does not make use of a magnetic compass. If operated in an environment with a strong magnetic field, a compass system could produce serious errors in vehicle position and heading readings and cause catastrophic UAV failures. However, in the case of the UAV goniometer, the accuracy would improve through the use of a compass system for heading correction.

Additional sources of error in the platform/sensor system are found in gimbal calibration in the tilt axis and during the process of physically mounting the spectrometer on the gimbal. Inconsistencies in either one or both of these procedures will lead to pointing offsets. The system could also be improved by deploying the spectrometer and a RGB camera in tandem, triggering both simultaneously. Camera and spectrometer could be aligned and calibrated in the laboratory to determine the spectrometer field of view in the camera image. The camera imagery could then be utilized to accurately calculate the position and pointing of the UAV using the structure from motion approach used in this study to evaluate the pointing accuracy (Section 2.2).

The UAV system in combination with the "mAngle" software enables users to plan, setup and perform a multiangular flight around a center point of interest efficiently and quickly (in less than 30 min, 10 min for the measurement flight itself). In addition, the UAV and spectrometer system is deployed in a single, easily portable package, making it highly mobile. Since the completion of this study, the system has been deployed at a number of other sites in Europe and New Zealand.

The large radius and thus big footprint of the UAV ensures a good averaging over the fine structure of the vegetation (e.g., leaves, shaded areas, stems). This was assessed by calculating standard deviation of multiple spectra at the same waypoint (Figure 6) and shows good agreement of consecutive spectra taken at the same WP. If smaller footprints are desired the flying radius can be reduced or the spectrometer can be equipped with a fore optic with a narrower FOV.

The results of the multiangular reflectance measurements acquired in this study are consistent with previous measurements characterizing common angular reflectance distribution over vegetation [46]. The common hotspot feature is clearly visible in the data and changes over time with sun angle. High levels of reflectance were found at the rather low tilt angle of 20° in the heading of the hotspot. As the tilt angle is lower than the hotspot feature, these high levels might be introduced by a viewing angle, whereas only the very top of the canopy is seen by the sensor (Figure 9). Along with the results of our accuracy assessment of UAV imagery pointing and of the spectral domain response, we are confident that we have utilized a novel platform-sensor combination to acquire a valid and valuable hyperspectral dataset.

The complete spectrum analysis emphasizes that BRDF effects are both wavelength and angle dependent. Around the hot spot the measured reflection is higher than in nadir, in both in the VIS and NIR part of the spectrum. For WPs towards the dark spot the reflectance is lower in most parts of the VIS and higher in the NIR. Overall, lower sensor tilt angles increase reflectance compared with the nadir position. While the NDVI reduces angular effects quite efficiently, these effects were a significant factor in TCARI. This distinction can be ascribed primarily to the differing formula structures of the two VIs. For the NDVI, the reflectance in the NIR dominates the nominator of the formula. Thus the differences due to the observation angle influence the index nominator and denominator in similar ways and the entire ratio only slightly changes. The TCARI formula does not provide such normalization. The reflection factors at the wavelength of the first part of the term (R700–R760) are differently influenced by the angle (Figure 8) and introduce strong fluctuations to the VI. Minor influences are introduced by the second term. The first part (R700–R550) of the second term is not strongly influenced, since both reflection factors of the wavelengths are affected similarly by the angle. However, the second component of TCARI again uses the R700 and R760 band ratio. This increases the variations in the second term of the formula caused by the differing observation angles. In combination, these factors produce the significant differences (up to 150 percent), which are seen in the TCARI values. Differing observation angles cause only minor fluctuations in REIP values. As seen with NDVI, formula deviation normalizes most of the variation in REIP values. However, it must be emphasized that, as for most VIs, the practical dynamic range of the REIP is narrower than what is theoretically possible. Thus even the small observation angle variances suggested by the REIPs results could lead to errors in interpreting this index if BRDF effects are disregarded. Other studies have been carried out for other VIs or vegetation cover [47–50] support the angular dependency found in this study.

Radiative transfer models show significant potential as tools for correcting angular influences introduced by solar effects or imaging sensors. They are based on existing theory of radiative transfer and plant physiology [22]. So far, real world multiangular data for various vegetation covers are rare and thus, a rigorous validation of the model is challenging. With the approach described in this study datasets for the validation and improvement of those methods may be generated. However, it has to be taken into account that SCOPE does not account for certain sensor variables such as FOV and FWHM. Due to the

footprint of the spectrometer, light reflected at different angles by the canopy is collected by the sensor. Thus, this might be one source for the increasing discrepancies towards low tilt angles observed in this study. Following studies could minimize this effect by using spectrometer fore optics with narrower FOV. A careful investigation on the difference between modeled and measured spectra go beyond the scope of this study but should be investigated in the future.

Based on this study, we strongly encourage the extensive compilation of multiangular datasets for various vegetation cover types and environments. A more sophisticated knowledge base regarding vegetation angular effects could also enable researchers to derive accurate complementary information through the use of angular measurements that capture vegetation features not typically visible from a nadir perspective [12]. Additionally, these results could help to understand influences of BRDF effects in imaging spectroscopy. Typically, current hyperspectral (image-frame and push broom) imaging systems as well as RGB systems have a FOV of up to 50° [35]. Thus, pixels captured towards the edges of the image have tilt angles of about 66°. As shown here, angular effects have a significant contribution to these observation angles and need to be taken into account during analysis. To improve the correction of these effects consecutive studies should examine tilt angles found in the FOV of common UAV and airborne sensors. This is foreseen within a number of parallel research activities that are ongoing and focused on improving models and collecting spectral databases. These include COST Action ES0903 EUROSPEC, COST Action ES1309 OPTIMISE, and the SPECCHIO online spectral database [33]. These projects could also serve as a basis for enhanced training of models leading to highly accurate correction methods.

5. Conclusions

This study presents a novel hyperspectral (338 to 823 nm) goniometer system based on an unmanned aerial vehicle (UAV) and specifically developed software. The approach allows measurements over inaccessible areas and without disturbing the surface cover. Using the system in an exemplary field experiment, we test the positioning and spectral accuracy (VIS < 6% CV, NIR < 1.5% CV) While a larger footprint can be analyzed, this UAV system does not provide the same absolute pointing accuracy as common ground based goniometers. With the presented field data we highlight the influence of angular effects on the spectrum (0.6 to 3 fold relative difference) and vegetation indices (up to more than 1.5 fold relative difference) and thus the necessity for correction of angular effects in remote sensing data. Radiative transfer models like SCOPE represent an opportunity for angular corrections, but differ especially for low tilt angles from the UAV goniometer data. The fast and flexible UAV goniometer contributes a technique to assess angular effects over any given land cover with low efforts. Based on this assessment of relevant reflection parameters a new way of UAV-driven plant parameter retrieval by the inclusion of oblique angels could be developed. Finally, we hope to contribute additional understanding to the broad and complex topic of BRDF in vegetation.

Acknowledgments

The authors thank Christian van der Tol for the preparation of the SCOPE exercise used in this study. Also, the authors acknowledge the funding of the CROP.SENSe.net and PhenoCrops project in the context of the Ziel 2-Programms NRW 2007–2013 “Regionale Wettbewerbsfähigkeit und Beschäftigung”

by the Ministry for Innovation, Science and Research (MIWF) of the state North Rhine Westphalia (NRW) and European Union Funds for regional development (EFRE) (005-1103-0018). We also acknowledge the contribution of Mr. Joseph Scepan of Medford, Oregon, USA, in producing this document.

Author Contributions

Andreas Burkart developed the measurement system and participated in data analysis that was designed and led by Helge Aasen. Luis Alonso created multiangular flight patterns and contributed practical expertise in bidirectional effects characterization and spectrometer calibration. Gunter Menz gave essential scientific advice and contributed a major part of lecturing of the manuscript. Georg Bareth participated in spectral data analysis and interpretation and discussion of the results. Uwe Rascher did supervise the methodologies and provided the fundamental question that led to the research.

Conflicts of Interest

The authors declare no conflict of interest.

References

1. Milton, E.J. Review article principles of field spectroscopy. *Remote Sens.* **1987**, *8*, 1807–1827.
2. Tian, Y.; Dickinson, R.E.; Zhou, L.; Zeng, X.; Dai, Y.; Myneni, R.B.; Knyazikhin, Y.; Zhang, X.; Friedl, M.; Yu, H. Comparison of seasonal and spatial variations of leaf area index and fraction of absorbed photosynthetically active radiation from Moderate Resolution Imaging Spectroradiometer (MODIS) and Common Land Model. *J. Geophys. Res* **2004**, *109*, doi:10.1029/2003JD003777.
3. Gnyp, M.L.; Yu, K.; Aasen, H.; Yao, Y.; Huang, S.; Miao, Y.; Bareth, G. Analysis of crop reflectance for estimating biomass in rice canopies at different phenological Stages Reflexionsanalyse zur Abschätzung der Biomasse von Reis in unterschiedlichen phänologischen Stadien. *Photogramm. Fernerkund. Geoinf.* **2013**, *2013*, 351–365.
4. Yu, K.; Leufen, G.; Hunsche, M.; Noga, G.; Chen, X.; Bareth, G. Investigation of leaf diseases and estimation of chlorophyll concentration in seven barley varieties using fluorescence and hyperspectral indices. *Remote Sens.* **2013**, *6*, 64–86.
5. Aasen, H.; Gnyp, M.L.; Miao, Y.; Bareth, G. Automated hyperspectral vegetation index retrieval from multiple correlation matrices with hypercor. *Photogramm. Eng. Remote Sens.* **2014**, *80*, 785–795.
6. Penuelas, J.; Pinol, J.; Ogaya, R.; Filella, I. Estimation of plant water concentration by the reflectance water index WI (R900/R970). *Int. J. Remote Sens.* **1997**, *18*, 2869–2875.
7. Mahlein, A.K.; Rumpf, T.; Welke, P.; Dehne, H.W.; Plümer, L.; Steiner, U.; Oerke, E.C. Development of spectral indices for detecting and identifying plant diseases. *Remote Sens. Environ.* **2013**, *128*, 21–30.
8. Barnes, W.L.; Pagano, T.S.; Salomonson, V.V. Prelaunch characteristics of the moderate resolution imaging spectroradiometer (MODIS) on EOS-AM1. *IEEE Trans. Geosci. Remote Sens.* **1998**, *36*, 1088–1100.

9. Nicodemus, F.E. Directional reflectance and emissivity of an opaque surface. *Appl. Opt.* **1965**, *4*, 767–773.
10. Schaepman-Strub, G.; Schaepman, M.E.; Painter, T.H.; Dangel, S.; Martonchik, J.V. Reflectance quantities in optical remote sensing—Definitions and case studies. *Remote Sens. Environ.* **2006**, *103*, 27–42.
11. Fassnacht, F.; Koch, B. Review of forestry oriented multi-angular remote sensing techniques. *Int. For. Rev.* **2012**, *14*, 285–298.
12. Schlerf, M.; Atzberger, C. Vegetation structure retrieval in beech and spruce forests using spectrodirectional satellite data. *IEEE J. Sel. Top. Appl. Earth Obs. Remote Sens.* **2012**, *5*, 8–17.
13. Morton, D.C.; Nagol, J.; Carabajal, C.C.; Rosette, J.; Palace, M.; Cook, B.D.; Vermote, E.F.; Harding, D.J.; North, P.R.J. Amazon forests maintain consistent canopy structure and greenness during the dry season. *Nature* **2014**, *506*, 221–224.
14. Peltoniemi, J.I.; Kaasalainen, S.; Naranen, J.; Matikainen, L.; Piironen, J. Measurement of directional and spectral signatures of light reflectance by snow. *IEEE Trans. Geosci. Remote Sens.* **2005**, *43*, 2294–2304.
15. Bourgeois, C.S.; Ohmura, A.; Schroff, K.; Frei, H.-J.; Calanca, P. IAC ETH goniospectrometer: A tool for hyperspectral HDRF measurements. *J. Atmos. Ocean. Technol.* **2006**, *23*, 573–584.
16. Buchhorn, M.; Petereit, R.; Heim, B. A Manual transportable instrument platform for ground-based spectro-directional observations (ManTIS) and the resultant hyperspectral field goniometer system. *Sensors* **2013**, *13*, 16105–16128.
17. Deschamps, P.-Y.; Bréon, F.-M.; Leroy, M.; Podaire, A.; Bricaud, A.; Buriez, J.-C.; Seze, G. The POLDER mission: Instrument characteristics and scientific objectives. *IEEE Trans. Geosci. Remote Sens.* **1994**, *32*, 598–615.
18. Barnsley, M.J.; Settle, J.J.; Cutter, M.A.; Lobb, D.R.; Teston, F. The PROBA/CHRIS mission: A low-cost smallsat for hyperspectral multiangle observations of the Earth surface and atmosphere. *IEEE Trans. Geosci. Remote Sens.* **2004**, *42*, 1512–1520.
19. Comar, A.; Baret, F.; Viénot, F.; Yan, L.; de Solan, B. Wheat leaf bidirectional reflectance measurements: Description and quantification of the volume, specular and hot-spot scattering features. *Remote Sens. Environ.* **2012**, *121*, 26–35.
20. Qin, W.; Goel, N.S. An evaluation of hotspot models for vegetation canopies. *Remote Sens. Rev.* **1995**, *13*, 121–159.
21. Andrieu, B.; Baret, F.; Jacquemoud, S.; Malthus, T.; Steven, M. Evaluation of an improved version of SAIL model for simulating bidirectional reflectance of sugar beet canopies. *Remote Sens. Environ.* **1997**, *60*, 247–257.
22. Tol, C.; Verhoef, W.; Timmermans, J.; Verhoef, A.; Su, Z. An integrated model of soil-canopy spectral radiances, photosynthesis, fluorescence, temperature and energy balance. *Biogeosciences* **2009**, *6*, 3109–3129.
23. Nolin, A.W.; Liang, S. Progress in bidirectional reflectance modeling and applications for surface particulate media: Snow and soils. *Remote Sens. Rev.* **2000**, *18*, 307–342.
24. Deering, D.W.; Eck, T.F.; Banerjee, B. Characterization of the reflectance anisotropy of three boreal forest canopies in spring–summer. *Remote Sens. Environ.* **1999**, *67*, 205–229.

25. Burkhart, J.F.; Bogren, W.S.; Storvold, R.; Pedersen, C.A.; Gerland, S. A new measure of BRDF, banking on UAS measurements. In Proceedings of the AGU Fall Meeting Abstracts, San Francisco, CA, USA, 13 December 2010; Volume 1, p. 3.
26. Hakala, T.; Suomalainen, J.; Peltoniemi, J.I. Acquisition of bidirectional reflectance factor dataset using a micro unmanned aerial vehicle and a consumer camera. *Remote Sens.* **2010**, *2*, 819–832.
27. Honkavaara, E.; Markelin, L.; Hakala, T.; Peltoniemi, J. The metrology of directional, spectral reflectance factor measurements based on area format imaging by UAVs. *Photogramm. Fernerkund. Geoinform.* **2014**, *2014*, 175–188.
28. Burkart, A.; Cogliati, S.; Schickling, A.; Rascher, U. A novel UAV-Based ultra-light weight spectrometer for field spectroscopy. *IEEE Sens. J.* **2014**, *14*, 62–67.
29. Kuusk, J. Dark signal temperature dependence correction method for miniature spectrometer Modules. *J. Sens.* **2011**, *2011*, doi:10.1155/2011/608157.
30. Busetto, L.; Meroni, M.; Crosta, G.F.; Guanter, L.; Colombo, R. SpecCal: Novel software for in-field spectral characterization of high-resolution spectrometers. *Comput. Geosci.* **2011**, *37*, 1685–1691.
31. Grenzdörffer, F.N. UAV based BRDF-measurements of agricultural surfaces with pfiffikus. In Proceedings of the UAV-g 2011, Conference on Unmanned Aerial Vehicle in Geomatics, Zurich, Switzerland, 14 September 2011; Volume XXXVI, pp. 1–6.
32. mAngle. Available online: https://github.com/wemperor/mAngle/releases (accessed on 8 January 2015).
33. Hueni, A.; Nieke, J.; Schopfer, J.; Kneubühler, M.; Itten, K.I. The spectral database SPECCHIO for improved long-term usability and data sharing. *Comput. Geosci.* **2009**, *35*, 557–565.
34. Sandmeier, S.R.; Itten, K.I. A field goniometer system (FIGOS) for acquisition of hyperspectral BRDF data. *IEEE Trans.Geosci. Remote Sens.* **1999**, *37*, 978–986.
35. Lucieer, A.; Malenovský, Z.; Veness, T.; Wallace, L. HyperUAS-imaging spectroscopy from a multirotor unmanned aircraft system. *J. F. Robot.* **2014**, *31*, 571–590.
36. Quemada, M.; Gabriel, J.; Zarco-Tejada, P. Airborne hyperspectral images and ground-level optical sensors as assessment tools for maize nitrogen fertilization. *Remote Sens.* **2014**, *6*, 2940–2962.
37. Blackburn, G.A. Spectral indices for estimating photosynthetic pigment concentrations: A test using senescent tree leaves. *Int. J. Remote Sens.* **1998**, *19*, 657–675.
38. Haboudane, D.; Miller, J.R.; Tremblay, N.; Zarco-Tejada, P.J.; Dextraze, L. Integrated narrow-band vegetation indices for prediction of crop chlorophyll content for application to precision agriculture. *Remote Sens. Environ.* **2002**, *81*, 416–426.
39. Guyot, G.; Baret, F. Utilisation de la haute resolution spectrale pour suivre l'etat des couverts vegetaux. *Spectr. Signatures Objects Remote Sens.* **1988**, *278*, 279–286.
40. Lichtenthaler, H.K.; Gitelson, A.; Lang, M. Non-destructive determination of chlorophyll content of leaves of a green and an aurea mutant of tobacco by reflectance measurements. *J. Plant Physiol.* **1996**, *148*, 483–493.
41. Gastellu-Etchegorry, J.P.; Guillevic, P.; Zagolski, F.; Demarez, V.; Trichon, V.; Deering, D.; Leroy, M. Modeling BRF and radiation regime of boreal and tropical forests: I. BRF. *Remote Sens. Environ.* **1999**, *68*, 281–316.

42. Kennedy, R.E.; Cohen, W.B.; Takao, G. Empirical methods to compensate for a view-angle-dependent brightness gradient in AVIRIS imagery. *Remote Sens. Environ.* **1997**, *62*, 277–291.
43. Wanner, W.; Strahler, A.; Hu, B.; Lewis, P.; Muller, J.; Li, X.; Schaaf, C.; Barnsley, M. Global retrieval of bidirectional reflectance and albedo over land from EOS MODIS and MISR data: Theory and algorithm. *J. Geophys. Res.-Atmos.* **1997**, *102*, 17143–17161.
44. Schlapfer, D.; Richter, R.; Feingersh, T. Operational BRDF effects correction for wide-field-of-view optical scanners (BREFCOR). *IEEE Trans. Geosci. Remote Sens.* **2015**, *53*, 1855–1864.
45. Peltoniemi, J.I.; Hakala, T.; Suomalainen, J.; Honkavaara, E.; Markelin, L.; Gritsevich, M.; Eskelinen, J.; Jaanson, P.; Ikonen, E. Technical notes: A detailed study for the provision of measurement uncertainty and traceability for goniospectrometers. *J. Quant. Spectrosc. Radiat. Transf.* **2014**, *146*, 376–390.
46. Strub, G.; Beisl, U.; Schaepman, M.; Schlaepfer, D.; Dickerhof, C.; Itten, K. Evaluation of diurnal hyperspectral HDRF data acquired with the RSL field goniometer during the DAISEX'99 campaign. *ISPRS J. Photogramm. Remote Sens.* **2002**, *57*, 184–193.
47. Kuusk, A. The angular distribution of reflectance and vegetation indices in barley and clover canopies. *Remote Sens. Environ.* **1991**, *37*, 143–151.
48. Epiphanio, J.N.; Huete, A.R. Dependence of NDVI and SAVI on sun/sensor geometry and its effect on fAPAR relationships in alfalfa. *Remote Sens. Environ.* **1995**, *51*, 351–360.
49. Leblanc, S.G.; Chen, J.M.; Cihlar, J. NDVI directionality in boreal forests: A model interpretation of measurements. *Can. J. Remote Sens.* **1997**, *23*, 369–380.
50. Verrelst, J.; Schaepman, M.E.; Koetz, B.; Kneubühler, M. Angular sensitivity analysis of vegetation indices derived from CHRIS/PROBA data. *Remote Sens. Environ.* **2008**, *112*, 2341–2353.

A4: Author´s additional scientific work

Peer Reviewed Paper

A. Burkart, T. J. Wrobel, A. Räsch, and U. Rascher, "Das Leuchten der Pflanzen," *Biol. unserer Zeit*, vol. 44, no. 3, pp. 182–186, Jun. 2014. – A Study that presents a new low-budget method of making chlorophyll-fluorescence visible to the human eye. By using a blue LED flashlight and red glasses in a dark room, the fluorescence signal is decoupled from the blue activator light. The same concept works with a consumer digital camera and several photographs and Kautsky-kinetics of fluorescence are presented.

A. Burkart, A. Schickling, M. P. Cendrero Mateo, T. Wrobel, M. Rossini, S. Cogliati, T. Julitta, and U. Rascher, "A method for uncertainty assessment of passive sun-induced chlorophyll fluorescence retrieval by using an infrared reference light" *IEEE Sensors Journal, 2015, in press,* This study describes the development of a sun-induced-fluorescence (SIF) measurement device that uses a novel infrared reference light. Using this active reference we could for the first time show the stable retrieval of SIF over time. We also were able to access the accuracy and uncertainty of the measurement system.

W. Timmermans, C. Van der Tol, J. Timmermans, M. Ucer, X. Chen, L. Alonso, J. Moreno, A. Carrara, R. Lopez, F. de la Cruz Tercero, H. L. Corcoles, E. de Miguel, J. A. G. Sanchez, I. Pérez, B. Franch, J.-C. J. Munoz, D. Skokovic, J. Sobrino, G. Soria, A. MacArthur, L. Vescovo, I. Reusen, A. Andreu, **A. Burkart**, C. Cilia, S. Contreras, C. Corbari, J. F. Calleja, R. Guzinski, C. Hellmann, I. Herrmann, G. Kerr, A.-L. Lazar, B. Leutner, G. Mendiguren, S. Nasilowska, H. Nieto, J. Pachego-Labrador, S. Pulanekar, R. Raj, A. Schikling, B. Siegmann, S. von Bueren, and Z. Su, "An overview of the regional experiments for land-atmosphere exchanges 2012 (REFLEX 2012) campaign," *Acta Geophys.*, Dec. 2014. – This paper describes the experiments performed during the REFLEX summerschool including hyperspectral airborne sensors and various field setups. The experiments were performed over scientific agricultural fields in Barrax Spain.

M. Rossini, L. Nedbal, L. Guanter, A. Ač, L. Alonso, **A. Burkart**, S. Cogliati, R. Colombo, A. Damm, M. Drusch, J. Hanus, R. Janoutova, T. Julitta, P. Kokkalis, J. Moreno, J. Novotny, C. Panigada, F. Pinto, A. Schickling, D. Schüttemeyer, F. Zemek, and U. Rascher, "Red and far-red sun-induced chlorophyll fluorescence as a measure of plant photosynthesis," *Geophys. Res. Lett.*, p. n/a–n/a, Feb. 2015. – This paper describes the measurement of red and far red SIF with the airborne sensor *HyPlant* and sophisticated ground based systems. A detergent that was sprayed on grassland induced an extreme variation in SIF, that could be tracked spatially and over time.

H. Aasen, A. Bolten, **A. Burkart** and G. Bareth, "Generating 3D Hyperspectral Information with Lightweight UAV Snapshot Cameras for Vegetation Monitoring: From Camera Calibration to Quality Assurance" – submitted – This work describes the calibration of a novel hyperspectral snapshot camera that is used on a rotary wing UAV. The study introduces a technique to generate 3D surface models from the captured images and overlay them with the hyperspectral information. A thorough quality assessment is performed and each pixel is tracked throughout the whole post-processing chain to provide the uncertainty information for each 3D point of the product.

U. Rascher, L. Alonso, **A. Burkart**, C. Cilia, S. Cogliati, R. Colombo, A. Damm, M. Drusch, L. Guanter, J. Hanus, T. Hyvärinen, T. Julitta, J. Jussila, P. Kokkalis, S. Kraft, T. Kraska, M. Matveeva, J. Moreno, O. Muller, C. Panigada, M. Pikl, F. Pinto, L. Prey, R. Pude, M. Rossini, A. Schickling, U. Schurr, D. Schüttemeyer, J. Verrelst, F. Zemek, "Sun-induced fluorescence - a probe of photosynthesis beyond greenness: First maps from the imaging spectrometer HyPlant" – submitted – This paper collects the first maps of sun-induced-fluorescence (SIF) as measured with the novel airborne sensor *HyPlant.*

S. Cogliati, M. Rossini, T. Julitta, M. Meroni, A. Schickling, **A. Burkart**, F. Pinto, U. Rascher, and R. Colombo, "Continuous and long-term measurements of reflectance and sun-induced chlorophyll fluorescence by using novel automated field spectroscopy systems," *Remote Sens. Environ.*, May 2015. – in Press – This paper describes an automated system with high resolution spectrometers, which continuously measures reflectance of plant canopies. The accurate calibration and fine spectral resolution allows the retrieval of sun-induced-fluorescence.

Conferences

"Rotary wing UAS based multiangular hyperspectral measurements over various vegetation" - **Andreas Burkart**, Helge Aasen, Luis Alonso, Georg Bareth, and Uwe Rascher - EGU General Assembly 2014 – Vienna AT – oral presentation.

"UAV based spectroscopy – achievements, challenges and results of hyperspectral measurements in Europe and New Zealand" – **A. Burkart**, S. von Bueren, A. Lobo and U. Rascher - COST Action ES0903 "EUROSPEC" Final Conference, 6-8 November 2013, Trento IT – oral presentation

"An airship as platform for remote sensing of plant phenology" – **A. Burkart**, U. Rascher– 9th International Airship Convention 2012, Ashfort UK – proceedings and oral presentation

"Spectroscopy Information Systems for Earth System Science" – A. Hueni, M. Jehle, A. Damm, **A. Burkart**, M. Schaepman – ESA PV 2013 - proceeding

"Introducing a novel miniaturized high performance spectrometer to measure vegetation using an octocopter" - **A. Burkart**, S. von Bueren, S. Cogliati, L. Alonso and U. Rascher - EARSEL Nante 2013 - poster

"Hyperspectral reflectance measurements over agricultural crops by an UAV based ultra-light weight microspectrometer - Ein fliegendes Hyperspektrometer" – 2. Workshop Unbemannte autonom fliegende Systeme (UAS) in der Landwirtschaft – **A. Burkart**, S. Cogliati and U. Rascher - 6. - 7. Mai 2013, Berlin – oral presentation

„Ableitung relevanter Parameter aus hochauflösenden Luftaufnahmen von Versuchsflächen" – **A. Burkart** and T. Malolepszy – GFP Züchtertagung 2014, Bonn – oral presentation

„From landscape to miniature – a processing chain from UAV data to a 3D printed model" – **A. Burkart**, T. Burkart, S. von Bueren and U. Rascher - 35. Wissenschaftlich-Technische Jahrestagung der DGPF Workshop on Laser Scanning Applications – Cologne, 2015 - poster